Effective Cancer Therapy Design Through the Integration of Nanotechnology

Jessica Won Hee Fisher

Thesis submitted to the faculty of the Virginia Polytechnic Institute and State University
in partial fulfillment of the requirements for the degree of

Master of Science
In
Biomedical Engineering

Marissa N. Rylander, Ph.D., Committee Chair
Harry C. Dorn, Ph.D., Committee Member
Scott T. Huxtable, Ph.D., Committee Member
Christopher G. Rylander, Ph.D., Committee Member

July 25, 2008
Blacksburg, VA

Keywords: multi-walled nanotubes, carbon nanohorns, tissue phantom, laser therapy, hyperthermia, heat shock proteins

Effective Cancer Therapy Design Through the Integration of Nanotechnology

Jessica Won Hee Fisher

ABSTRACT

Laser therapies can provide a minimally invasive treatment alternative to surgical resection of tumors. However, therapy effectiveness is limited due to nonspecific heating of target tissue, leading to healthy tissue injury and extended treatment durations. These therapies can be further compromised due to heat shock protein (HSP) induction in tumor regions where non-lethal temperature elevation occurs, thereby imparting enhanced tumor cell viability and resistance to subsequent therapy treatments. Introducing nanoparticles (NPs), such as multi-walled nanotubes (MWNTs) or carbon nanohorns (CNHs), into target tissue prior to laser irradiation increases heating selectivity permitting more precise thermal energy delivery to the tumor region and enhances thermal deposition thereby increasing tumor injury and reducing HSP expression induction. This research investigates the impact of MWNTs and CNHs in untreated and laser-irradiated monolayer cell culture, tissue phantoms, and/or tumor tissue from both thermal and biological standpoints. Cell viability remained high for all unheated NP-containing samples, demonstrating the non-toxic nature of both the nanoparticle and the alginate phantom. Up-regulation of HSP27, 70 and 90 was witnessed in samples that achieved sub-lethal temperature elevations. Tuning of laser parameters permitted dramatic temperature elevations, decreased cell viability, and limited HSP induction in NP-containing samples compared to those lacking NPs. Preliminary work showed MWNT internalization by cells, which presents imaging and multi-modal therapy options for NT use. The lethal combination of NPs and laser light and NP internalization reveals these particles as being viable options for enhancing the thermal deposition and specificity of hyperthermia treatments to eliminate cancer.

Acknowledgements

I would like to thank my Lord and Savior, Jesus Christ, who has given me new life and provided me with these opportunities and skills to do this research for His glory. I also thank my husband, Mark, for his continual love and encouragement through the entire span of my research. Without his constant humor and creativity, this adventure would have not been the same or as fun. He truly deserves a standing ovation. I would also like to thank my advisor, Dr. M. Nichole Rylander, whose dedication, invaluable guidance, support, and ever-present optimism has fueled my ability to conduct this research. I am truly blessed and honored to have been mentored by her. I thank my committee members, Dr. Harry Dorn, Dr. Scott Huxtable, and Dr. Chris Rylander, whose advice and insight have helped propel this work forward. Thank you to my collaborators at Wake Forest University, who have helped in innumerable ways. I would also like to thank Anjali Hirani for her training and advice with cell culture work and her humor. Thank you for making the lab fun. Also, I thank Dr. Nicole L. Polyachenko for her great ideas and wise counsel in regards to nanotubes and sodium alginate.

I would also like to thank my parents and brother, Rick and Ann and Willie, and my family for their continuous encouragement, love, and support. You have helped me get to where I am and I am so grateful for your love. I thank all my friends in Blacksburg and beyond whose loving support and encouragement helped me during my graduate career.

This research was supported by the National Science Foundation (NSF) under grant CBET-0731108, Institute of Critical Technology and Applied Science Fellowship, and Advance VT Research Development Grant.

Table of Contents

List of Figures vii
List of Tables xii
Chapter 1: Introduction 1
1.1. Cancer: disease, detection, and treatment 1
1.1.1. Cancer: the disease 1
1.1.2. Detection and diagnosis 1
1.1.3. Treatment and recurrence 2
1.2. Heat shock proteins 4
1.2.1. Molecular roles 4
1.2.2. Indications of apoptosis prevention in cancer cells by HSPs 5
1.3. Nanotechnology: Multi-walled carbon nanotubes 6
1.3.1. Definition and applications 6
1.4. Nanotechnology: Carbon nanohorns 10
1.4.1. Definition and applications 10

Chapter 2: Hyperthermia treatment of PC3 and RENCA cells using MWNTs 12
2.1. Experimental materials and methods 13
2.1.1. Cell culture 13
2.1.2. Multi-walled nanotubes 14
2.1.3. Laser-thermocouple system setup 14
2.1.4. Spectrophotometer and optical setup 15
2.1.5. Cell viability 15
2.1.6. HSP immunostaining 16
2.1.7. MWNT internalization 17
2.2. Experimental results 17
2.2.1. Optical properties 17
2.2.2. Temperature and heat generation 19
2.2.3. Cell viability 24

2.2.4. HSP expression 27
2.2.5. MWNT internalization 32
2.3. Discussion and conclusions 35

Chapter 3: Hyperthermia treatment of tissue phantoms and tumors using MWNTs 40
3.1. Experimental materials and methods 41
3.1.1. Sodium alginate phantom creation 41
3.1.2. Tumor implantation and MWNT injection 43
3.1.3. Laser and temperature measurement system setup 43
3.1.4. Cell viability 44
3.1.5. Tissue processing and H&E staining 45
3.1.6. HSP immunostaining 45
3.2. Experimental results 45
3.2.1. Temperature for phantoms 45
3.2.2. Cell viability of phantoms 46
3.2.3. H&E staining and HSP expression of tissue 48
3.3. Discussion and conclusions 51

Chapter 4: Hyperthermia treatment of PC3 cells using CNHs 53
4.1. Experimental materials and methods 53
4.1.1. Nanohorn fabrication 53
4.1.2. Nanohorn structure and imaging 54
4.1.3. Temperature and heat generation 54
4.1.4. Cell viability 54
4.2. Experimental results 55
4.2.1. Nanohorn structure and imaging 55
4.2.2. Temperature and heat generation 55
4.2.3. Cell viability 57
4.3. Discussion and conclusions 58

Chapter 5: Future Prospects.....60
5.1. Multi-walled nanotubes 60
5.1.1. Cell culture.....60
5.1.2. Phantoms and *in vivo* mouse tumor study 60
5.2. Nanohorns.....61

References.....62

List of Figures:

Chapter 1:

Figure 1.1: Male lower abdominal anatomy.
http://www.cancer.gov/cancertopics/wyntk/prostate/page2 1

Chapter 2:

Figure 2.1: External beam laser setup for cell heating.....15

Figure 2.2: Absorbance curve for 0.1 mg/ml MWNT in ddH_2O (baseline corrected). Deionized water in a fluorometer was used as the baseline curve. Scan rate 600nm/min 18

Figure 2.3: Spectral data of various fullerenes and imaging particles dispersed in PBS with 1% Pluronic F-127. Note the preferential absorption peak of fullerenes in the UV-Vis range but the absence of NIR absorption.....19

Figure 2.4: Temperature plot for various nanoparticles or material heated with a 1064 nm laser at 3W for 30 sec.....20

Figure 2.5: Close-up view of temperature increase of non-NIR-specific particles and water heated with a 1064 nm laser at 3W for 30 sec 20

Figure 2.6: Temperature profile during sub-lethal laser heating of 3W for 90 sec of (A) PC3 cells without NTs and (B) PC3 cells with MWNT. TC0 is located 4 mm from laser center, TC1 is located 7 mm from laser center 21

Figure 2.7: Temperature increase of sub-lethal heating (3W, 90 sec) of media in the absence and presence of 0.1 mg/ml MWNTs. n=6, σ range: 2.10 and 3.41°C 22

Figure 2.8: Temperature plot of lethal heating of media (A) without and (B) with 0.1 mg/ml MWNTs. TC0 is located 4 mm from laser center and TC1 is located 7 mm from laser center 23

Figure 2.9: Temperature increase of lethal heating (3W, 5 min) of media in the absence and presence of MWNTs. N=6, σ range: 2.25-6.52°C.....23
Figure 2.10: Cell viability staining with trypan blue of PC3 cells near laser center. (A) Unheated cells without NTs, (B), Unheated cells with MWNTs, (C) Sub-lethal heated cells without NTs, (D) Sub-lethal heated cells with MWNT, (E) Lethal heated cells without NTs, and (F) Lethal heated cells with MWNT. Red arrows indicate MWNT clusters. Scale bars are 100 μm.....25
Figure 2.11: Cell viability staining with trypan blue of RENCA cells near laser center. (A) Unheated cells without NTs, (B) Unheated cells with MWNTs, (C) Sub-lethal heated cells without NTs, (D) Sub-lethal heated cells with MWNT, (E) Lethal heated cells without NTs, and (F) Lethal heated cells with MWNT. Red arrows indicate MWNT clusters. Scale bars are 100 μm 26
Figure 2.12: Cell viability of (A) PC3 and (B) RENCA for various heating levels. –NT: no MWNT, +NT: 0.1 mg/ml MWNT; –Laser: unheated, subL: 3W for 90 sec, Lethal: 3W for 5 min. n=3 except in lethal cases; σ_{PC3} range: 0.27-2.45%, σ_{RENCA} range: 0.27-0.89%.....27
Figure 2.13: HSP fluorescent microscope images of unheated and laser heated PC3 cells with and without MWNTs. These cells have been stained separately for HSP27, 70, and 90. NL: no laser; Sub-L: sub-lethal laser; L: lethal laser; noNT: no MWNTs; NT: MWNTs. Scale bars are 50 μm.....28
Figure 2.14: HSP fluorescent intensities of unheated and laser heated PC3 cells with and without MWNTs. These cells have been stained separately for HSP27, 70, and 90. NL: no laser; Sub-L: sub-lethal laser; LL: lethal laser; noNT: no MWNTs; NT: MWNTs. N=3 (* group: N=2), σ_{HSP27}=2.23-11.77AU, σ_{HSP70}=0.35-6.74AU, σ_{HSP90}=1.04-6.49AU.....29

Figure 2.15: HSP fluorescent microscope images of unheated and laser heated RENCA cells with and without MWNTs. These cells have been stained separately for HSP27, 70, and 90. NL: no laser; Sub-L: sub-lethal laser; L: lethal laser; noNT: no MWNTs; NT: MWNTs. Scale bars are 50 μm.....30

Figure 2.16: HSP fluorescent intensities of unheated and laser heated RENCA (R) cells with and without MWNTs. These cells have been stained separately for HSP27, 70, and 90. NL: no laser; Sub-L: sub-lethal laser; LL: lethal laser; noNT: no MWNTs; NT: MWNTs. N=3 (* group: N=2; # group: N=1), σ_{HSP27}=0.48-1.87AU, σ_{HSP70}=2.67-4.77AU, σ_{HSP90}=1.58-8.37AU.....31

Figure 2.17: HSP fluorescent intensities of unheated and laser heated PC3 and RENCA cells with and without MWNTs. These cells have been stained separately for HSP27, 70, and 90. NL: no laser; Sub-L: sub-lethal laser; LL: lethal laser; noNT: no MWNTs; NT: MWNTs. N=3 (* group: N=2; # group: N=1).....32

Figure 2.18: Microscope image of MWNT clusters (arrows) near unheated PC3 cells. Magnification: 400x.....32

Figure 2.19: Brightfield image of MWNT incubated with RENCA cells. Black length bar is 100 μm. See MWNT aggregates encircled the nucleus (red circle).....33

Figure 2.20: DAPI-stained nuclei of RENCA cells overlaid on bright field images. Unheated non-NT samples (A, B) and samples with 0.1 mg/ml MWNT added 24 hours earlier (C-F). MWNT aggregates show up as black clusters around the nuclei (see arrows). Scale bars are 25 μm.....34

Chapter 3:

Figure 3.1: Lexan mold setup for tissue phantom creation. Note the filters are placed on either side of metal mold to shape phantoms into 1-2 mm thick phantoms.....42

Figure 3.2: Tissue phantoms shown here, 0.1 mg/ml MWNT phantom (left) and non-NT phantom (right) 42
Figure 3.3: Nude mice bearing RENCA tumors subcutaneously. Red circle indicates the location of one tumor 43
Figure 3.4: External beam laser setup for mouse experiments 44
Figure 3.5: Tumor half in liquid OCT (pre-freezing). Black area is MWNTs (see arrow) 45
Figure 3.6: Temperature profile during laser heating of 3W for 45 sec as a function of various radial positions of (A) non-NT phantom and (B) MWNT phantom. All thermocouples were positioned 1 mm in depth. TC0 is located 3 mm from center, TC2 is located 4 mm from center, TC1 is located 6 mm from center, and TC3 is located 7 mm from center 46
Figure 3.7: Representative image of trypan blue staining of (A) unheated PC3 phantom and (B) unheated PC3 phantom immersed in methanol. Similar results were seen at all depth positions within phantoms. Magnification: 100x 47
Figure 3.8: Cell viability staining with trypan blue of PC3-seeded phantoms. Trypan blue enters dead or dying cells while viable cells exclude the dye. (A) Unheated phantom without NTs, (B) unheated phantom with MWNTs, (C) heated phantom without NTs, and (D) heated phantom with MWNT. Magnification: 100x. Note: black arrows indicate examples of dead cells 48
Figure 3.9: H&E staining of a section of RENCA mouse tumor. Note MWNT clustering (arrow) 49
Figure 3.10: Magnified area of MWNT clumping in H&E stained section of RENCA mouse tumor. Note MWNT clustering (arrow). Scale bar is 100 μm 49
Figure 3.11: HSP staining of RENCA mouse tumors. (A) Growth control, (B) MWNT control, (C) Saline with laser irradiation, and (D) MWNT with laser irradiation. Scale bar is 10 μm 50

Figure 3.12: HSP90 staining of RENCA mouse tumors. (A) Growth control, (B) MWNT control, (C) Saline with laser irradiation, and (D) MWNT with laser irradiation. Scale bar is 50 μm 51

Chapter 4:

Figure 4.1: TEM images of $Gd_3N@C_{80}$@SWNH taken by collaborators at ORNL. (A) Low magnification TEM image showing the flower-like structure of the functionalized carbon SWNHs filled with $Gd_3N@C_{80}$ metallofullerenes, 20 nm scale bar; (B) High magnification micrograph from the SWNH edge showing the carbon nanohorn structure, as well as individual fullerene particles trapped inside cones, 5 nm scale bar; (C) STEM-HAADF image from the edge of a functionalized SWNH containing $Gd_3N@C_{80}$. Bright dots are the individual metal particles, 2 nm scale bar; (D) A bright field image from the same area showing SWNH caps of single graphene sheets (see arrow), 2 nm scale bar.....55

Figure 4.2: Temperature plots of lethal heating (3W, 5 min) of PBS with 1% PL-127 (A) without and (B) with 0.1 mg/ml CNHs. (TC0 is 4 mm from laser center and TC1 is 7 mm from laser center 56

Figure 4.3: Temperature elevation without and with CNHs at lethal laser level (3W, 5min). Concentration of CNH was 0.1 mg/ml in PBS. N=3, σ = 2.6-3.2°C 56

Figure 4.4: Trypan Blue staining of PC3 cells: (A) unheated without CNH, (B) unheated with CNH, (C) lethal heating without CNH, and (D) lethal heating with CNHs. Scale bar is 100 μm 57

Figure 4.5: Cell viability of PC3 cells. Note the significant reduction in viable cells with lethal and CNHs. n=3, σ range: 0.49 - 3.64% 58

*Unless otherwise noted, all images are original to the author.

List of Tables:

Chapter 1:

Table 1.1: TNM staging system for cancer [16] 3
Table 1.2: HSP Locations and specific functions 4

Chapter 2:

Table 2.1: Antibodies used for HSP27, 70, and 90 immunostaining 17
Table 2.2: Summary of mean intensities of each PC3 group with its associated standard deviation. N=3, except *N=2 29
Table 2.3: Summary of mean intensities of each RENCA group with its associated standard deviation. N=3, except *N=2 31

Chapter 1: Introduction

1.1. Cancer: disease, detection, and treatment

1.1.1. Cancer: the disease

Estimates in 2007 state that one in six men in the United States will be diagnosed with prostate cancer in his lifetime. It is estimated that there will be over 218,000 new cases and over 27,000 deaths related to prostate cancer this year. It is also the second most common cancer and second leading cause of cancer death for men in the US [1, 2]. Prostate cancer affects the prostate gland, located below the bladder and around the urethra in men. Figure 1.1 depicts the surrounding human anatomy.

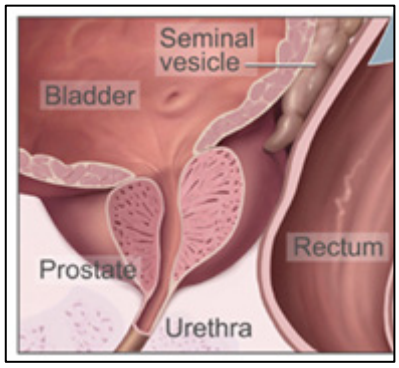

Figure 1.1. Male lower abdominal anatomy. http://www.cancer.gov/cancertopics/wyntk/prostate/page2.

Prostate cells can begin to mutate and can metastasize into surrounding tissue, such as bone. It is not clear what causes prostate cancer. However, there are several risk factors associated with prostate cancer, such as family history, race, diet, and age, with age being the main factor. In the United States, most men with prostate cancer are older than 65 [3].

1.1.2. Detection and diagnosis

Evaluating the blood for prostate-specific antigen (PSA) levels and conducting a digital rectal exam (DRE) are two ways to screen for prostate cancer [2]. If tissue looks suspicious, a biopsy is taken. Pathologists evaluate a biopsy using a subjective rubric called the Gleason scoring system which gives an overall summary of progression and aggressiveness of the cancer. A cancer's grade is based on comparison of the prostate tissue as seen under a microscope to a

discrete model structure. The scale runs from 1 to 5, where 1 represents cells that are very nearly normal, and 5 represents cells that do not resemble native-normal cells. Two grades of the most prevalent tissue structures are summed to create a Gleason score between 2 and 10. The more advanced the cancer is, the higher its Gleason score [4, 5].

1.1.3. Treatment and recurrence

Prostate cancer has a high cure rate provided that the cancer is found early and the patient has a low Gleason score. Conventional cancer methods include surgical removal of tumor tissue, which is effective for removing well-defined, accessible tumors located within non-vital tissue. However, this therapy method is highly invasive and possesses high tissue morbidity, making it unsuitable for treating small, poorly-defined tumors or tumors within vital tissue. Minimally invasive therapies, such as thermal therapies, are being investigated for better treatment of these types of tumors. These therapies can provide minimally invasive treatment alternatives to conventional resection procedures, reducing complication rates and decreasing the length of hospital stays. Exposing tissue to elevated temperatures, or hyperthermia, is being used to combat cancer. Thermal stress causes denaturation of proteins within cells which causes irreversible cell damage. Lethal levels of heating (high thermal dose) will result in apoptosis. Thermal therapies use a variety of delivery methods, such as laser-induced thermal therapy [6-9], microwave and radiofrequency (RF) ablation [10, 11], magnetic thermal ablation [12, 13], and focused ultrasound [14].

Even though prostate cancer has a high "cure rate," the effectiveness of these cures is complicated by higher recurrence rates. Kattan developed a pre-operative nomogram to predict the probability of a patient living recurrence-free for five years [15]. Clinical stage refers to the extent or severity of a patient's cancer. Staging is important because it helps doctor plan patient treatment, estimate prognosis, and identify suitable clinical trials for specific patients. The TNM staging system is one of the most commonly used staging system. This system is based on the size and extent of primary tumor (T), presence of distant metastasis (M), and extent of spread to regional lymph nodes (N) [16]. Table 1.1 describes this staging system.

Table 1.1. TNM staging system for cancer [16].

Primary tumor (T)		Regional Lymph Nodes (N)		Distant Metastasis (M)	
Category	**Description**	**Category**	**Description**	**Category**	**Description**
TX	Primary tumor cannot be evaluated	NX	Regional lymph nodes cannot be evaluated	MX	Distant metastasis cannot be evaluated
T0	No evidence of primary tumor	N0	No regional lymph node involvement	M0	No distant metastasis
Tis	Carcinoma in situ (early cancer not spread to neighboring tissue)	N1, N2, N3	Involvement of regional lymph nodes (number and/or extend of spread)	M1	Distant metastasis
T1, T2, T3, T4	Size and/or extent of primary tumor				

In the early 1990s, researchers reported that the 10-year clinical recurrence rates in a majority of T1-T2 (N0: no cancer in lymph nodes, M0: no cancer spread to distant body parts) patients following radical prostatectomy (RP) and radiotherapy (RT) were 28% and 33%, respectively [17, 18]. A study by Walsh et al. reported the 5-year clinical recurrence rates following RP and RT were up to 7% and 24%, respectively, and their 10-year clinical recurrence rates were up to 31% and 44%, respectively [19].

Even thermal therapy effectiveness is limited due to nonspecific heating of target tissue which often leads to healthy tissue injury. Due to the lack of heating specificity, treatment volumes and durations are limited by the maximum temperature near the probe tip and the expanding thermal boundary. Treatment of larger tumor volumes with hyperthermia therapies results in longer treatment times and generation of poorly defined lesion boundaries because of slow thermal diffusion from the heating source. In addition to these limitations, hyperthermia therapies can frequently be compromised due to the induction of molecular chaperones, known as heat shock proteins (HSP), in regions of the tumor where non-lethal temperature elevation occurs [20, 21]. The success of thermal therapies is characterized most often according to the equivalent thermal dose (the equivalent time that a tissue was at $T = 43^{o}C$, which is the threshold for thermal injury) and the associated temperature dependent cellular injury [22]. However, with thermal induction of HSP and the subsequent protection of tumor cells, understanding both cellular injury and HSP expression to characterize the cellular response to laser therapies and their effectiveness is critical.

1.2. Heat shock proteins

1.2.1. Molecular roles

The HSP family of proteins is labeled according to molecular weight (in kilodaltons, kDa). These proteins reside in several sub-cellular compartments as well as within the cytosol in normal cells [23]. Table 1.2 lists known HSP along with their determined functions and locations [24].

Table 1.2. HSP Locations and Specific Functions.

Family	Chaperone Members	Cellular Compartment	Function
HSP100	HSP104	Cytoplasm	Thermotolerance
HSP90	HSP90 Grp94	Cytoplasm Endoplasmic Reticulum	Stabilize inactive forms of certain hormone receptors until hormone is present; interaction with certain protein kinases to help their transit to plasma membranes; prevent aggregation of denatured proteins; and interact with immunophilins
HSP70	HSC70 HSP70 Bip/GRP78 GRP75	Cytoplasm/Nucleus Cytoplasm/Nucleus ER Mitochondria	Stabilize prefolded/unfolded structures towards translocation/ folding; assembly of Immunoglobins; target old protens to lysosomes for degradation; protein secretion; antigen presentation; thermotolerance; interaction with certain immunosuppressants
HSP60	HSP60	Mitochondria	Stabilize prefolded structures towards folding/assembly; re-export of precursors to membrane space
HSP40	HSP40	Cytoplasm/Nucleus	Chaperone activity; essential co-chaperon activity with HSP70 to enhance ATPase rate and substrate release
Small HSP	HSP27 αA and αB-crystallins	Cytoplasm Cytoplasm	Prevents polypeptide aggregation; thermotolerance through stabilization of microfilaments; possible roles in cell growth and differentiation

Rylander MN: **Design of Hyperthermia Protocols for Inducing Cardiac Protection and Tumor Destruction by Controlling Heat Shock Protein Expression.** University of Texas at Austin, Biomedical Engineering; 2005.

Low levels of HSP are found in unstressed cells to inhibit improper protein aggregation and direct new proteins to target organelles for final packaging, degradation, or repair [23]. However, in response to stress, HSP levels increase to help refold and repair denatured proteins and assist in synthesizing new proteins [13, 14, 25]. Various stimuli can trigger up-regulation of HSP, including environmental stresses (chemicals, heat shock, heavy metals), pathophysiological state (fever, hypertrophy, inflammation, viral infection), and non-stressful conditions (cell cycle, growth) [26]. Elevated expression of HSP were found in cells subjected to environmental challenges, such as elevated temperatures, drugs, UV irradiations, glucose deprivation, cytoskeletal perturbation, or other stresses [27]. Non-lethal thermal stress up-regulates expression of HSP within the tissue, enhancing cell viability and resistance to other therapies, such as chemotherapy and radiation therapy which are often used in combination with hyperthermia. Higher levels of HSP can lead to increased tumor recurrence [20, 21]. As a result, applied thermal stress associated with hyperthermia can induce the offsetting effects of HSP up-regulation and cell necrosis [20, 21, 28].

1.2.2. Indications of apoptosis prevention in cancer cells by HSPs

During ineffective hyperthermia treatments, cells are exposed to sub-lethal temperatures, increasing HSP levels which inhibit apoptosis and spare tumor cells. While HSPs perform critical functions (protein refolding and repair) within normal cells, the up-regulated expression of HSPs in cancer cells has been implicated in many roles of therapeutic resistance which includes multi-drug resistance [29], regulation of apoptosis [30-32], and modulation of p53 functions [33] for a large range of neoplastic tissues. Even though there are many HSPs that are thermally induced, previous research has shown HSP27 and HSP70 to be the most significantly induced as a result of thermal stress [34-36] with HSP90 being investigated as well. Each of these HSPs promotes survival mechanisms of a cell by interacting with Akt, a serine/threonine protein kinase that is a critical regulator of cell survival and proliferation [27, 37].

Over-expression of HSP27 is a poor prognostic marker in invasive prostatic carcinoma in humans [38]. Elevated levels of HSP70 have been observed in breast and cervical cancers [39, 40] and have a proven role in cell proliferation and drug resistance [41]. HSP70 and HSP27 over-expression has also been linked to the synergistic effect of hyperthermia on radio and chemotherapies [42]. HSP90 is abundant in eukaryotes and is localized in the cytoplasm of cells.

However, after heat shock, it can travel to the nucleus [43]. It also inhibits apoptosis, providing a protective role for the cell [44]. Investigating one of the primary pathways of apoptosis reveals how HSP interaction can inhibit this process. Upon apoptotic stimuli, cytochrome c is released from the mitochondria and then it binds to a protein called Apaf-1. This complex recruits pro-caspase-9 (the unprocessed pro-form of a proteolytic enzyme caspase-9). Once this pro-form is cleaved, caspase-9 becomes active and initiates the process of apoptosis. HSP27, 70, and 90 have been shown to inhibit at different stages in the initiation phase of apoptosis. HSP27 binds to cytochrome c, preventing its binding to Apaf-1. HSP90 binds to Apaf-1 and prevents its binding to cytochrome c. HSP70 prevents oligomerised Apaf-1 from recruiting pro-caspase-9 [24, 27, 45].

Therefore HSP induction, and thus protection, occurs if the temperature within any part of the target tissue (i.e. tumor) is sub-lethal or the heating duration is insufficient to fully coagulate proteins in any portion of the tissue, sparing cancer cells and making them more resistant to other therapies. Because of this, HSP27, 70, and 90 expression needs to be used to give both an indirect measure of heat delivery and cellular response which will allow evaluation of the effectiveness of various therapies for tumor destruction.

To overcome the limitations of traditional hyperthermia therapies, researchers are investigating various methods to enhance therapy selectivity and thermal deposition using nanoparticles [46, 47]. Nanomaterials, such as Fe/Co graphitic-shell nanocrystals, gold nanoshells, single walled nanotubes (SWNTs), and multi-walled nanotubes (MWNTs), are being investigated for their potential role as heat delivery vehicles for laser ablation of tumors. Many of these nanoparticles have excellent thermal properties, such as high thermal conductivities, which would improve the thermal deposition and specificity for laser treatment [22, 46-56].

1.3. Nanotechnology: Multi-walled carbon nanotubes

1.3.1. Definition and applications

Nanotechnology refers to a field which uses a category of materials that have at least one dimension between one nanometer and one micron. For comparison, a human hair is 60 μm in diameter and red blood cells are 7 μm in diameter while a C60 nanoparticle could be 1 nm in diameter. Nanoparticles are generally classified based on their dimensionality, morphology, composition, uniformity, and agglomeration [57].

Carbon nanotechnology refers to carbon materials within this size range. There are three forms of carbon, specifically graphite, diamond, and fullerenes. The fullerene form was discovered by Kroto, Smalley, and Curl in 1985 [58]. Within the fullerene family, there are two structures: spherical (called Buckeyballs) and tubular (called nanotubes). Their morphology is dependent on the number and arrangement of their carbon atoms. Carbon nanotubes (CNTs or NTs) are composed of graphene sheets of sp2 bonded carbon atoms rolled seamlessly into a tubular form, capped at their ends by fullerene hemispheres. The two major configurations of CNTs are single-walled (characterized by a single graphene tube) or multi-walled (characterized by several concentric tubes nested within each other). For SWNTs, the diameter and length of CNTs varies between 1.5-3.0 nm and 20-1000 nm and 5.0 -100 nm and 1-50 microns for multi-walled CNTs, respectively.

Currently, a wide variety of carbon nanotubes can be created. These CNTs can be metallic or semiconducting, which is function of the chirality of the tube. Chirality refers to the property of non-superposition; a nanotube and its mirror image cannot be superimposed on each other. Nanotubes can be "rolled" into different chiralities, thus possessing different electrical and thermal properties (metallic and semi-metallic) [25, 59].

There are several techniques employed to produce nanotubes in relatively large quantities, including arc discharge, laser ablation, and chemical vapor deposition (CVD). In CVD, a specific catalyst initiates tube growth on a substrate, which can yield highly aligned NTs. Choosing this catalyst affects properties of the tubes themselves [25, 60, 61]. If iron oxide particles are used, iron will be incorporated into the structure of the NT and MRI could be employed to visualize the nanotube-target site (i.e. a tumor) [62].

With increasing material variety, carbon nanomaterials have become the focus of much research for biomedical applications [46, 50, 51, 56, 63]. Currently, researchers are investigating various methods to enhance the selectivity and thermal deposition of these therapies [46, 47]. Many types of nanoparticles, such as Fe/Co graphitic-shell nanocrystals, gold nanoshells, single walled nanotubes (SWNTs), and multi-walled nanotubes (MWNTs), are being investigated for their potential role as heat delivery vehicles for laser ablation of target tissue [22, 46-56].

Although gold nanoshells, SWNTs, and MWNTs greatly enhance the effectiveness of laser therapy due to their ability to act as antennae for electromagnetic energy, carbon nanotubes (CNTs) are receiving much attention due to their stunning qualities, including remarkable

strength, hardness, electrical and thermal conductivity, and antenna properties. Embodied in this tubular form, CNTs are unlike all other allotropes of carbon. Along the axial direction, the tube is stronger than steel, harder than diamond, and carries greater current density than copper [52]. CNTs are the best known conductor of heat [64]. Absorption of light causes the tubes to oscillate and the electromagnetic energy to be converted into heat. Because of their high aspect ratio, the electric field within their localized area is enhanced, increasing heat generation of the tube [65-68].

Unlike other thermal conductors, the oscillator strength of CNTs grows as the number of dipole oscillators squared, making them ballistic conductors. Thus, CNTs have potential to generate enormous amounts of heat per unit mass [67, 68]. In addition, CNTs are strong absorbers in the near infrared (NIR) region of the spectrum, which includes wavelengths of 700–1,100 nm [53, 54]. CNTs have an absorption peak within this wavelength range [46, 69, 70]. The antenna properties of MWNTs are far superior to the SWNTs and nanoshells. MWNTs can absorb approximately three times the light as SWNTs, which is critical to permit reduction of the typical light attenuation associated with scattering in irradiated skin and subcutaneous tissue by NIR laser light. Due to the lack of NIR-absorbing chromophores in most tissue, NIR light is transmitted through tissue with scattering-limited attenuation and minimal heating. NIR light has been shown to penetrate tissue at depths up to 2-4 cm with power well below a threshold of normal tissue damage. Since typically NIR irradiation may be applied through the skin to kill embedded cancers, the decreased light intensities required to heat with MWNTs may reduce damage to dermal layers, particularly when the cancer lies at the deeper end of the NIR penetration range (2-4 cm). MWNTs must be illuminated with electromagnetic radiation to produce heat, and are therefore not toxic in the absence of radiation [53, 54]. Within this region, CNTs contained within tumors remain capable of absorbing infrared radiation and producing heat while skin remains mostly transparent to this range of wavelengths. Previous work has shown that MWNTs couple with 1064 nm incident light and generate heat with remarkable efficiency [55]. Introducing CNTs within the target tissue can greatly enhance thermal deposition by increasing the amount and specificity of thermal energy.

A second advantage of MWNTs is that they have broad bandwidth compared to the specific resonance absorptions of SWNTs and nanoshells, allowing them to be activated by broader bandwidths of electromagnetic radiation. A third distinction of MWNTs as compared to

nanoshells is their ability to act as magnetic resonance imaging (MRI) agents when filled with iron. Iron is a well known contrast agent for MRI, a procedure used routinely in diagnostic radiology. The dual functionality of MWNTs as both imaging and treatment agents is an attractive option as it allows MWNTs to be used to localize the tumor, serve as the ablative agent, and monitor tumor ablation. This should improve our ability to precisely target therapy to the tumor [53, 54]. Due to the extremely high potential benefit of including MWNTs in laser therapy, this study will focus on measuring the cellular response and thermal enhancement effects of these particles in laser therapy.

Internalization of nanoparticles into cells is of particular interest since this interaction between cells and nanoparticles is a critical issue which will determine any future biological application of these particles. Nanoparticle induced toxicity is a major concern and area of research [71]. However, internalization of NPs could be used to delivery therapeutic or imaging agents into diseased cells. Developing new strategies for the delivery of therapeutic agents into cells is necessary due to poor cellular penetration of many small molecules and some macromolecules, including drugs, proteins, and nucleic acids [72]. Use of these loaded nanoparticles could allow for better diagnosis, treatment, and monitoring of disease. Many researchers are investigating the use of nanoparticles as delivery vehicles for therapeutically active molecules [63, 73-75].

Studies have shown various nanoparticles being internalized by several cell types, including endothelial cells [76], pulmonary epithelium [77-83], gastrointestinal epithelium [84], red blood cells [85, 86], platelets [87], and nerve cells [88]. Cellular uptake and subcellular localization depend on chemistry, size, and shape of the particular nanoparticle [89]. It is proposed that NP internalization occurs through two routes. Passive uptake occurs through diffusion across the lipid bilayer, similar to a "nanoneedle," which allows NPs to perforate the cell membrane without causing cell death [90, 91]. Another route of NP internalization is through adhesive interaction [92, 93] (endocytosis). What initiates this uptake is not fully understood and is thought to be factors such as van der Waals forces, electrostatic charges, steric interactions, or interfacial tension effects [86, 94]. Nanoparticles have been found in the outer-cell membrane [76, 95], cytoplasm [76, 95], lipid vesicles [76, 96], mitochondria [89, 97], along the nuclear membrane [95, 98], or within the nucleus [76, 89, 98]. Studies have shown functionalized MWNTs (lengths between 0.5-2 μm, 20-30 nm diameter) to cross the cell

membrane of multiple cell types [63]. This phenomenon warrants further investigation as it could give additional useful features to the use of NPs in cancer therapy by adding other modes of therapy (i.e. reactive oxygen species generation, drug delivery) and imaging options.

In addition to carbon nanotubes, we will explore a highly under-investigated nanoparticle, called a carbon nanohorn (CNH), which has intrinsically lower toxicity and larger loading potential for imaging cargo, such as gadolinium (Gd).

1.4. Nanotechnology: Nanohorns

1.4.1. Definition and applications

Recently, the carbon nanohorn (CNH) was recognized as a member of the fullerene family [99, 100]. A single CNH has a similar structure to a pudgy single-wall carbon nanotube (SWNT) with one closed end with a cone-shaped cap (horn) [101]. CNHs have diameters of approximately 2-5 nm. Due to strong van der Waals forces, CNHs form spherical assemblies with an overall diameter of 50-100 nm (average: 80 nm) [100, 102]. Based on their morphology, these CNH agglomerates are classified into dahlia, bud, and seed types [103]. In the dahlia-like aggregates, CNHs protrude from the surface of the aggregate like the petals of a dahlia flower. For "bud-like" aggregates, CNHs do not protrude from the surface of the aggregate.

CO_2 laser vaporization of pure graphite at room temperature is one method to produce carbon nanohorn (CNH) aggregates. Kasuya et al. found that a large mass of ambient gas at high pressure was required for the formation of the "dahlia-like" aggregates. They also discovered that as the gas mass and pressure decreased, the "bud-like" CNH aggregates were formed. In other words, using different buffer gases at 760 Torr affected the morphology of CNHs, creating "dahlia-like" CNH aggregates (yield of 95%) with Ar gas and "bud-like" aggregates (yield of 70 or 80%) with either N_2 or He gas [103]. CNHs are produced without the use of any metal catalysts and are entirely metal-free [100, 104]. This fact enabled researchers to investigate the pure toxicological effects of CNHs without the complication of metal inclusion [104]. CNHs have been shown by *in vitro* and *in vivo* testing to be nontoxic in the short term, thus making them a promising, more biocompatible nanomaterial [99, 104, 105].

Because of a rough external surface and large pore volume, investigators are already using CNHs as catalyst supports [106, 107], hydrogen and methane storage media [108-111], and super-capacitor electrodes [112]. These surface/volume properties are useful features within the

biomedical field to enable absorption and containment of therapeutic drugs, genes, proteins, or imaging contrast agents [100, 105, 113-117]. Researchers have already successfully incorporated drugs such as cisplatin and dexamethasone into CNHs for controlled releases [115, 116]. This distinctive spherical structure and size may give CNHs potential advantages over conventional nanoparticles, such as nanorods and nanotubes, for intracellular delivery. Spherical nanoparticles of moderate size have shown improved cellular uptake efficiency over rod-shaped nanoparticles [118]. Researchers have also shown the ability of CNHs to couple with NIR light to generate heat and destroy microbes and viruses [48, 49].

Objective to research

The goal of this research was to characterize the heat delivery and cellular response to the inclusion of CNTs and CNHs in laser therapy. There is limited information on how inclusion of nanoparticles within tissues will affect their optical and thermal properties. Characterizing the thermal and optical properties associated with inclusion of CNTs or CNHs in tissue is crucial to predicting the tissue response to nanoparticle-mediated laser therapies. An understanding of all of these aspects of the interaction of CNTs or CNHs with cells and tissues is essential to developing cancer therapies utilizing both nanoparticles and laser therapy. Specifically, thermal effects of CNTs and CNHs were assessed based on temperature elevations and optical properties were acquired based on absorption within the NIR region. Cellular response was evaluated based on cell viability and HSP expression. These experimental results will help improve and validate a laser therapy model, which can offer insight into hyperthermia therapy design for cancer patients, fine-tuning treatments to each patient. Optimized therapy would more effectively eradicate cancer tissue and reduce the risk of tumor recurrence.

Chapter 2: Hyperthermia treatment of PC3 and RENCA cells using MWNTs

The effect of laser heating in combination with MWNTs was investigated with *in vitro* cell studies. This initial study will provide insight into the relationship between laser parameters (power, heating duration) and MWNT properties (length, concentration) to temperature elevation and cellular response (HSP expression and cellular damage/lethality). Also, understanding if and where the MWNTs are located within the cells themselves will determine future uses of these particles as carriers of imaging agents or therapeutically active molecules to provide multi-modal therapy options for the treatment of cancer. All of this information will help guide future *in vivo* studies. Because of their role in apoptosis inhibition, HSP27, 70, and 90 expression are included with cell viability as measures of effectiveness of a thermal cancer therapy.

Three levels of laser heating were investigated: (1) no heat (control), (2) "sub-lethal" heating, and (3) "lethal" heating. Exclusion or inclusion of MWNTs (0.1 mg/ml) in each of these heating groups shows their effects with NIR irradiation. The main difference between the two heating regimes was heating time (laser power is kept constant). Preliminary data is reported in previously published work [119]. Use of two cancer cell lines showed that the proposed combined therapy with MWNT inclusion was broad enough to be effective for more than one type of cancer. Temperature, cell viability, and HSP expression serve as points of comparison between MWNT-coupled samples (i.e. tumor cells) and unheated samples.

The purpose of this chapter is to measure the effects of MWNT inclusion on optical absorbance, heat generation, cell viability, and HSP expression on NIR laser irradiated monolayer cell cultures. Initial investigation of MWNT internalization is also presented. Spectrophotometric measurements confirmed the preferential absorption of MWNTs to ~1064 nm light by the presence of an absorption peak. Temperature tests confirmed this result, comparing MWNTs to other nanoparticles which lacked this absorption peak. Longer heating time resulted in a higher maximum temperature and larger temperature elevation for all samples. MWNT samples showed higher maximum temperatures and larger temperature elevations compared to their non-NT counterparts, which displayed the ability of MWNTs to couple to NIR light to generate heat. Similar cell viability and HSP expression was seen in all control samples, showing MWNTs to be nontoxic. Comparable viability between control and sub-lethal groups showed that MWNT laser therapy needed to be tuned. Elevated HSP expression was seen in

sub-lethal MWNT and lethal non-NT samples where cells received a sub-lethal thermal dose that would not kill and eliminate HSP induction. There was 100% lethality for lethally heated MWNT samples where temperatures rose above 60°C. HSP27 and 70 expression levels were similar to basal levels for lethally heated MWNT samples. However, HSP90 expression was higher in lethal groups compared with basal level. The ability of the MWNT to cross the cell membrane was witnessed within the RENCA cell control groups. Incubation of 24 hr caused at least 40% of cells to appear to have internalized MWNTs. This phenomenon was not perceivable in heated groups, where incubation time was less than 20 minutes. This phenomenon requires further research since this action would provide additional advantages to MWNT use in cancer therapy by supplying other modes of therapy (i.e. reactive oxygen species generation, chemo-drug delivery) and imaging options for diagnosing and monitoring target tissue.

This research shows the ability of MWNTs to increase local temperature while using a wavelength of light known to be transparent to tissue. Their inclusion would minimize healthy tissue damage by lowering the necessary power or heating time to eradicate cancer cells and eliminate HSP induction and tumor cell protection.

2.1. Experimental materials and methods

2.1.1. Cell culture

A human androgen-independent prostate cancer cell line, PC3, was purchased from American Type Culture Collection (Manassas, VA) and used in these cell experiments. RPMI 1640 media with L-glutamine (Mediatech, Manassas, VA) was supplemented with 10% FBS and 1% Pen-Strep (Sigma-Aldrich). A murine renal cancer cell line, RENCA, was provided by Dr. Heather Hatcher (Wake Forest University Baptist Medical Center) and was used in RENCA cell culture experiments. RENCA media was the same formulation as PC3 media with an addition of 1% sodium pyruvate (Mediatech, Manassas, VA). Cell cultures were kept in a 5% CO_2 incubator at 37°C in T25 (25 cm^2 area) membrane cap flasks. For cell experiments, cell monolayer cultures were grown on coated 2-chamber glass slides (Fisher Scientific) in a density of 100,000 cells/chamber (1-2 ml volume) and left to seed for 24 hr before experimentation. During MWNT heating, culture media was removed and sterile-filtered eagle minimum essential medium (Sigma-Aldrich) was mixed with 0.1 mg/ml MWNTs and used during heating. Using this media prevented media protein coagulation, which is toxic to cells.

2.1.2. Multi-walled nanotubes

Multi-walled carbon nanotubes (MWNTs) were fabricated by chemical vapor deposition (CVD) at Wake Forest University using an iron catalyst amount of 600 mg Fe, as described previously [55, 120]. Briefly, ferrocene was dissolved in pyridine and was fed into the preheater (200°C). The volatilized reaction gas was swept into the reactor by hydrogen carrier gas. To cut the nanotubes to an appropriate length, NTs were sonicated for 20 hr in a 3:1 sulfuric-nitric acid solution. This process yielded NTs with an average length of 900 nm, verified by TEM. This length was used because of its ability to couple to NIR light, described by antennae theory and shown in previous work. In short, a nanotube length of at least half the laser light wavelength is needed to properly transform the light into heat [55, 67, 68]. After sonication, nanotubes were later filtered and dried. Then, the nanotubes were placed in deionized water in a stock concentration of 2 mg/ml with 1% w/v Pluronic F-127 (PL-127) and sonicated for 20 min to uniformly disperse the NTs within solution. PL-127 at a 1% concentration was chosen based on its biocompatibility and proven dispersion abilities of NTs [121-123]. The resulting stock solution was steam autoclaved for 20 min to sterilize. A final solution concentration of 0.1 mg/ml MWNT was used in all experiments.

2.1.3. Laser-thermocouple system setup

A continuous wave (CW) laser with a beam diameter of 5 mm (YLR-10-1064-LP, IPG Photonics) was used to heat all test groups. Laser irradiance of 15.3 W/cm^2 (3W, 5 mm beam diameter) and a heating time of 1.5 or 5 min were used for sub-lethal and lethal monolayer cell culture experiments, respectively. The laser light was coupled to a fiber optic probe that allowed incident light on the center of the culture slide. Two hypodermic thermocouples were placed in the media of the culture chamber at known distances (4 mm and 7 mm from laser center) to measure real-time temperature elevations. A National Instruments thermocouple reader (USB-9211) and VI Logger Lite software were used to record temperature data during the experiments. Figure 2.1 shows a picture of this laser setup.

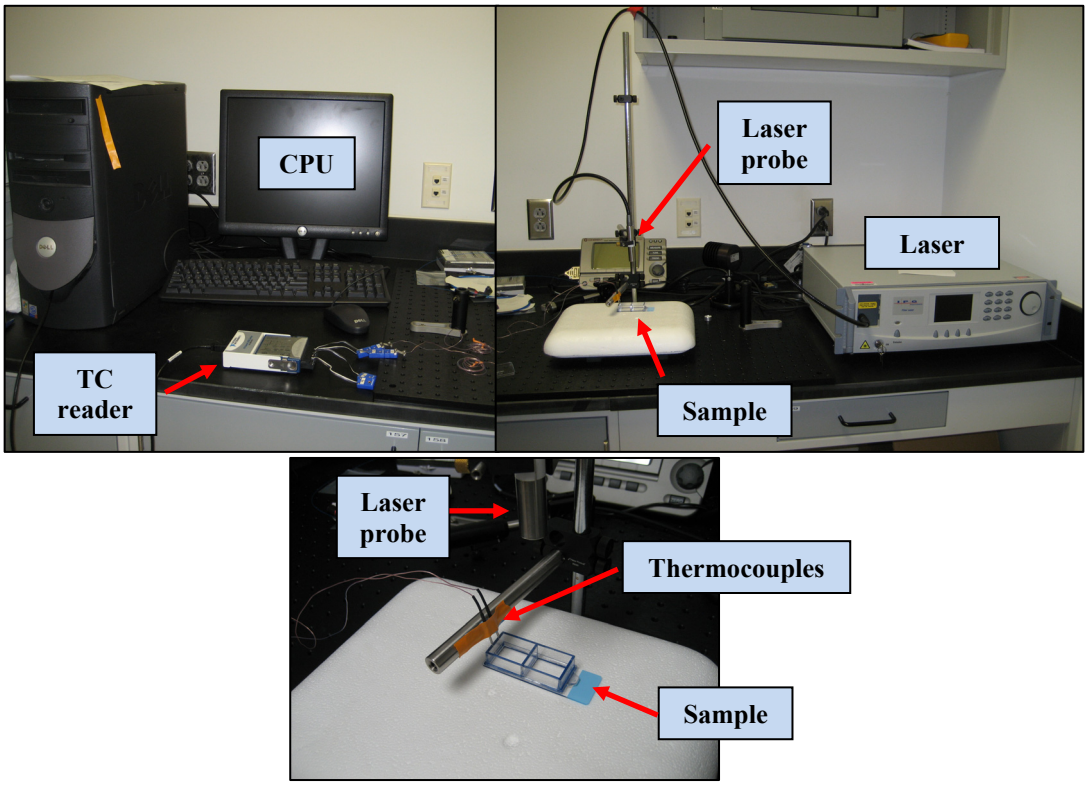

Figure 2.1. External beam laser setup for cell heating.

2.1.4. Spectrophotometer and optical setup

A double-beam Cary 5000 spectrophotometer (Varian, Inc.) was used to assess optical properties of all liquid samples. Particles were made water-soluble and dissolved in phosphate buffered saline (PBS) or deionized water (ddH_2O) for optical assessment. Liquid samples were placed in fluorometer or self-masked cuvettes (Starna Cells) and held in the internal DRA integrating sphere cuvette holder. This setup would account for scattering effects of the samples.

2.1.5. Cell viability

Trypan blue cell viability studies for unheated MWNT controls were carried out at 16, 24, and 48 hr post-seeding. Cell viability of lased samples was assessed at 16 hr post-heating using sterile-filtered 0.4% trypan blue solution (Sigma-Aldrich). For monolayer cell experiments, 0.4% trypan blue solution was diluted in warmed PBS at a ratio of 1:1. Briefly, culture media was removed and samples were rinsed with warmed PBS twice. Diluted trypan blue solution was placed on samples for 5 min at room temperature. Trypan blue was removed

and the samples were rinsed with PBS twice. PBS was placed on samples during imaging. A Leica DM IL or Leica DMI6000B microscope was used to capture cell viability pictures.

2.1.6. HSP immunostaining

Fluorescent immunostaining was used to visualize HSP27, 70, and 90 expression in control and heated cell samples with and without MWNTs. HSP expression was measured at 16 hr post-heating which has been shown as the time of peak HSP expression [124]. All incubation steps were carried out in the 37°C incubator (5% CO_2). Briefly, cells were rinsed with warmed PBS, fixed with Histochoice fixative MB (Electron Microscopy Sciences, Hatfield, PA) for 20 minutes, rinsed with PBS, and permeabilized by 0.5% Triton X-100 (diluted in deionized water) to allow antibody staining. After cell cultures were rinsed with PBS, a blocking buffer of 5% normal goat sera (Santa Cruz Biotechnology, Inc.) diluted in PBS was incubated with cell culture for 1 hr. Next, a primary antibody for HSP27 (dilution: 1:100), HSP70 (dilution: 1:500), or HSP90 (dilution: 1:100) from Assay Designs was diluted in 1.5% normal goat sera and incubated with its corresponding cell culture for 1 hr. The fluorescent secondary antibodies Cyanine2 (Cy2, for HSP27, dilution: 1:300), AMCA (for HSP70, dilution: 1:50), or Rhodamine Red-X (RRX, for HSP90, dilution: 1:50) from Jackson Immunoresearch, was first diluted in deionized water and further diluted in PBS. After slides were rinsed with PBS to remove residual unbound primary antibodies, each secondary antibody was incubated with its corresponding sample for 1 hr. Slides were rinsed, mounting media applied, and cover slips sealed before imaging. The slides were imaged on a Leica DMI6000B microscope. Photoshop Elements 6.0 was used to assess average intensity measurements of sample cells. Table 2.1 gives the antibody pairings and dilutions.

Table 2.1. Antibodies used for HSP27, 70, and 90 immunostaining.

Protein	Primary Antibody	Primary Dilution	Secondary antibody	Secondary dilution
HSP27	Mouse Anti-HSP27, biotin-conjugated monoclonal	1:100	Goat Cy2-streptavidin	1:300
HSP70	Rabbit Anti-HSP70 polyclonal	1:500	Goat Anti-rabbit AMCA	1:50
HSP90	Rat Anti-HSP90 monoclonal	1:100	Goat Anti-rat RRX	1:50

2.1.7. MWNT internalization

RENCA cells were seeded for 24 hr and then incubated with 0.1 mg/ml MWNTs for 24 hr. Cells were washed with warmed PBS, fixed with Histochoice MB fixative (Electron Microscopy Sciences, Hatfield, PA) for 20 min, washed with PBS 3 times, permeabilized with 0.5% Triton X-100, and washed with PBS 3 additional times. Mounting media with DAPI (Vector Labs, Inc.) was placed on samples and coverslips were sealed on the slides. A Leica DMI6000 microscope was used to take brightfield and DAPI fluorescent images. The Leica Application Software Advanced Fluorescence program was used to overlay images to locate nuclei and NTs.

2.2. Experimental results

2.2.1. Optical properties

A spectrophotometer scan was taken of the UV-Vis-NIR range from 200-1200 nm. A grating change occurred at 850 nm. Deionized water (ddH_2O) in a fluorometer was taken as a baseline. A scan of 0.1 mg/ml MWNTs in ddH_2O was taken and baseline-corrected to account for the effects of cuvette and water absorption in order to isolate the optical properties of the MWNTs themselves. Figure 2.2 shows the absorbance curve of ddH_2O and MWNTs (baseline-corrected).

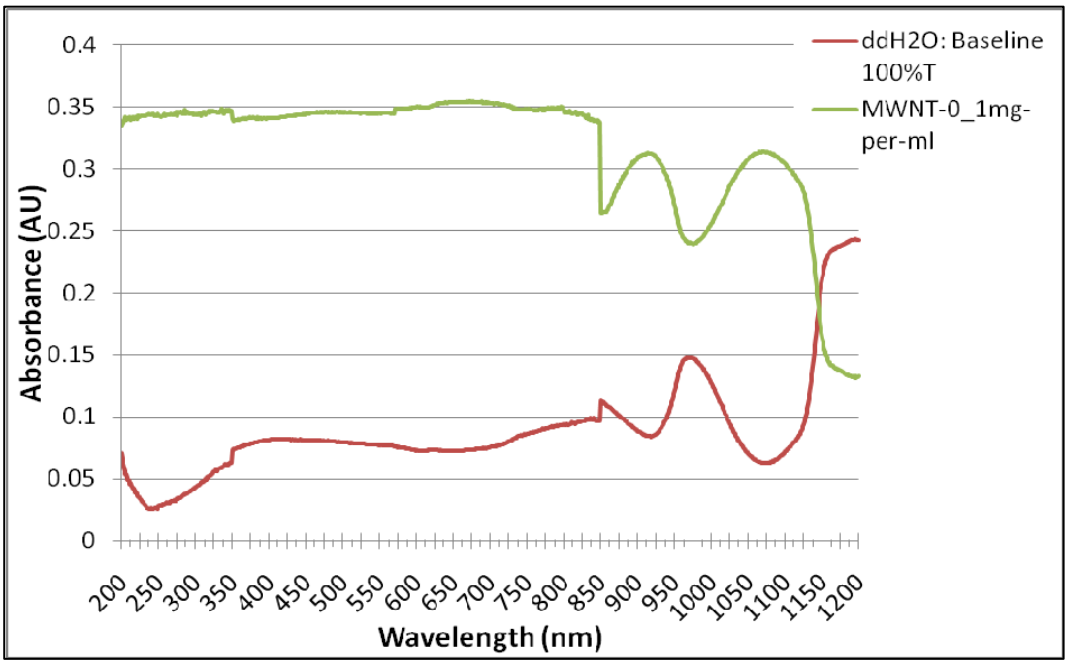

Figure 2.2. Absorbance curve for 0.1 mg/ml MWNT in ddH_2O (baseline corrected). Deionized water (ddH_2O) in a fluorometer was used as the baseline curve. Scan rate 600nm/min.

In order to compare the absorption of MWNTs with other fullerenes, another scan was taken of other particles alone or within C_{60} and C_{80} fullerenes to assess their absorption within the NIR region. Figure 2.3 shows the lack of NIR absorption (near that of water) but a high absorbance in the UV range, which has been shown by other researchers [125].

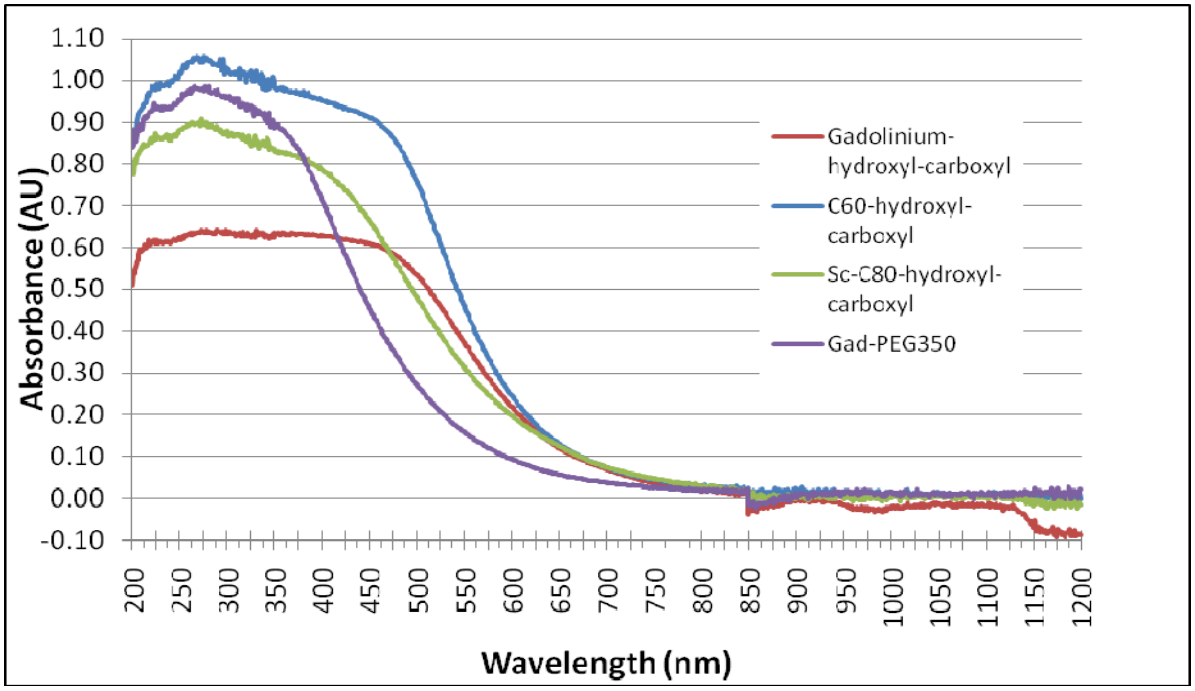

Figure 2.3. Spectral data of various fullerenes and imaging particles dispersed in PBS with 1% Pluronic F-127. Note the preferential absorption peak of fullerenes in the UV-Vis range but the absence of NIR absorption.

2.2.2. Temperature and heat generation

An absorption peak is indicative of preferential absorption of that range of wavelengths. In the case of MWNTs, absorption of those preferred wavelengths translates to increased heat generation. To test this theory, a 96-well cell plate was used to assess the temperature of various nanoparticle samples during laser irradiation. One thermocouple was placed just outside of the laser beam profile. 100 µL of solution of each particle was heated with a 1064 nm (NIR) CW laser for 30 sec at 3W power. Figure 2.4 shows that MWNT solution heated significantly. A close-up view of the other particles shows little difference between water and particle (Figure 2.5).

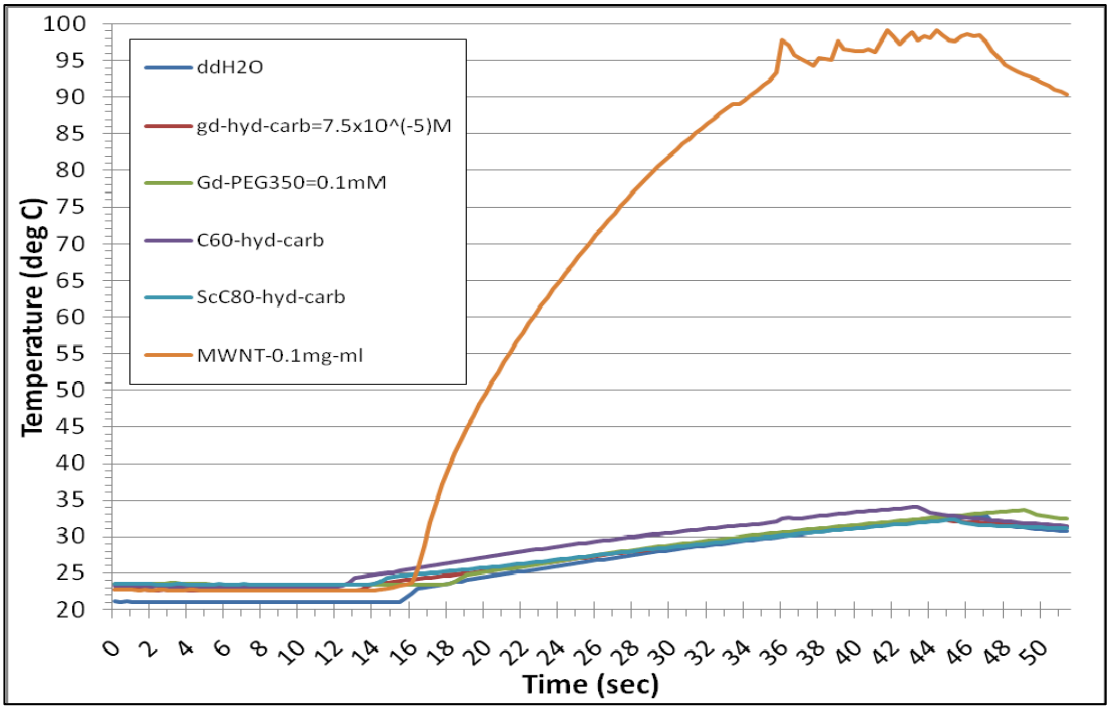

Figure 2.4. Temperature plot for various nanoparticles or material heated with a 1064 nm laser at 3W for 30 sec.

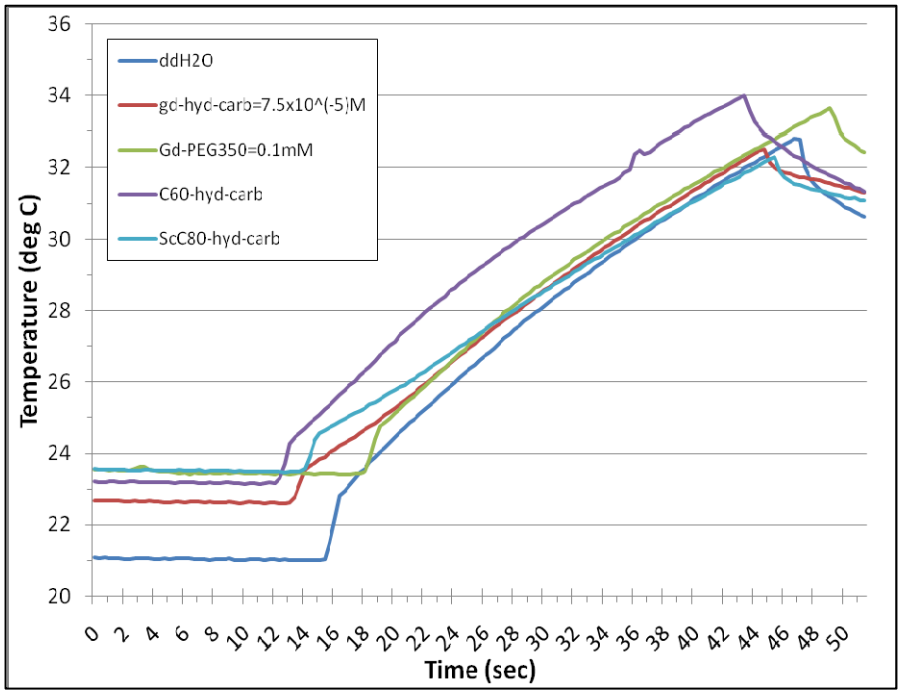

Figure 2.5. Close-up view of temperature increase of non-NIR-specific particles and water heated with a 1064 nm laser at 3W for 30 sec.

The next step was temperature measurements as PC3 cells underwent laser irradiation with and without MWNT inclusion. The subsequent HSP expression and cell viability would be measured for these same samples and correlated with this temperature. Temperature measurements were obtained from thermocouples placed at known radial positions from the laser center (TC0 and TC1 located 4 mm and 7 mm from laser center, respectively). During sub-lethal heating (3W, 90 sec), higher temperature elevations were observed in cell cultures with MWNT inclusion compared to non-NT cultures. Maximum temperatures in these non-NT and MWNT cultures were near 28.73°C and 53.31°C, respectively, with a standard deviation (σ) of 1.79 and 3.88°C respectively. Figure 2.6 is an example of temperature curves acquired real-time during sub-lethal heating. Mean temperature elevation was 5°C and 30°C for non-NT and MWNT samples, respectively. Temperature elevations for non-NT and NT samples had standard deviations of 2.10 and 3.41°C, respectively. Figure 2.7 shows the marked difference the inclusion of MWNTs made with respect to temperature rise in 90 sec of irradiation during sub-lethal laser heating.

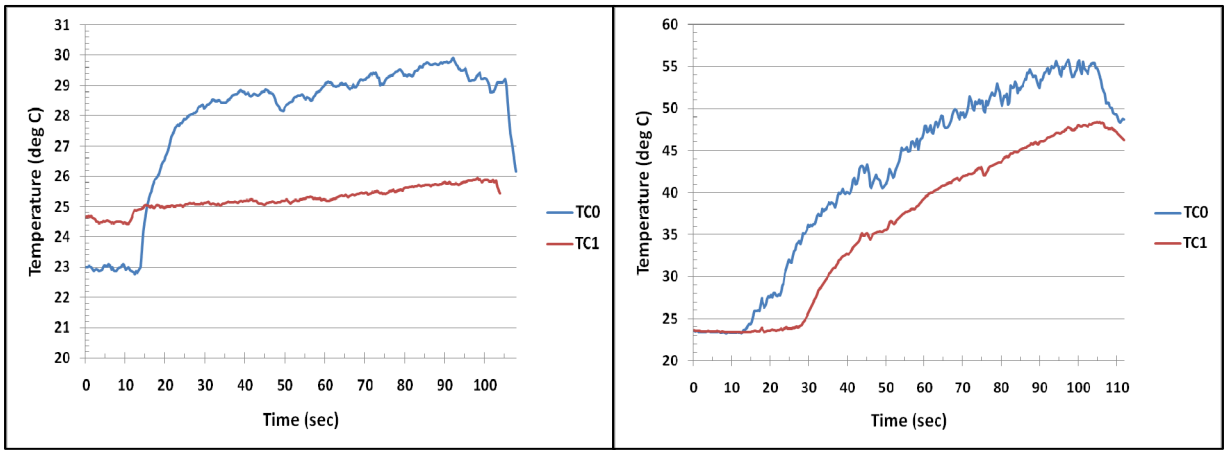

Figure 2.6. Temperature profile during sub-lethal laser heating of 3W for 90 sec of (A) PC3 cells without NTs and (B) PC3 cells with MWNT. TC0 is located 4 mm from laser center, TC1 is located 7 mm from laser center.

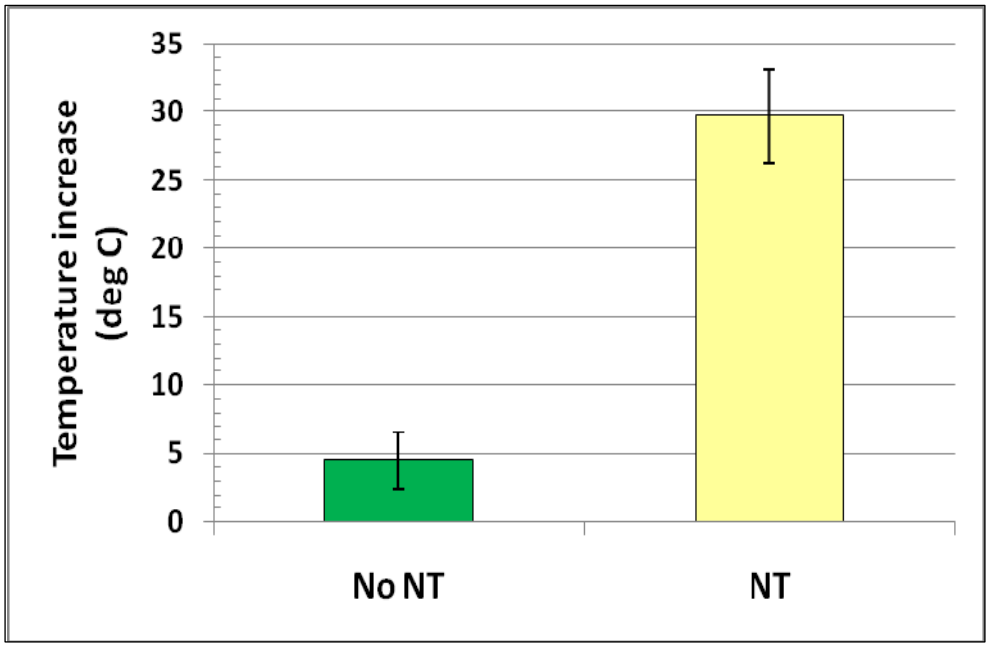

Figure 2.7. Temperature increase of sub-lethal heating (3W, 90 sec) of media in the absence and presence of 0.1 mg/ml MWNTs. n=6, σ range: 2.10 and 3.41°C.

Laser heating at the lethal level (3W, 5 min) revealed higher maximum temperatures and larger temperature increases for both non-NT and MWNT samples compared to their respective sub-lethal groups. Mean maximum temperatures for non-NT and MWNT samples were 33.55°C and 67.43°C, respectively, with standard deviations ranging from 4.41-6.74°C. Temperature elevations for non-NT and MWNT samples were 7.12°C and 42.87°C, respectively. Temperature elevation for these samples had standard deviations ranging from 2.25-6.52°C. Figure 2.8 shows a typical temperature plot of non-NT and MWNT samples. Similar to sub-lethal heating, MWNT samples displayed larger temperature elevations compared to non-NT samples, as seen in Figure 2.9.

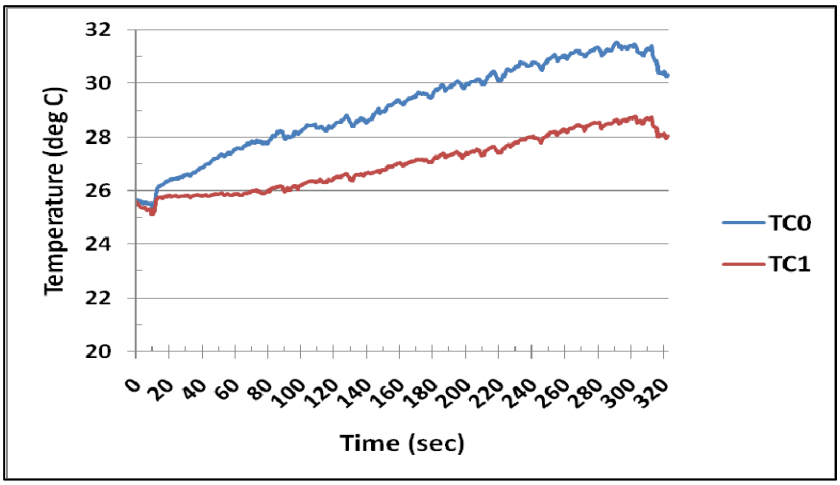

(A)

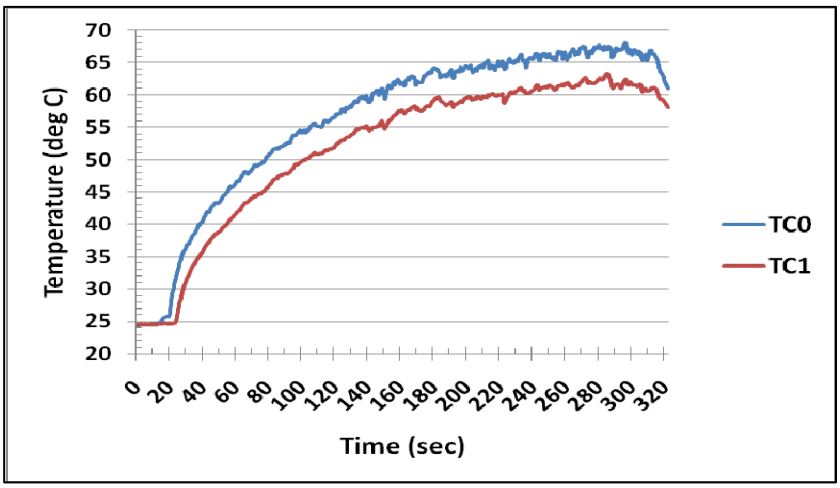

(B)

Figure 2.8. Temperature plot of lethal heating of media (A) without and (B) with 0.1 mg/ml MWNTs. TC0 is located 4 mm from laser center and TC1 is located 7 mm from laser center.

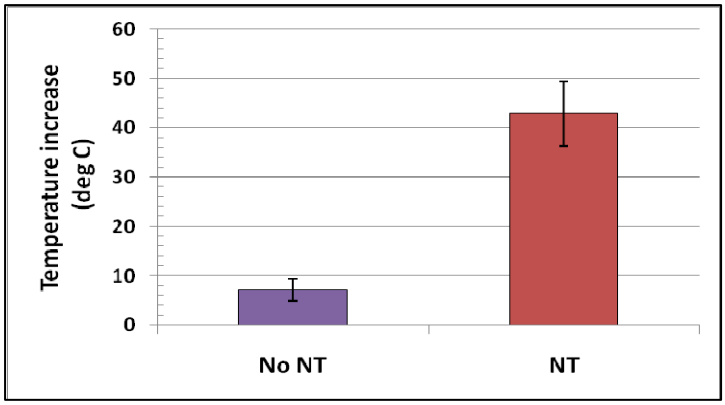

Figure 2.9. Temperature increase of lethal heating (3W, 5 min) of media in the absence and presence of MWNTs. N=6, σ range: 2.25-6.52°C.

2.2.3. Cell viability

Staining with trypan blue allows visualization of the amount of dead cells within a cell population. The relatively large size of trypan blue dye and the selective transport mechanisms of a cell membrane mean that trypan blue can only enter dead or dying cells whose membranes have become permeable enough while viable cells with intact membranes exclude the dye. With this technique, we were able to compare cell viability between the various cell cultures. Several pictures were taken of each cell population with viable and dead cells counted and averaged for a particular sample. Unheated PC3 cell cultures with and without MWNTs showed high cell viability. Sub-lethal heating of cell cultures without MWNTs maintained high cell viability, similar to control (unheated) samples. Although significant temperature elevations were observed in the sub-lethally heated MWNT samples, these elevations were below the threshold necessary for irreversible thermal injury and cell death. Therefore, cell viability remained high. Increasing heating time allowed MWNTs to effectively enhance thermal deposition and increase temperatures to lethal limits that resulted in 0% viable cells. For non-NT cell cultures, lethal heating did not affect cell viability as it remained similar to cell viability of controls. Figure 2.10 shows representative images of cell viability attained from trypan blue staining of PC3 cell culture groups near laser center. Black dots are clusters of nanotubes which are indicated with arrows.

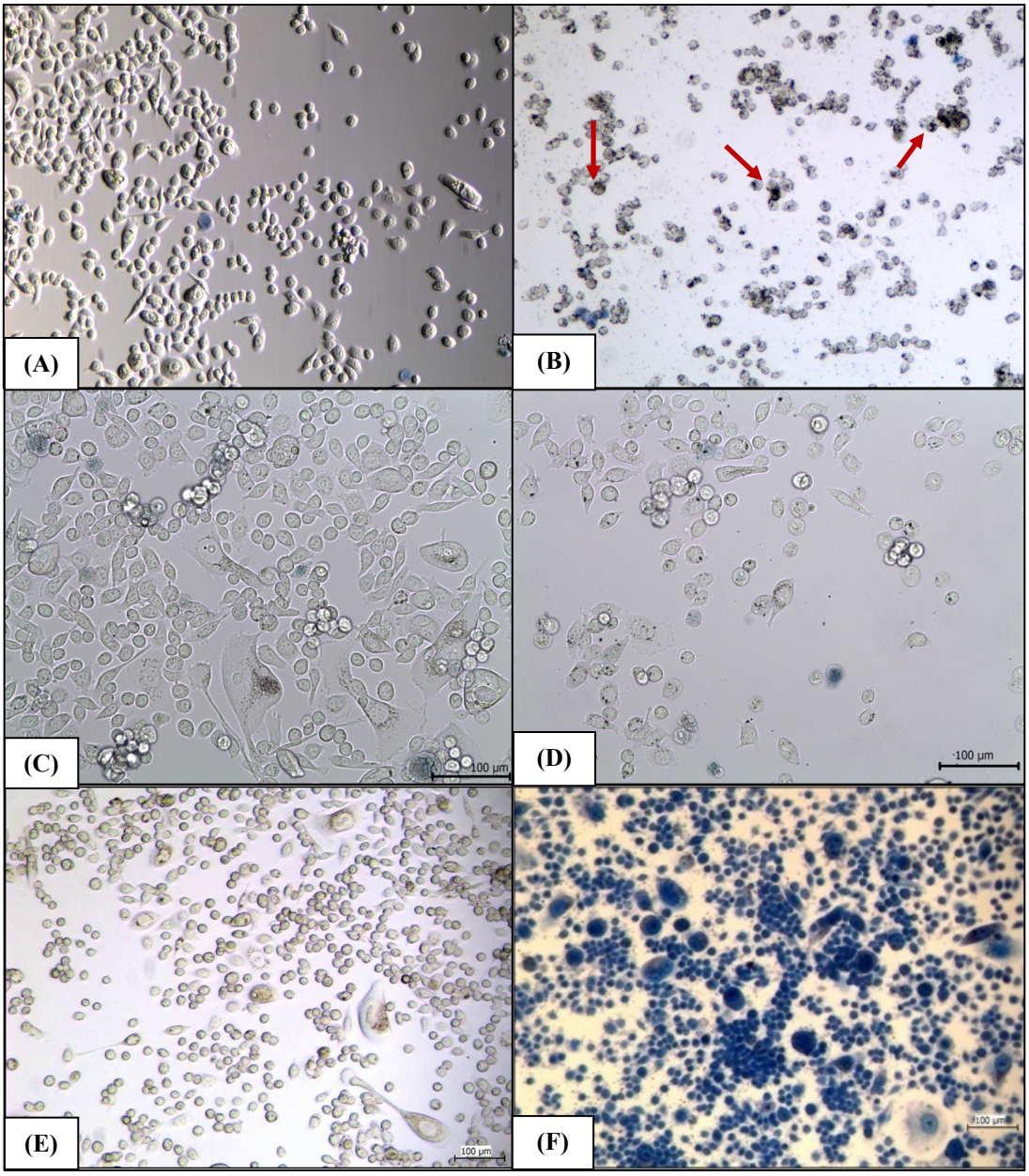

Figure 2.10. Cell viability staining with trypan blue of PC3 cells near laser center. (A) Unheated cells without NTs, (B), Unheated cells with MWNTs, (C) Sub-lethal heated cells without NTs, (D) Sub-lethal heated cells with MWNT, (E) Lethal heated cells without NTs, and (F) Lethal heated cells with MWNT. Red arrows indicate MWNT clusters. Scale bars are 100 µm.

RENCA cells showed similar cell viability at the different heating levels compared to the PC3 cells samples. Figure 2.11 shows RENCA cells stained with trypan blue.

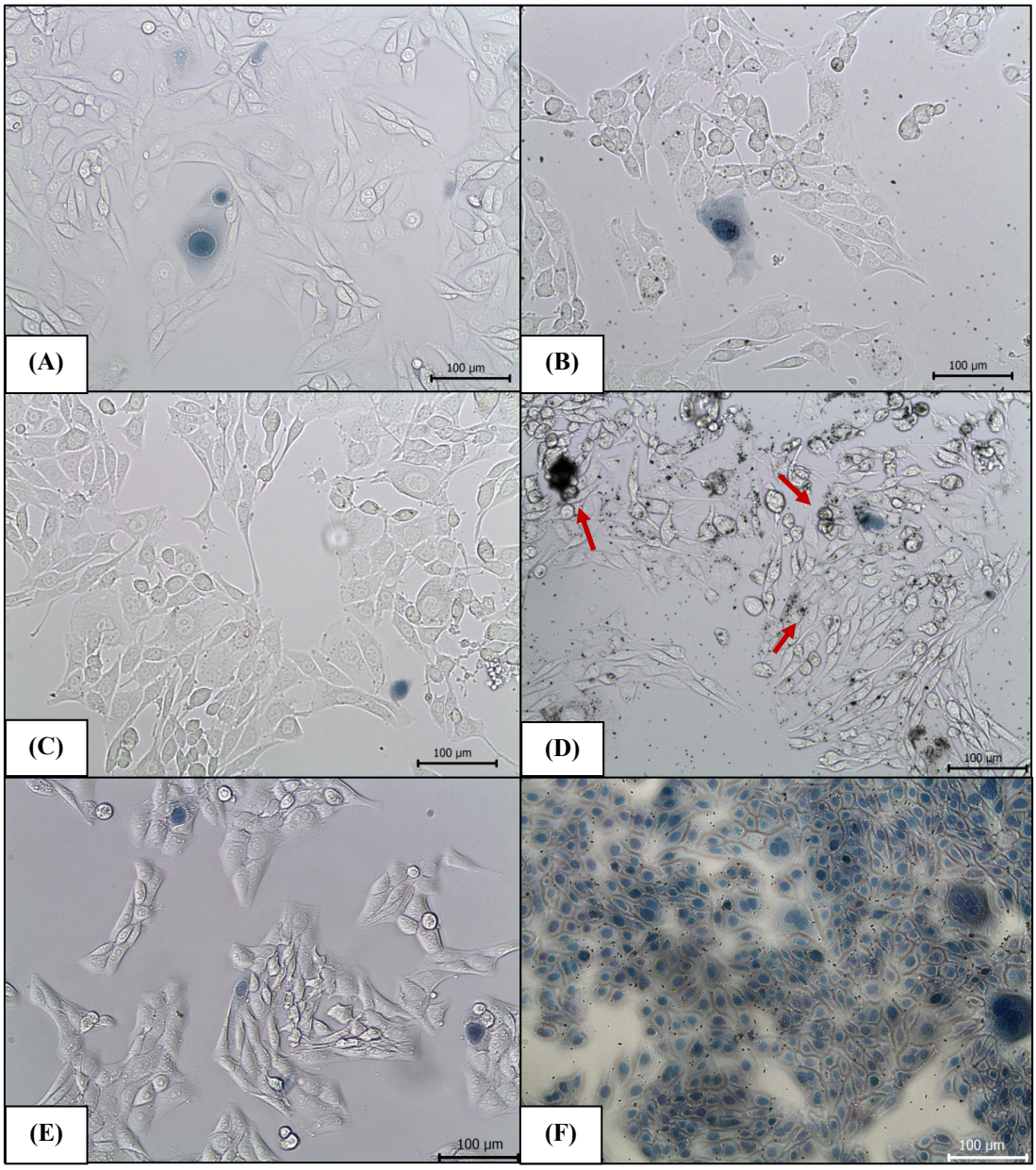

Figure 2.11. Cell viability staining with trypan blue of RENCA cells near laser center. (A) Unheated cells without NTs, (B) Unheated cells with MWNTs, (C) Sub-lethal heated cells without NTs, (D) Sub-lethal heated cells with MWNT, (E) Lethal heated cells without NTs, and (F) Lethal heated cells with MWNT. Red arrows indicate MWNT clusters. Scale bars are 100 µm.

The cell viability is shown graphically for PC3 and RENCA cells at the various heating conditions in Figure 2.12A and 2.12B, respectively. The only significant difference in cell viability was seen in the lethal-laser heated MWNT group, where cell death is 100%. Cell viability for PC3 and RENCA cells had standard deviations ranging from 0.27-2.45% and 0.27-0.89%, respectively.

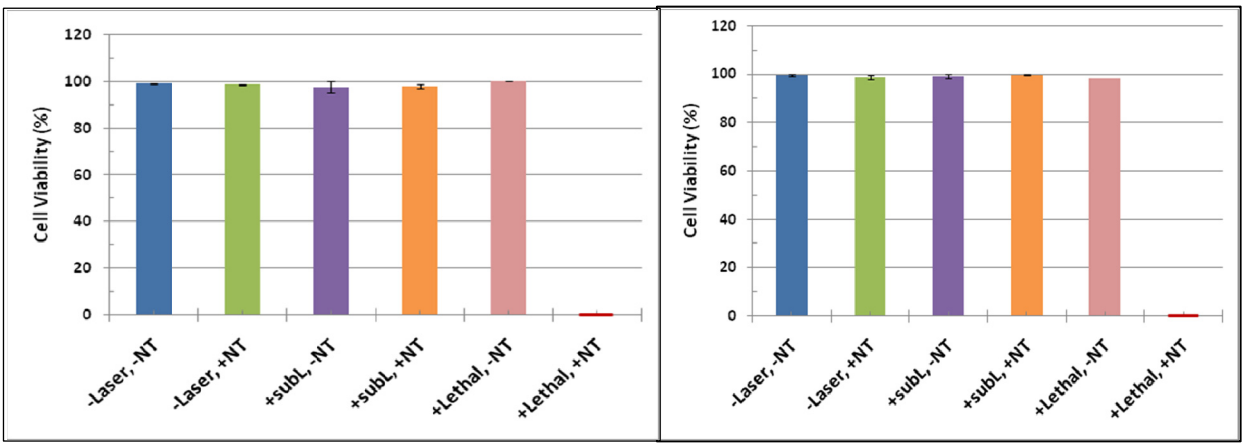

Figure 2.12. Cell viability of (A) PC3 and (B) RENCA for various heating levels. –NT: no MWNT, +NT: 0.1 mg/ml MWNT; –Laser: unheated, subL: 3W for 90 sec, Lethal: 3W for 5 min. n=3 except in lethal cases; σ_{PC3} range: 0.27-2.45%, σ_{RENCA} range: 0.27-0.89%.

2.2.4. HSP expression

Since new and multi-species primary and secondary antibodies were being used, these antibodies were first tested for feasibility on monolayer cell culture with and without constant temperature water bath heating. These tests showed these dyes can be used to image HSP27, 70, and 90. The up-regulation of HSP in the water bath heated samples indicated the feasibility of these primary and secondary antibodies for future HSP staining.

At 16 hr post-laser heating, laser irradiated and unheated samples were stained for HSP27, 70 and 90. There was little difference between the control (unheated) and sub-lethal non-NT groups. In lethal MWNT samples, HSP27 and 70 expression was near basal levels while HSP90 was above its basal level. Up-regulated expression of HSP27, 70, and 90 was seen in sub-lethal heated MWNT and lethal heated non-NT samples. Figure 2.13 shows the HSP expression intensity of these PC3 groups. Graphically, these fluorescent intensities of PC3 cells are shown in Figure 2.14. Note the higher intensity of sub-lethal with MWNT and lethal without MWNTs groups. Intensity measurements for PC3 groups for HSP27, 70, and 90 had standard deviations ranging from 2.23-11.77AU, 0.35-6.74AU, and 1.04-6.49AU, respectively. Table 2.2 summarized the mean intensities of each PC3 group with its associated standard deviation.

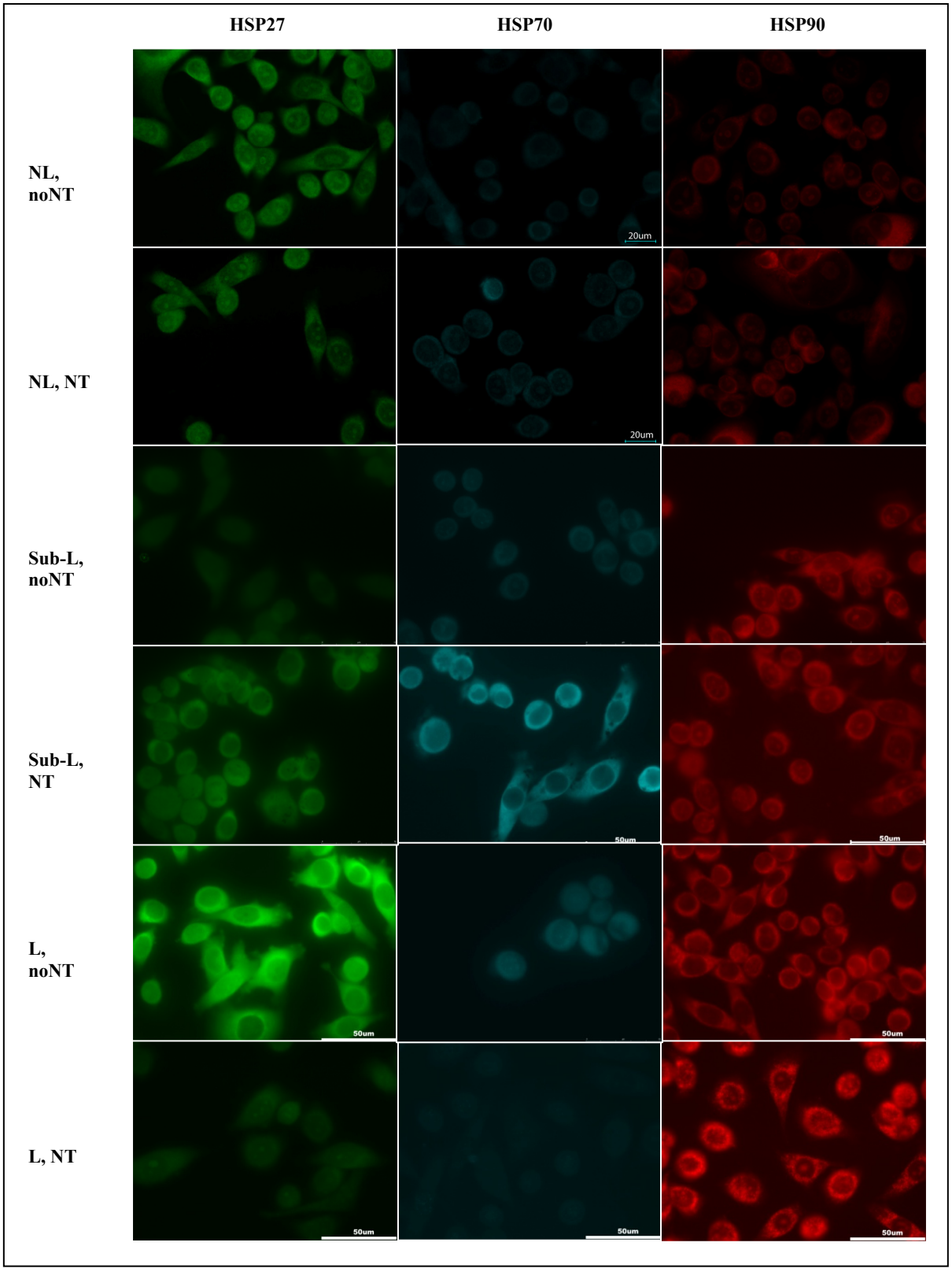

Figure 2.13. HSP fluorescent microscope images of unheated and laser heated PC3 cells with and without MWNTs. These cells have been stained separately for HSP27, 70, and 90. NL: no laser; Sub-L: sub-lethal laser; L: lethal laser; noNT: no MWNTs; NT: MWNTs. Scale bars are 50 μm.

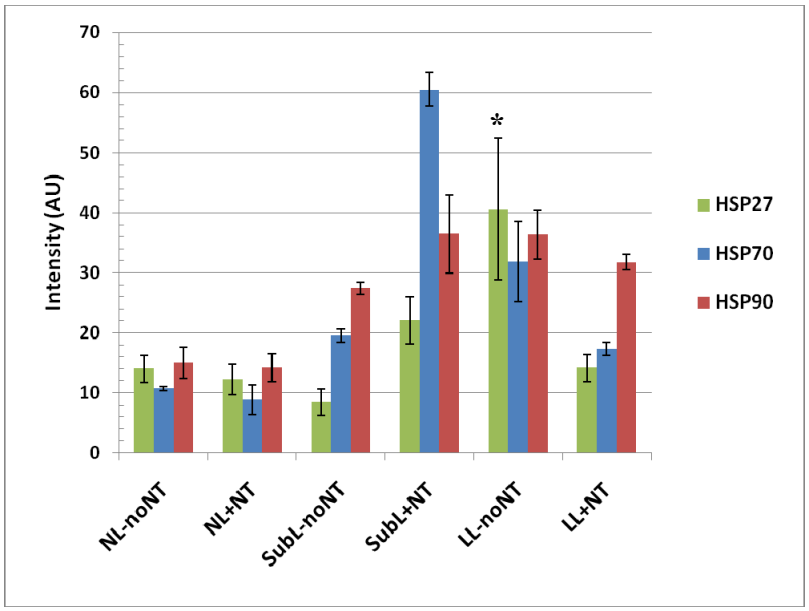

Figure 2.14. HSP fluorescent intensities of unheated and laser heated PC3 cells with and without MWNTs. These cells have been stained separately for HSP27, 70, and 90. NL: no laser; Sub-L: sub-lethal laser; LL: lethal laser; noNT: no MWNTs; NT: MWNTs. N=3 (* group: N=2), σ_{HSP27}=2.23-11.77AU, σ_{HSP70}=0.35-6.74AU, σ_{HSP90}=1.04-6.49AU.

Table 2.2. Summary of mean intensities of each PC3 group with its associated standard deviation. N=3, except *N=2.

	Mean Intensity±SD (AU)		
PC3 Group	**HSP27**	**HSP70**	**HSP90**
NL-noNT	13.93±2.26	10.68±0.35	14.97±2.66
NL+NT	12.17±2.55	8.76±2.45	14.15±2.28
SubL-noNT	8.41±2.23	19.49±1.05	27.39±1.04
SubL+NT	22.08±3.89	60.44±2.81	36.38±6.49
LL-noNT*	40.60±11.77	31.79±6.74	36.33±4.08
LL+NT	14.06±2.23	17.30±1.06	31.71±1.31

Similar HSP studies were carried out with RENCA cells, to see if the proposed therapy would be applicable to more than one type of cancer. Figure 2.15 gives fluorescent images of HSP27, 70, and 90 of RENCA cells under various laser heating conditions and Figure 2.16 shows the resulting fluorescent intensities. Note the higher expression of HSPs in the sub-lethal with NTs and lethal without NTs groups. Also, more HSP90 has translocated into the nucleus for lethal-MWNT samples as seen in Figure 2.15. Intensity measurements for HSP27, 70, and 90 had standard deviations ranging from 0.48-1.87AU, 2.67-4.77AU, and 1.58-8.37AU,

respectively. Table 2.3 gives a summary of mean intensities of each group with its associated standard deviation.

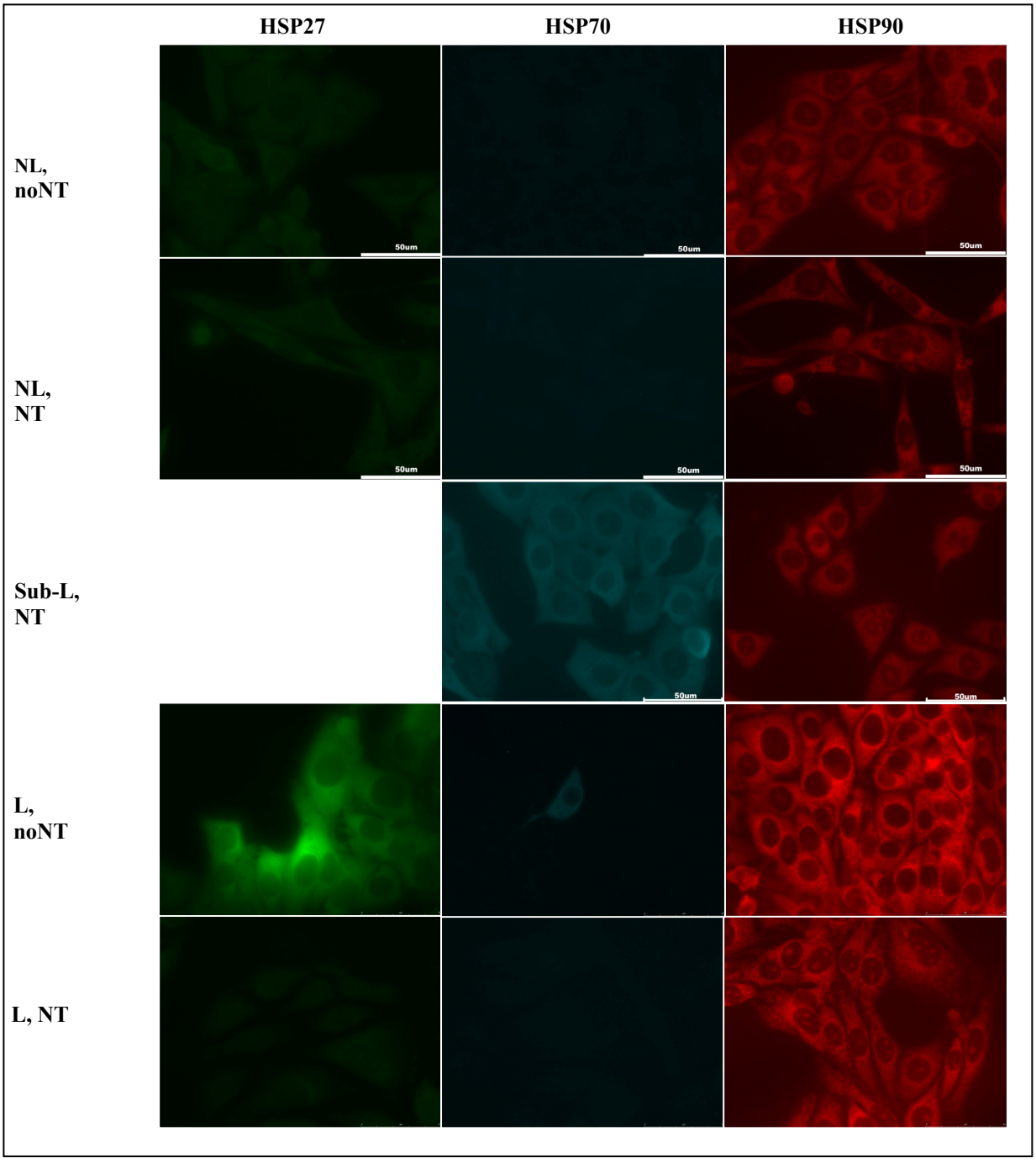

Figure 2.15. HSP fluorescent microscope images of unheated and laser heated RENCA cells with and without MWNTs. These cells have been stained separately for HSP27, 70, and 90. NL: no laser; Sub-L: sub-lethal laser; L: lethal laser; noNT: no MWNTs; NT: MWNTs. Scale bars are 50 μm.

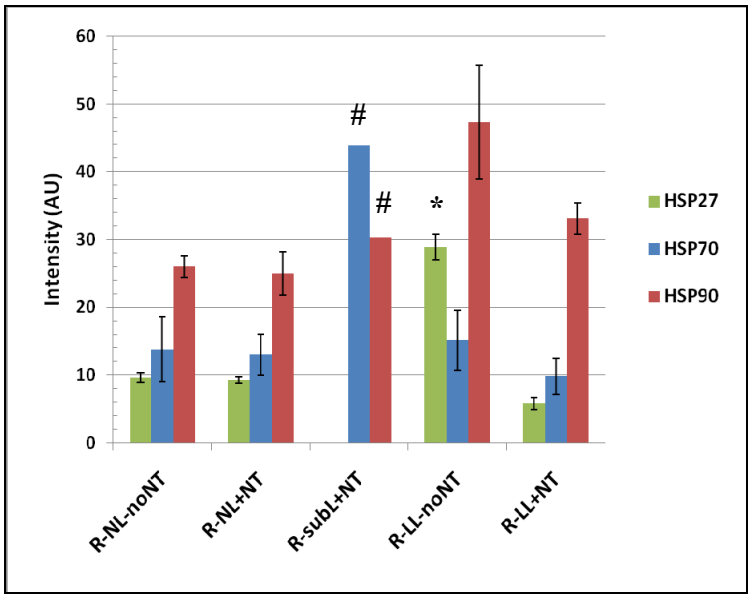

Figure 2.16. HSP fluorescent intensities of unheated and laser heated RENCA (R) cells with and without MWNTs. These cells have been stained separately for HSP27, 70, and 90. NL: no laser; Sub-L: sub-lethal laser; LL: lethal laser; noNT: no MWNTs; NT: MWNTs. N=3 (* group: N=2; # group: N=1), σ_{HSP27}=0.48-1.87AU, σ_{HSP70}=2.67-4.77AU, σ_{HSP90}=1.58-8.37AU.

Table 2.3. Summary of mean intensities of each RENCA group with its associated standard deviation. N=3, except *N=2.

	Mean Intensity±SD (AU)		
RENCA Group	**HSP27**	**HSP70**	**HSP90**
NL-noNT	9.63±0.67	13.78±4.77	26.01±1.58
NL+NT	9.22±0.48	12.98±3.03	24.99±3.15
LL-noNT*	28.88±1.87	15.09±4.43	47.33±8.37
LL+NT	5.76±0.88	9.80±2.67	33.09±2.31

Comparing the two cell lines, similar trends are seen. Higher levels of HSP27 and 90 are seen in the sub-lethal with MWNTs and lethal without MWNTs groups. HSP70 is up-regulated in the sub-lethal with MWNTs groups. Figure 2.17 shows the HSP fluorescent intensity for all samples.

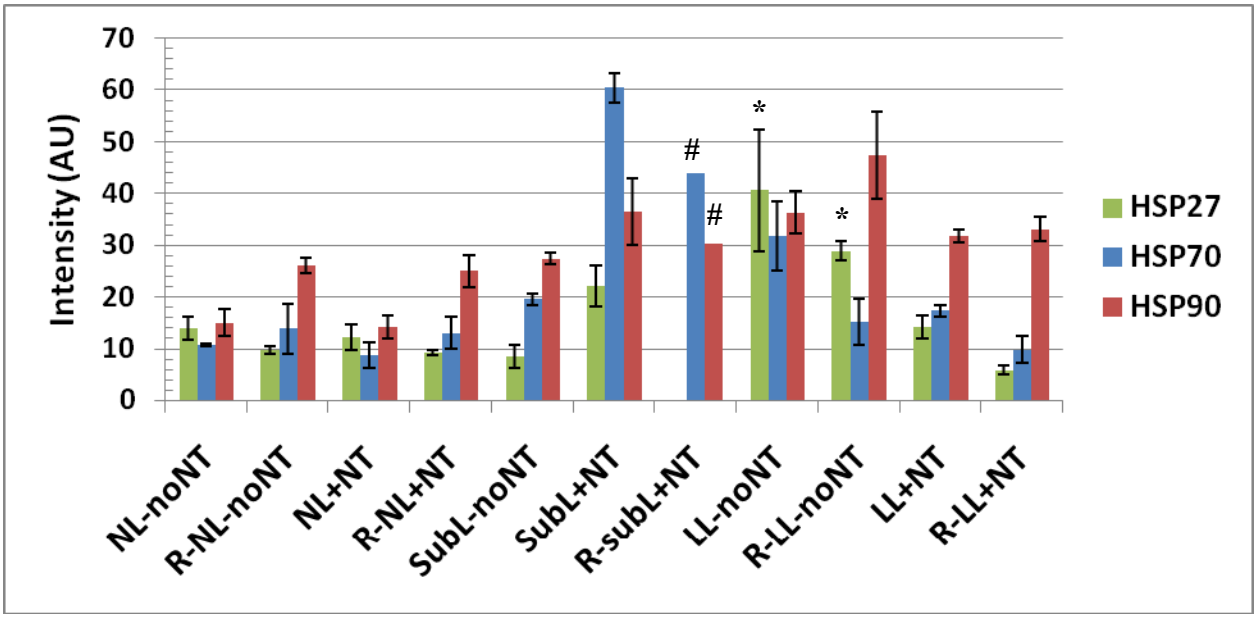

Figure 2.17. HSP fluorescent intensities of unheated and laser heated PC3 and RENCA cells with and without MWNTs. These cells have been stained separately for HSP27, 70, and 90. NL: no laser; Sub-L: sub-lethal laser; LL: lethal laser; noNT: no MWNTs; NT: MWNTs. N=3 (* group: N=2; # group: N=1).

2.2.5. MWNT internalization

In heated MWNT samples, MWNTs localized around the cells but not inside them. Figure 2.18 shows a magnified image of heated cells with MWNTs, indicated by white arrows. However, in unheated RENCA cells, which were incubated with MWNTs for 24 hr, MWNTs appear to have entered the cell through the cell membrane but did not enter into the nucleus (see Figure 2.19).

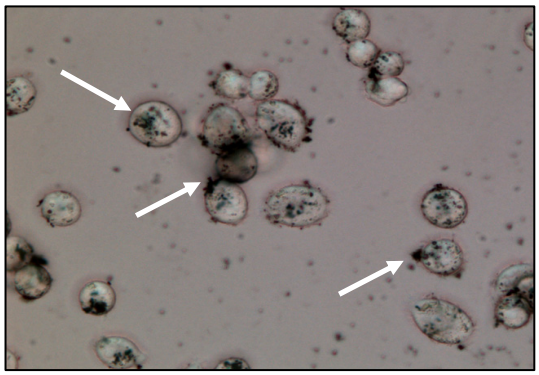

Figure 2.18. Microscope image of MWNT clusters (arrows) near unheated PC3 cells. Magnification: 400x.

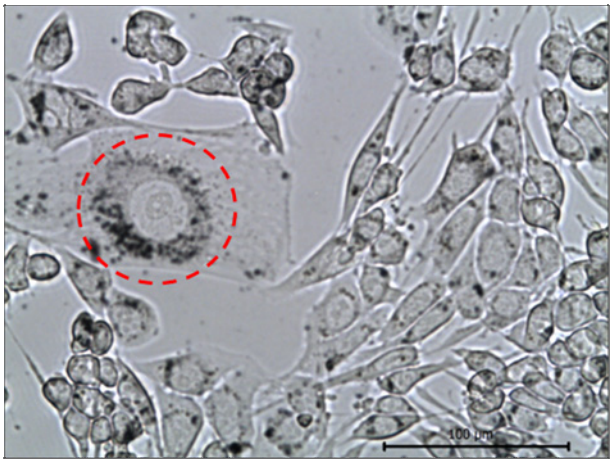

Figure 2.19. Brightfield image of MWNT incubated with RENCA cells. Black length bar is 100 µm. See MWNT aggregates encircled the nucleus (red circle).

DAPI staining of DNA allowed imaging of cell nuclei. These initial images seemed to indicate that these MWNT aggregate passed through the cell membrane but did not translocate into the nucleus. MWNT aggregates showed up as black clusters that surround the nucleus, highlighted by white arrows in Figure 2.20. This phenomenon was seen in approximately 40% of the population of RENCA cells, both large and small.

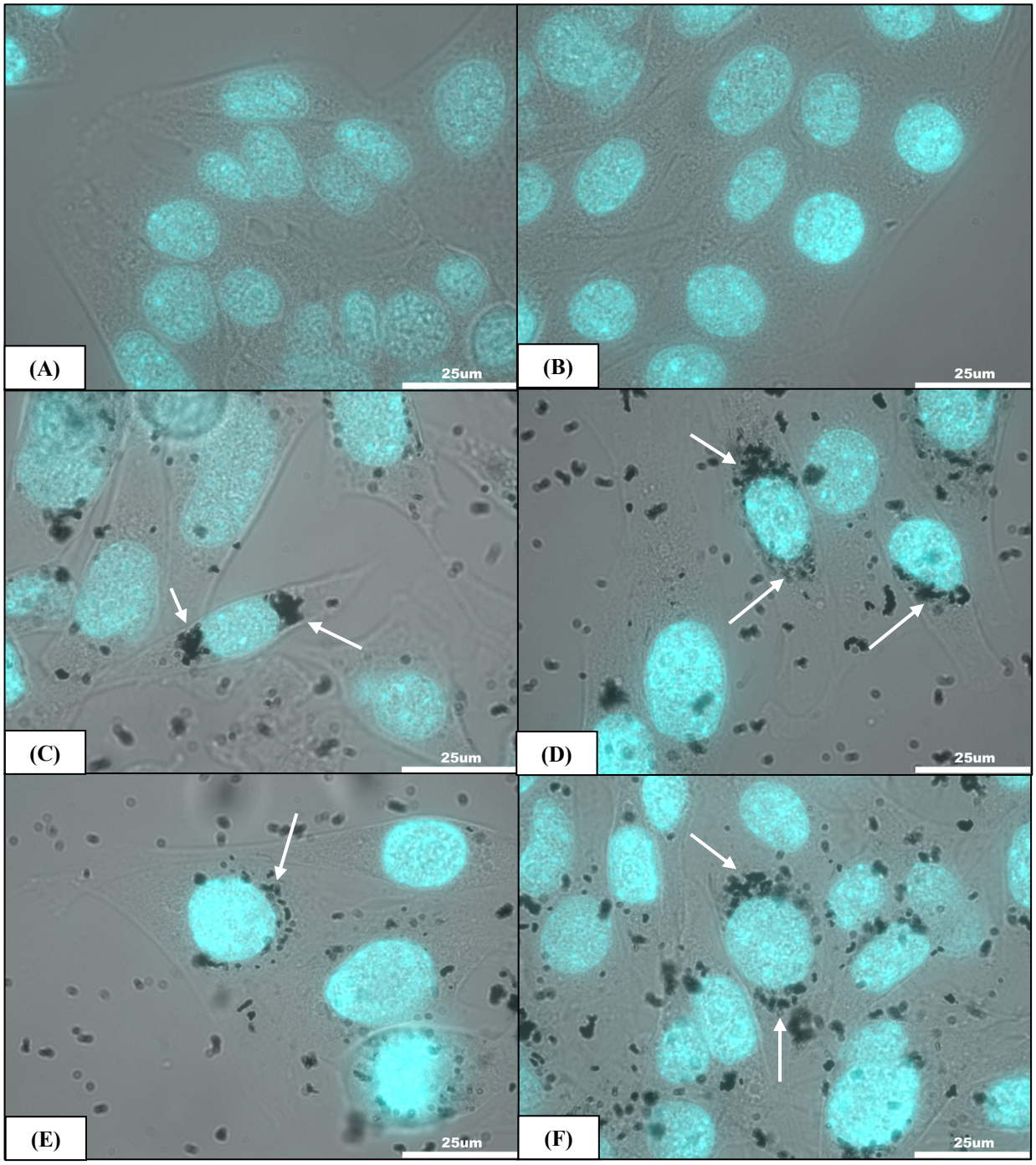

Figure 2.20. DAPI-stained nuclei of RENCA cells overlaid on bright field images. Unheated non-NT samples (A, B) and samples with 0.1 mg/ml MWNT added 24 hours earlier (C-F). MWNT aggregates show up as black clusters around the nuclei (see arrows). Scale bars are 25 μm.

2.3. Discussion and conclusions

MWNTs are effective enhancers of heat generation upon NIR irradiation. Their inclusion in laser therapy dramatically increased temperature elevation and cell death and diminished HSP expression. They possessed no inherent cell toxicity in the absence of laser irradiation making them a promising option for improving thermal dose deposition and specificity.

Cell viability revealed that MWNTs are not inherently toxic to cells as evidenced by the high cell viability count in the unheated MWNT cell cultures with little difference compared to non-NT cells. The lack of HSP induction in the presence of unheated MWNTs indicated that these particles are not producing enough environmental stress signals that would initiate HSP up-regulation, as described in **Chapter 1**. Toxicity is a long debated subject with regards to nanotubes. With many variables affecting NT chemical properties and structure, toxicity is not an easy measure to delineate. It has been found that the surface chemistry of NTs is critical in determining their *in vivo* behavior. Pristine carbon nanotubes have very hydrophobic surfaces and are highly nonspecific in binding to biological species [126, 127]. By modifying the surface chemistry of NTs, these particles can be made more inert (less toxic) and resistant to nonspecific biological species and uptake [128]. Adding the biocompatible surfactant Pluronic F-127 coats the NT surface and thus makes the NT more biocompatible and water soluble [123]. This could lead to complex micelle formation in aqueous systems which would decrease NT availability to cells, and offer lower toxicity effects [121, 129].

Fullerenes filled with various imaging agents (gadolinium and scandium) showed lower NIR absorption but a high absorbance in the UV range, which has been shown by other researchers [125]. This low NIR absorbance resulted in low temperature elevations upon irradiation with NIR light. The temperature rise exhibited in these samples was similar to that witnessed in NIR irradiation of deionized water. However, an absorption peak, as seen in the MWNT sample, reveals the ability of MWNTs to couple with NIR and generate heat. The large difference in temperatures observed between laser heating of non-NT and MWNT cultures showed the thermal enhancement imparted by MWNT inclusion when coupled to NIR light. The antennae effects of MWNTs can be utilized for specifically targeting tumor tissue and selectively heating that tissue to lethal levels using NIR of 1064 nm, a wavelength to which tissue is mostly transparent.

For all heated samples, measured temperatures close to the laser beam (4 mm from laser center or less) were higher than measured temperatures farther away. This phenomenon was more pronounced in monolayer cells with MWNT inclusion. For sub-lethal laser heating (3W, 90 sec), laser treatment alone (no NTs) had little effect on cells from either a cell viability or HSP induction standpoint. This treatment did not up-regulate HSP27, 70, and 90 expression in cell monolayer culture when compared to the basal HSP levels, indicating that little thermal stress was given to the cells. By comparing the temperature, cell viability, and HSP data, it can be concluded that little thermal injury or damage was imparted to these cells, leaving them unharmed and viable. This evidence verified the transparency of cells to NIR laser light, with little heat deposition within the non-NT culture. Unaided by heat delivery agents like MWNTs, NIR laser application would need to apply higher power or much longer heating times in order to eradicate tumor cells and prevent HSP up-regulation and future therapy resistance. Under the same laser parameters, heated samples containing MWNT produced more HSP expression than the non-NT or control samples. This higher HSP expression was expected since maximum temperatures were within the HSP up-regulation temperature range (44-60°C) and lethal temperature limits were not exceeded [34-36, 124]. Even though 50-55°C is well above the prescribed lethal temperature limit used in most thermal therapies (43°C), cells were not heated for an adequate amount of time to effectively thermally damage and kill cells, which would eliminate HSP expression. This induction of HSP at these laser parameters revealed that an increase in laser power or lasing time was needed to effectively eliminate HSP expression within the MWNT target area.

Tuning of one laser therapy parameter (i.e. heating time) had a drastic effect on heat generation and therapy outcome when coupled with MWNTs. When heating time was increased from 90 sec to 5 min, an increase in maximum temperature is seen in both NT and non-NT groups. However, increasing of laser power or heating time alone may not be adequate to eliminate all cancer cells that did not contain MWNTs. There still existed a significant temperature difference between the NT and non-NT samples. Heating of the non-NT cultures gave temperatures that are not lethal to cells. During lethal laser heating (3W, 5 min), inadequate heating of prostate and renal cancer cells induced higher expression of HSP27, 70, and 90 within the non-NT samples. The lethal laser settings alone were not harmful enough to cause cell death or stop HSP induction by cells. When NIR laser light was coupled with

MWNTs, the resulting therapy produced much higher temperatures, reaching temperature above the fatal temperature of 60°C [24]. Lethally heated MWNT samples exhibited low levels of HSP27 and 70, similar to basal (control) expression, revealing the destruction of cancer cells before significant induction of HSP began. However, HSP90 levels in this lethal MWNT group were higher than the control groups. This discrepancy could be due to the fact that HSP90 is one of the most abundant proteins expressed in cells, accounting for 1-2% of all cellular proteins in unstressed cells [130]. The exact temperature that a particular group of cells was experiencing is not known since the thermocouples measure only the temperature of surrounding media. Another possibility is the temperature activation versus destruction of HSP90 compared to the other HSPs. HSP90 may not be as sensitive to thermal stress as HSP27 and HSP70 thereby requiring a higher thermal dose for protein denaturation. In order for HSP90 to be "activated" so it can become a fully functional molecular chaperone, oligomerization of the protein is required. Oligmerization of HSP90 is triggered by heat shock and allows it to perform molecular chaperone duties like bind substrate proteins and prevent irreversible protein aggregation [131, 132]. Even though oligomerization of HSP90 occurs quickly as soon as temperature increases, Garnier et al. showed that cations, like calcium, influenced this process by lowering the temperature threshold of oligomer formation of HSP90 [131]. A rise in intracellular calcium, as witnessed during heat stress, decreases HSP90 thermostability and could account for HSP90 oligomerizing easier and becoming fully functional to perform its molecular chaperone duties [131, 133].

Even with significant enhancement of thermal properties, this therapy combination of NIR light and MWNTs needed tuning, as shown by the sub-lethal setting on MWNT samples with respect to cell viability and HSP induction. Laser parameters (heating time, heating power) were further tuned to give adequate temperature rise to kill MWNT-targeted tumor cells and to eliminate HSP expression within the tumor. This optimization would destroy cancerous tissue but minimize damage and impart HSP protection to surrounding healthy cells (or cells not near MWNTs). Thus, there is a need to optimize this therapy by using computational models as well as increasing heating specificity with agents such as MWNTs. These experimental results will aid in the improvement and validation of a laser therapy model, which can offer insight into hyperthermia therapy design for cancer patients, optimizing treatments to each patient. A properly tailored therapy would reduce the risk of tumor recurrence.

Because of poor cellular penetration of many therapeutically active molecules, new strategies for the delivery of therapeutic agents into cells is necessary [72]. Several groups have shown that SWNTs and MWNTs can be internalized by a variety of cell types to act as delivery vehicles to cells [63, 73-75]. Cell internalization of MWNTs sparks debate since this process is very dependent on nanotube and cell characteristics and properties. A critical parameter in these studies is the type of carbon nanotubes used, which is determined by: (i) the preparation and manufacturing process, (ii) the structural characteristics of the CNTs, and (iii) the surface characteristics of the CNTs including the characteristics of the functional groups at the CNT surface [134]. This complexity of cellular uptake as well as the variety of NT material types accounts for the difficulty in studying MWNT internalization in cells.

One research group took fluorescently labeled (FITC) functionalized CNTs (concentration: 2-200 μg/ml, diameter: 20-30 nm, length: 0.5-2 μm) and showed that they entered a variety of cell types within hours of initial cell contact [63]. Because of the types of cells that they studied, the researchers concluded that internalization is not solely dependent on endocytosis of the particle although other studies have shown endocytosis as a main gateway of nanoparticles into the cell [63, 92, 135]. MWNT internalization has been proposed based on the cylindrical shape and high aspect ratio, like a "nanosyringe," reported [90] and simulated [136]. Functionalized MWNTs have been shown to penetrate the plasma membrane of mammalian HeLa cells and translocate into the cytoplasm [90, 137].

In heated cultures, MWNTs were only incubated with the cells during heating (no more than 20 min). This was not sufficient time for MWNTs to be internalized into the cells. However, in unheated groups where the MWNTs were incubated with the cells for 24 hr, MWNT aggregates appeared to have crossed the membrane but remained excluded from the nuclear envelope in approximately 40% of the cell population. Working to stain other intracellular components (lysosomes, ER, Golgi Apparatus) will help to understand the pathways they use to enter cells and where they localize within cells. Using phase contrast methods for microscopic imaging will provide a better image to show if the NTs are gathered around the nuclei outside of the membrane or inside of it. Another factor that may have aided in membrane permeation was the use of Pluronic F-127 as a surfactant to disperse MWNTs in aqueous solution. Nonionic surfactants, like Pluronic block copolymers, are known to be less toxic and less irritating to biological systems and have been shown to affect the permeability of biological

membranes by solubilizing the lipid membrane [138-145]. They have also been used as penetration enhancers in transdermal delivery systems [146]. It is unknown whether Pluronic played a role in MWNT internalization. This internalization warrants further investigation since this would provide additional advantages to MWNT use in cancer therapy by supplying other modes of therapy (i.e. reactive oxygen species generation, chemo-drug delivery) and imaging options for diagnosing and monitoring target tissue.

Chapter 3: Hyperthermia treatment of tissue phantoms and tumors using MWNTs

Tissue representative phantoms can provide a closer approximation to tissue than *in vitro* cultures and provide a way to measure responses more similar to that found *in vivo* without requiring the use of animals. Phantoms provide a three dimensional environment to cells that more closely resembles cells within tumor tissue. This tool permits refinements of therapies prior to animal sacrifice. For instance, phantoms permit volumetric measurement of temperature and provide HSP expression and cell death as a function of three dimensional position. This information would be used to optimize therapy parameters before moving into animal tissue. With several options available, we chose sodium alginate as the main material of our phantoms.

Sodium alginate is a polysaccharide derived from brown seaweed which has the ability of to form a gel when it comes in contact with certain divalent cations, such as calcium. Alginate has been used in the commercial food industry as an emulsifier, thickener, and stabilizer since its properties were discovered in the 1930s [147]. Alginate has also been used within the biomedical realm in the manufacturing of surgical dressings [148] but has gained increased interest for its function as a scaffold for encapsulation and immunoprotection of transplanted cells, such as non-autologous islet cells for diabetes treatment [149, 150]. It has also been used to protect recombinant cells delivering tumor-suppressing agents [151, 152] and growth hormone [153]. Alginates have also served as culture scaffolds for a variety of cell types, including chondrocytes, bone-marrow stromal cells, islets, myoblasts, fibroblasts, Schwann cells, kidney cells, epithelial cells, and hepatocytes. These cell-seeded scaffolds that encapsulate bone-marrow stromal cells and chondrocytes could provide for the healing of bone and cartilage defects [154-156]. However, a lack of research exists using this alginate as a scaffold for thermal therapy evaluation. Initial testing showed the alginate would retain its stiffness and structure during laser heating while other gels would melt. Because of its biocompatibility with many cell types, this alginate was used to provide three-dimensional architecture to simulate cancerous tumor tissue.

In vivo studies, such as subcutaneous tumors on animals, allow testing of therapy options in a comparable complex, three-dimensional living environment and situation to that of human cancer. Superficial tumors are used because they are easy to grow, monitor, and extract. They

also provide an easily accessible target tissue for NIR light excitation of MWNTs. Injection of MWNTs intratumorally allow for the initial proof of concept of this therapy by guaranteeing the presence of MWNTs within the tumor and bypassing complex surface modifications needed to attach elusive antibodies for proteins that are expressed exclusively by cancer cells.

The focus of this chapter is the evaluation of the effects of MWNT inclusion onheat generation and cell viability of NIR-irradiated tissue phantoms. This chapter also provides an initial assessment of HSP expression within tumor tissue. Temperature profiles and cell viabilities of phantoms were assessed for different heating regimes with and without MWNTs: (1) unheated and (2) NIR laser heated phantoms (3W power for 45 sec). Both types of phantoms showed the dependence of temperature on position within the phantom. Higher temperatures were seen close to the surface and closer to the laser beam with decreasing thermal effects in deeper or farther (radial) positions. This effect was more pronounced in MWNT phantoms compared to non-NT ones. MWNT phantoms showed higher temperatures and larger temperature elevations than non-NT phantoms as well as decreased cell viability near the laser beam profile.For *in vivo* studies, HSP expression and cell damage were examined in unheated growth control, unheated MWNT-injected, laser heated saline-injected, and laser heated MWNT-injected tumors. Preliminary HSP27, 70, and 90 staining of the growth control and unheated MWNT tumors showed low levels of HSP. The MWNT irradiated tumor showed areas of higher HSP where tissue experienced sub-lethal temperatures that would induce the HSP response. The saline irradiated tumor had higher HSP levels than unheated tumors but lower HSP levels compared with the MWNT tumor. This induction indicated that sub-lethal temperatures were present in this imaged area. Further investigation is needed to correlate magnetic resonance temperature imaging (MRTI) temperature maps (being produced at Wake Forest University) to variable HSP expression within an irradiated tumor.

3.1. Experimental materials and methods

3.1.1. Sodium alginate phantom creation

Sodium alginate, Protanal LF 10/60 (FMC Biopolymer, Drammen, Norway), a low viscosity alginate with a mean G/M (guluronate / mannuronate) ratio of 70% and mean molecular weight of 180 kDa [157], was stirred vigorously with deionized water to a 3% w/v concentration (3g / 100 ml) for 1 hour. The alginate was sterile filtered through a 0.45 μm

membrane. For the alginate-MWNT solution, MWNT stock solution was added to the alginate solution to yield a 0.2 mg/ml NT concentration and vortexed for 60 seconds. PC3 cells were suspended in complete media by pipette mixing. The cell-media solution was added to the alginate solution or the alginate-NT solution in a 1:1 volume ratio and mixed by gentle pipetting, giving a final NT concentration of 0.1 mg/ml. A total of $1x10^6$ cells/phantom was suspended in the structure. To crosslink the phantom, a previous method was modified [147]. Briefly, sterile 80 mM $CaCl_2$ solution was poured into a shallow, sterile dish. Molds were used to constrain the phantom solution (Figure 3.1). The resulting phantoms are shown in Figure 3.2.

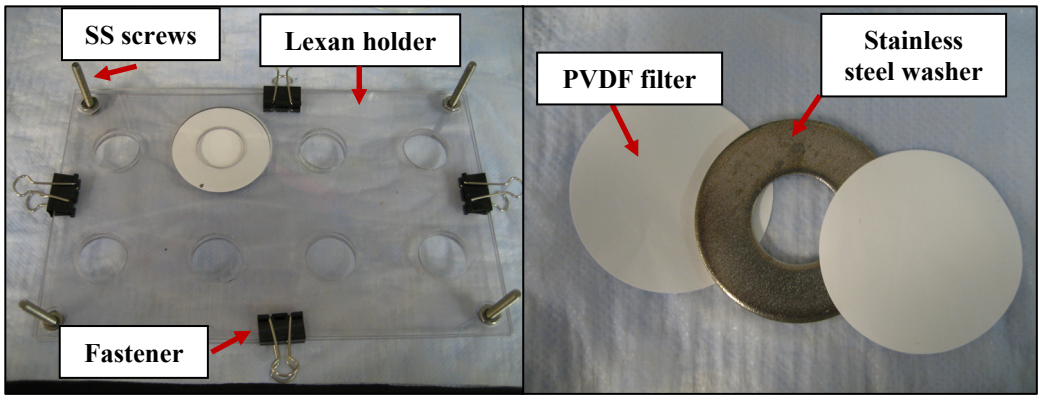

Figure 3.1. Lexan mold setup for tissue phantom creation. Note the filters are placed on either side of metal mold to shape phantoms into 1-2 mm thick phantoms.

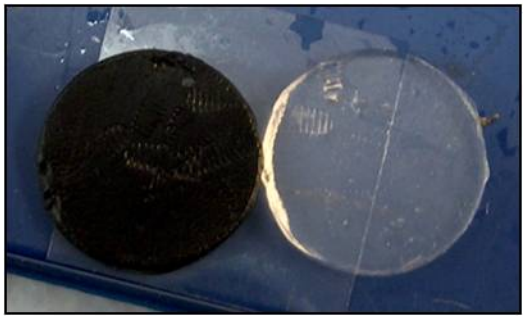

Figure 3.2. Tissue phantoms shown here, 0.1 mg/ml MWNT phantom (left) and non-NT phantom (right).

All containers and mold components were placed inside a sterile biological hood. These molds were soaked in 70% ethanol for 15 minutes. Then, they were placed in PBS to soak for 2 minutes. PVDF filters (Millipore; 5 μm pore size) were placed in the $CaCl_2$ solution for 5

minutes. The mold was assembled aseptically and the alginate was slowly pipetted to fill the mold and the entire assembly was secured and placed into the $CaCl_2$ bath for 20 minutes. The phantoms were de-molded and washed with PBS and immediately lased. After heating, the phantoms were placed in sterile dishes and covered with complete media for 16 hours.

3.1.2. Tumor implantation and MWNT injection

A murine renal cancer cell line, RENCA, was provided by Dr. Heather Hatcher (Wake Forest University Baptist Medical Center). RENCA cells were injected subcutaneously into the flanks of host nude mice. Within two weeks, tumors were removed and cut into smaller pieces and each piece implanted under the skin of experimental nude mice. Tumors grew for 2 weeks to allow tumor diameters to be between 5 and 10 mm. Once tumors were an appropriate size, 200 μL of either saline or 2 mg/ml MWNT stock solution was injected via a 27.5 gauge needle. This injection would yield 0.1 mg/ml MWNT concentration within the mouse tumor, which was estimated to have a blood volume of approximately 2 ml. Tumors were irradiated 24 hr post-injection and were sacrificed 16 hours post-heating. Figure 3.3 shows RENCA subcutaneous tumors.

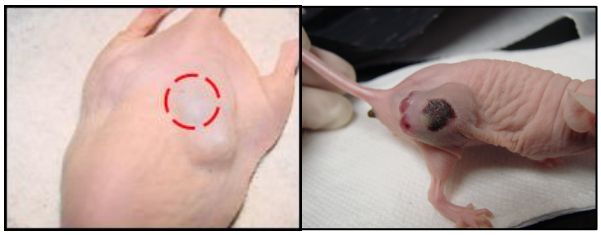

Figure 3.3. Nude mice bearing RENCA tumors subcutaneously. Red circle indicates the location of one tumor.

3.1.3. Laser and temperature measurement system setup

A continuous wave (CW) laser with a beam diameter of 5 mm (YLR-10-1064-LP, IPG Photonics) was used to heat mouse tumors. Laser irradiance of 15.3 W/cm^2 (3W, 5 mm beam diameter) was used. A heating time of 30 seconds was used to heat the tumors and 45 seconds to heat phantoms. Four hypodermic thermocouples (Omega) were placed at specified depths and radial positions in the phantoms for real-time temperature measurements during heating. Figure 3.4 shows the laser setup for tumor heating.

Figure 3.4. External beam laser setup for mouse experiments.

For tumor tissue within the MRI machine, three MR-compatible thermal probes (Luxtron m3300, LumaSense Technologies) were inserted into the tumor with an additional probe measuring room temperature to provide absolute temperature measurements. Magnetic resonance temperature imaging (MRTI) was used to measure temperature. MRTI makes use of the physical property that the resonance frequency of a proton is proportional to temperature [158]. Relative temperature maps can be made from measuring the phase change between two complex MR images and converted into absolute thermal measurements by calibration with the thermal probes.

3.1.4. Cell viability

A concentration of 0.4% trypan blue solution was used for phantom experiments. Briefly, media was removed and phantoms were rinsed with warmed PBS twice. Trypan blue solution was placed on samples for 5 minutes at room temperature. Trypan blue was removed and the samples were rinsed with PBS twice. PBS was placed on samples during imaging. A Leica DM IL or Leica DMI6000B microscope was used to capture cell viability pictures. Pictures were taken at known depths of interest in the phantoms (0, 0.5, 1.0, and 1.5 mm depth).

3.1.5. Tissue processing and H&E staining

Mouse RENCA tumors were removed at 16 hr post-lasing. Tumors were cut in half, one half being fixed in 10% neutral buffered formalin and the other half being frozen in OCT. Figure 3.5 shows one tumor half in liquid OCT. The tumors were sent to AML Labs (Rosedale, MD) for tissue processing and sectioning. The formalin-fixed tumor was embedded in paraffin, sectioned at 5 μm thickness, and stained with hematoxylin and eosin (H&E). The frozen tissue was sectioned at 5 μm thickness onto glass slides (Fisher Scientific).

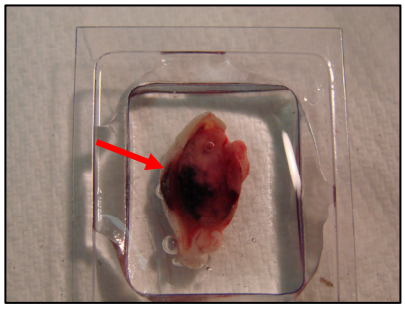

Figure 3.5. Tumor half in liquid OCT (pre-freezing). Black area is MWNTs (see arrow).

3.1.6. HSP immunostaining

Please see **Chapter 2** for process details. Tissue sections (on slides) were thawed at room temperature for 20 min. Tissue slides were then sealed with Secure-seal® hybridization chambers (Grace BioLabs) to aid liquid handling during staining and reduce chance of evaporation or tissue section loss. This chamber was removed and a coverslip secured prior to imaging. A Leica DMI6000B microscope was used to capture HSP images, using LASAF software.

3.2. Experimental results

3.2.1. Temperature for phantoms

Laser heating trials with the phantoms (MWNT and non-NT) showed higher temperature elevation than what was seen in initial cell experiments. Significant heating was confined to the first 1.5 mm in depth and minimal temperature elevation occurred outside of the 7 mm radius. Therefore, we restricted our experiments to this region of interest. Figure 3.6A is the temperature profile in the radial direction at 1-1.5 mm depth during heating of a non-NT phantom while

Figure 3.6B is heating of a MWNT phantom. The highest temperatures were seen closer to the laser beam and irradiated surface and decreased as depth from surface and radial distance from beam center increased.

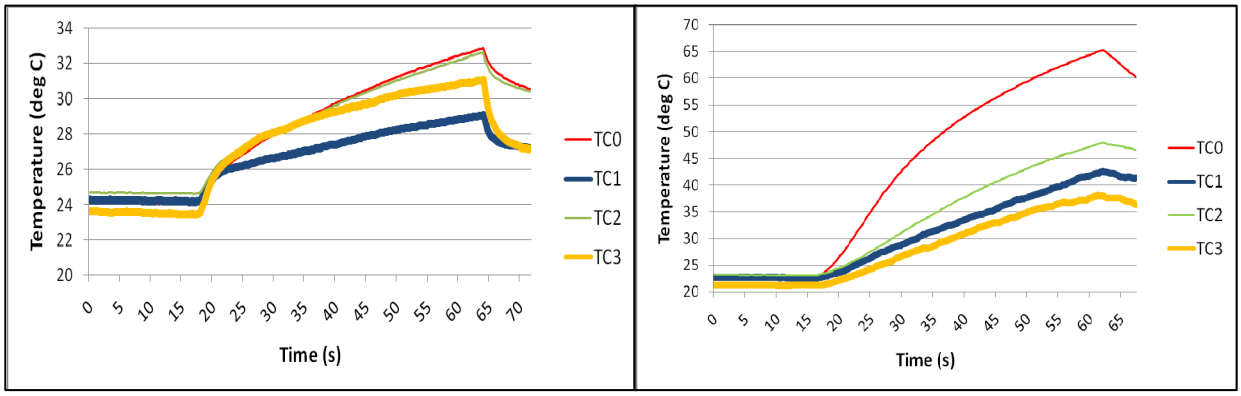

(A) **(B)**

Figure 3.6. Temperature profile during laser heating of 3W for 45 sec as a function of various radial positions of (A) non-NT phantom and (B) MWNT phantom. All thermocouples were positioned 1 mm in depth. TC0 is located 3 mm from center, TC2 is located 4 mm from center, TC1 is located 6 mm from center, and TC3 is located 7 mm from center.

3.2.2. Cell viability of phantoms

Trypan blue (concentration: 0.4%) was verified as a useful measurement of cell viability for cells contained within alginate phantoms. Dye penetration effectiveness was tested using positive controls of PC3 cell seeded phantoms immersed in methanol for 10 minutes at room temperature while negative controls were PC3 cell seeded in unheated phantoms. Figure 3.7 depicts the successful penetration and staining of dead cells with trypan blue. Trypan blue successfully infiltrated every part of the phantom and continues to properly stain dead cells. This fact indicated that any unstained cells are viable not unreachable.

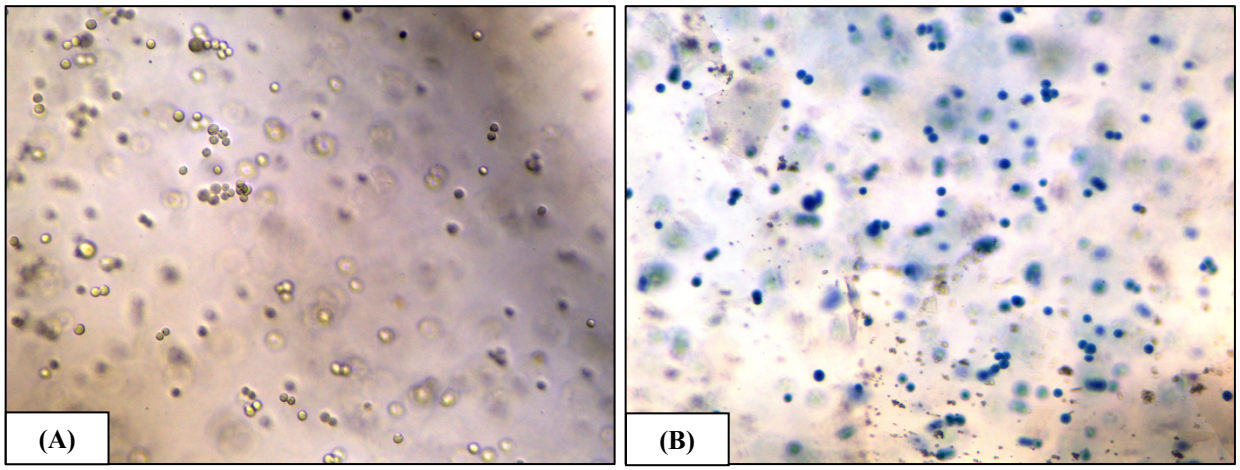

Figure 3.7. Representative image of trypan blue staining of (A) unheated PC3 phantom and (B) unheated PC3 phantom immersed in methanol. Similar results were seen at all depth positions within phantoms. Magnification: 100x.

For control (unheated) phantoms with and without MWNTs, trypan blue staining showed comparable high cell viability. Heated non-NT phantoms did not show any difference in cell viability compared to unheated controls. In all these cases, there was no significant difference between cell viability from 0 (top surface), 0.5, 1.0, and 1.5 mm depths within the phantoms. Upon laser heating, MWNT phantoms experienced a decrease in cell viability near the surface and closer to the laser beam area. In heated MWNT phantoms, the majority of cell death occurred within the top 1.5 mm depth. At all relevant depths of the heated MWNT phantoms, cell viability was lowest near laser center and increased with increasing radial distance from laser center. Within MWNT heated phantoms, increased cell viability was observed with increasing depth from the irradiated surface and radial distance away from the laser beam. Figure 3.8 shows trypan blue staining for all phantom cases at the top surface. In heated phantoms, the bottom right corner was laser center.

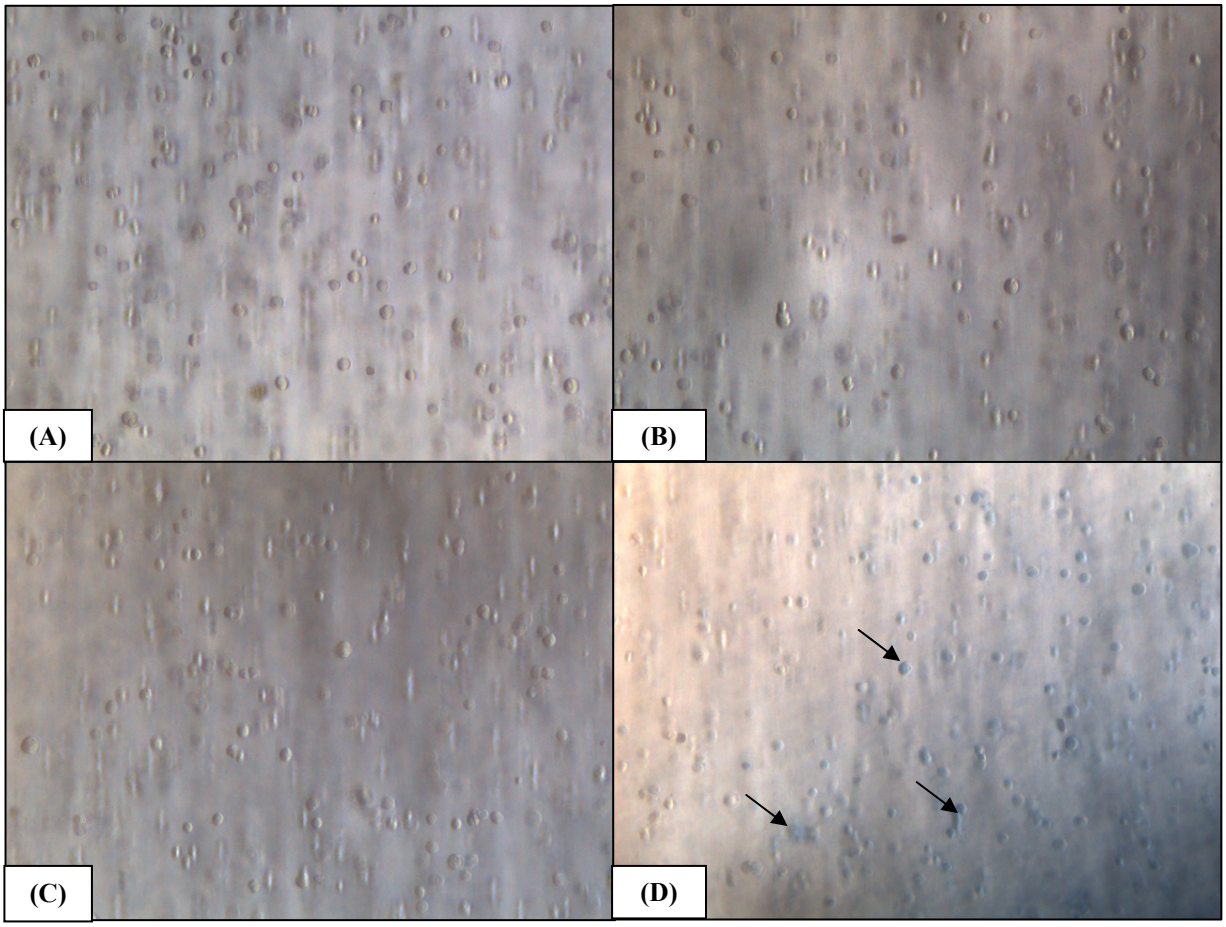

Figure 3.8. Cell viability staining with trypan blue of PC3-seeded phantoms. Trypan blue enters dead or dying cells while viable cells exclude the dye. (A) Unheated phantom without NTs, (B) unheated phantom with MWNTs, (C) heated phantom without NTs, and (D) heated phantom with MWNT. Magnification: 100x. Note: black arrows indicate examples of dead cells.

3.2.3. H&E staining and HSP expression of tissue

RENCA tumor tissue was stained with hematoxylin and eosin (H&E) to assess tissue morphology and subsequent structure alterations from inclusion of MWNT and laser heating as shown in Figure 3.9. Higher magnification of some MWNT clumping is displayed in Figure 3.10. Preliminary data indicated that MWNTs clump in certain areas of the tumor (see arrows). MWNT are shown as black clusters, usually near needle track areas.

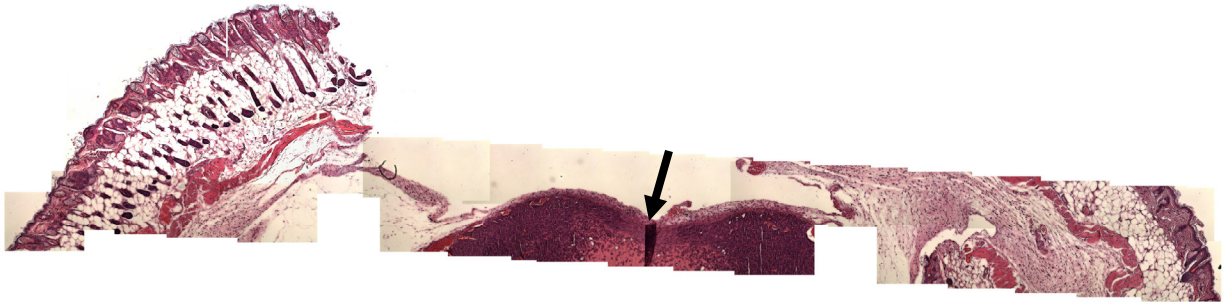

Figure 3.9. H&E staining of a section of RENCA mouse tumor. Note MWNT clustering (arrow).

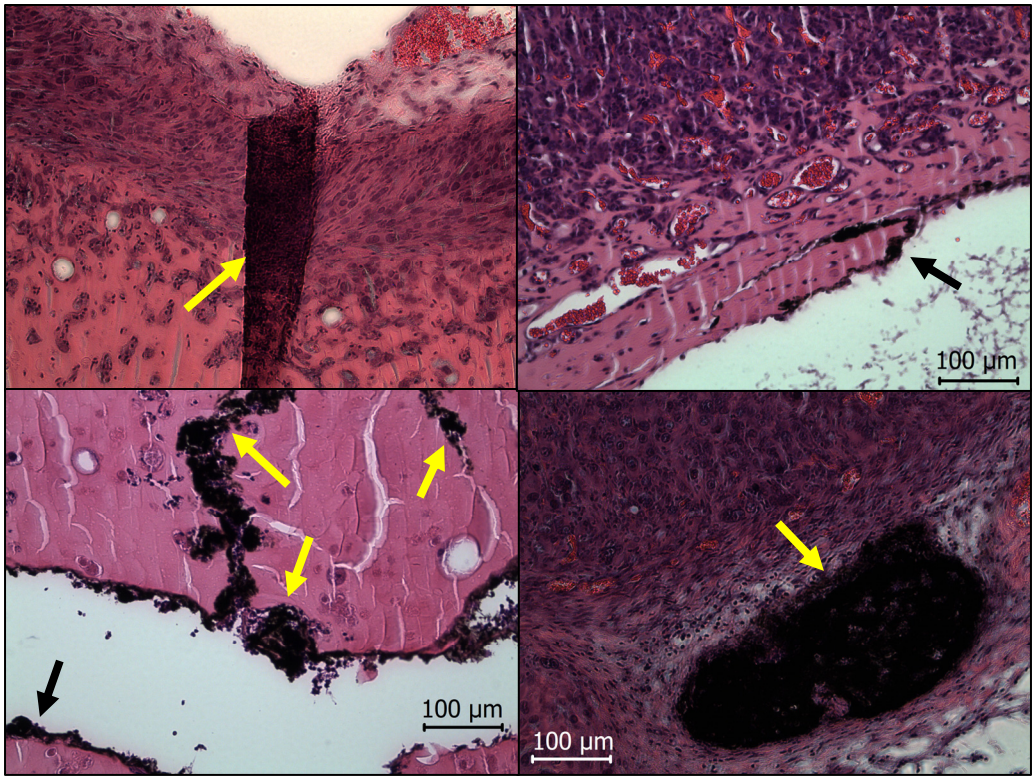

Figure 3.10. Magnified area of MWNT clumping in H&E stained section of RENCA mouse tumor. Note MWNT clustering (arrow). Scale bar is 100 µm.

HSP staining was conducted on tissue samples from 4 tumors: (1) growth control, (2) MWNT alone (no heating), (3) saline with laser heating, and (4) MWNT with laser heating. Images were difficult to resolve due to lower cell number and slightly altered tissue morphology due to freezing. Figure 3.11 shows these tumors and their HSP levels.

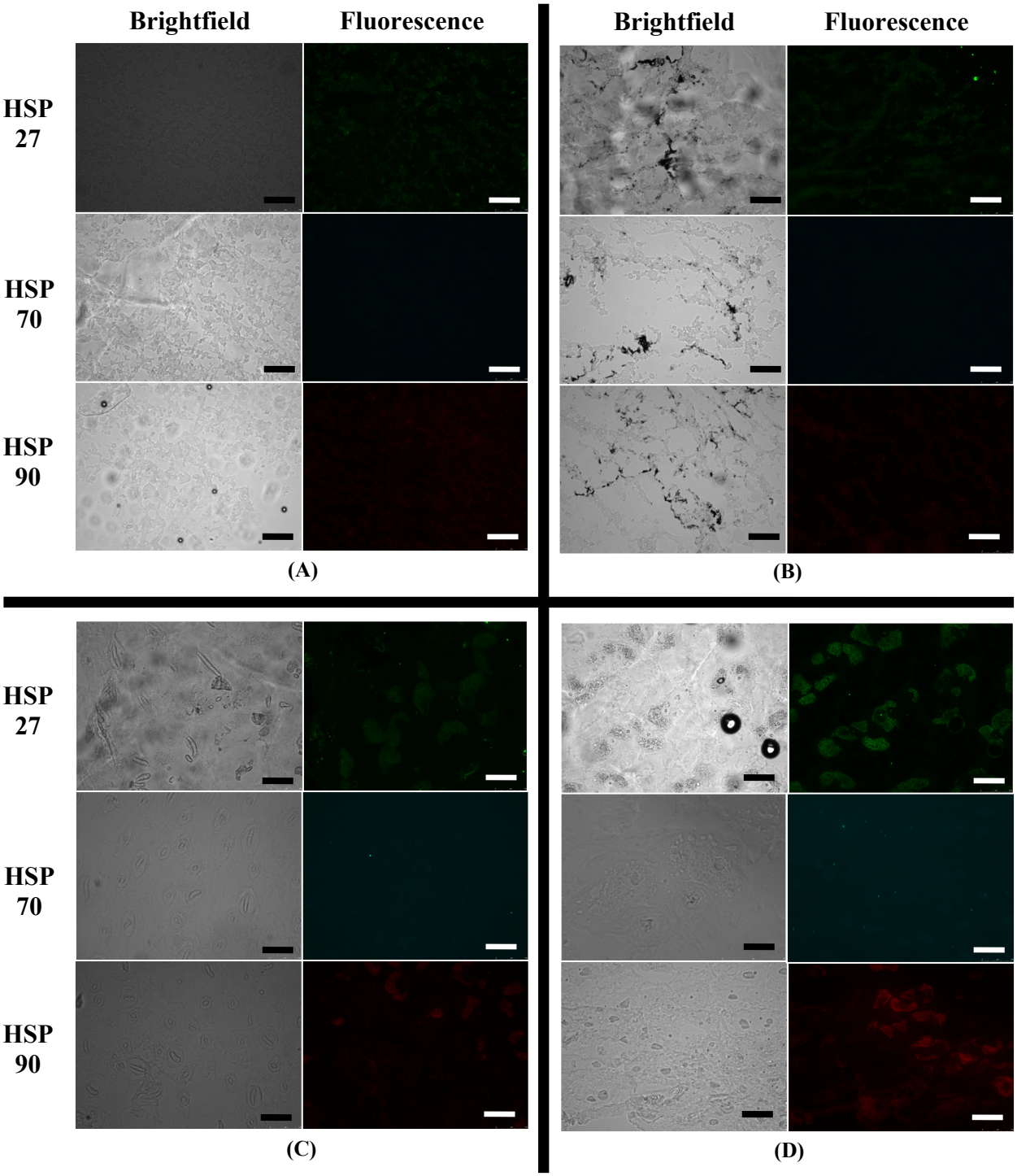

Figure 3.11. HSP staining of RENCA mouse tumors. (A) Growth control, (B) MWNT control, (C) Saline with laser irradiation, and (D) MWNT with laser irradiation. Scale bar is 10 μm.

Initial investigations show very low basal levels of HSP within the control (unheated) tissue. In the heated groups, all HSP had higher expression (within the imaged area) compared to control sections. Heated MWNT tissue showed higher HSP expression than heated saline tissue. Figure 3.12 shows a higher magnified image of HSP90 in tumor tissue.

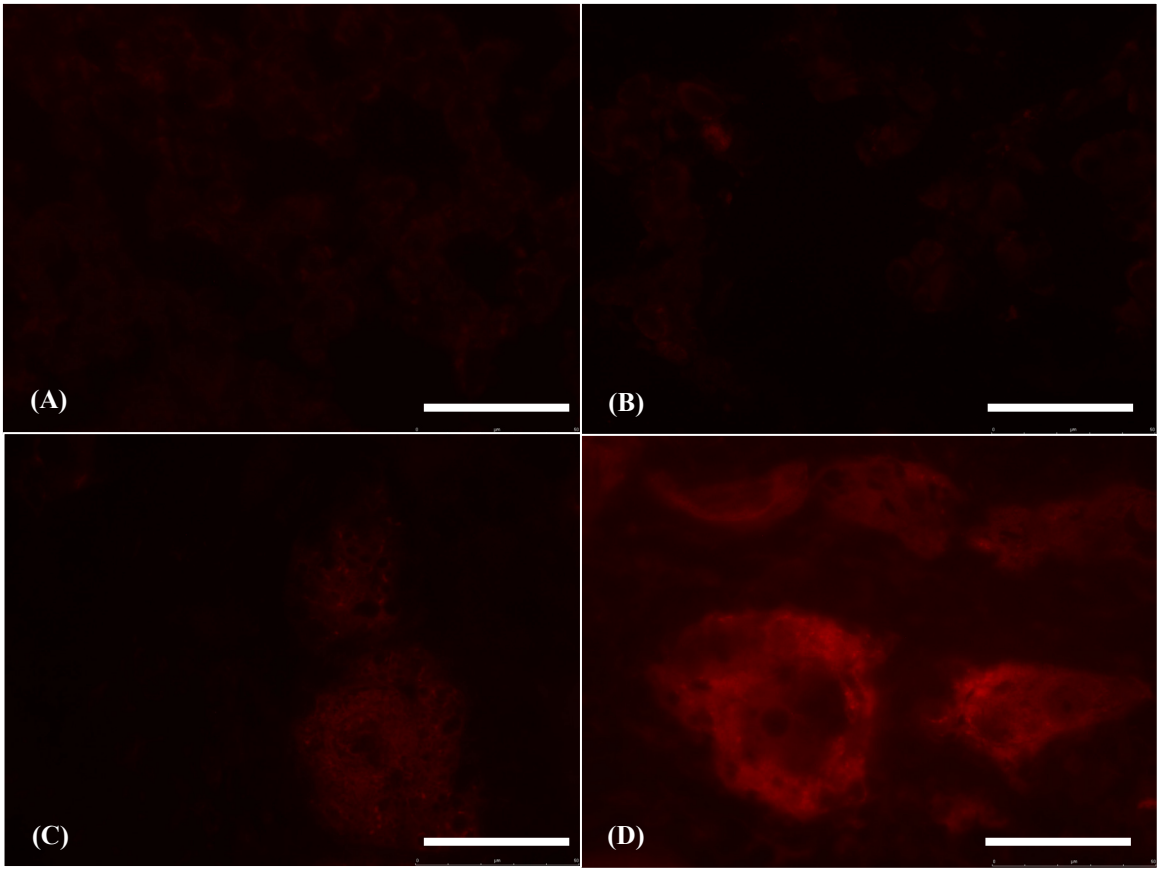

Figure 3.12. HSP90 staining of RENCA mouse tumors. (A) Growth control, (B) MWNT control, (C) Saline with laser irradiation, and (D) MWNT with laser irradiation. Scale bar is 50 μm.

3.3. Discussion and conclusions

Phantoms with MWNTs produced much higher temperatures compared to non-NT phantoms. The largest temperature elevations in either phantom occurred at the top surface with decreasing temperature elevations with increasing depth. Similar depth-dependent temperature profiles have been shown in previous *in vivo* work with nanoshells [34]. Measured temperatures showed a radial-dependence as well, higher temperatures present closer to the laser beam. These findings are similar to results from preliminary *in vivo* work and may suggest that these

phantoms may better replicate what happens in tissue heating. This temperature distribution was more drastic in MWNT phantoms. A small temperature rise was seen in the non-NT phantoms, however, this temperature rise was not sufficient to affect cell viability. This data showed that the current laser treatment alone cannot kill cells. For identical heating conditions, the MWNT samples produced a significantly greater amount of heat. Comparing the temperature rises between non-NT and MWNT phantoms revealed a similar trend in that the highest temperature elevations occur within the MWNT phantoms. This work also showed that the alginate itself is not coupling to the NIR light but that it is the MWNTs that produced the high temperature rise.

The phantom data showed that the alginate itself is not toxic to prostate cancer cells. In preliminary work, these cells remained viable for more than 2 days within the alginate scaffold. Other work documented cells remaining viable and proliferating within sodium alginate scaffolds for up to 10 weeks [157]. Unheated MWNT phantoms revealed that the MWNTs were not toxic to the cells, as shown in previous research [55]. Under laser heating, the cells within the non-NT phantoms underwent little thermal stress and showed no significant change in cell viability. However, phantoms containing MWNTs exhibited an area of dead cells after heating, centered around the laser beam and closer to the irradiated surface. This significant difference in cell viability between lased phantoms with and without MWNTs illustrates the heat delivery potential of MWNTs and their use as a more specific heat delivery vehicle to target tissue. With optimized laser settings, their inclusion would increase tissue temperatures to lethal levels and increase cell death within a target tissue, as shown in previous work [55]. These phantoms may better replicate what occurs during tissue heating since these results are comparable to preliminary *in vivo* studies where lasing resulted in tissue burn and subsequent tumor regression.

Initial *in vivo* data showed promise for HSP visualization within tissue. HSP intensities were higher in both lased tumors when compared to unheated ones. This observation indicated that certain areas of the lased tumor tissue experience sub-lethal thermal doses which up-regulated HSP. Future work is required to image and compare HSP intensity at different locations within the tumor and compare these values to MRTI temperature mapping data to understand the correlation between temperature and HSP expression. Also, future work will include consulting a pathologist to gain understanding on the H&E stained tissue structure and its markers for tissue health and damage.

Chapter 4: Hyperthermia treatment of PC3 cells using CNHs

Carbon nanohorns (CNHs) are receiving increased interest in the biomedical field. These nanoparticles are entirely metal free (biocompatible), possess large surface areas, contain large cavities (for drug or imaging agent inclusion), have unique spherical shape, and absorbs NIR light to generate heat. These properties make them advantageous for enhancing thermal therapies [48, 49].

The purpose of this chapter is to examine the thermal and biological effects of CNH inclusion in monolayer cell cultures during NIR laser therapy. Specifically, this chapter addresses the effects of CNHs on heat generation and cell viability. In this study, CNHs (0.1 mg/ml) were heated with PC3 cells to assess their thermal properties and implications for use with thermal cancer therapies. Two thermal settings were used: (1) control (unheated) and (2) lethal laser setting (3W, 5 min). There was a large difference in maximum temperature (31.4°C for non-CNH and 60.5°C for CNH samples) and temperature elevation (7.5°C for non-CNH and 36.3°C for CNH samples). Cell viability remained high in all groups except the lethal laser group with CNH inclusion (cell viability = 4.85%). These data showed that CNH were not inherently toxic to the cells, but combined with NIR, can kill cancer cells.

Because of their large cavities, particles can be incorporated into their structure. Groups have already begun inserting drugs, imaging agents, and other nanoparticles [105, 106, 113, 115, 116, 159-162]. Dr. Harry Dorn's group has already inserted $Gd_3N@C_{80}$ inside CNHs and collaborators at ORNL have imaged these particles. Being able to use this particle as both an imaging and therapy agent is useful to image tumor areas, thermally eradicate the tissue, and better monitor the target tissue. The results from this study show lethal combination of CNH and laser light as being a viable option for enhancing the thermal deposition and specificity of hyperthermia treatments for elimination of cancer or other unwanted tissue.

4.1. Experimental materials and methods

4.1.1. Nanohorn fabrication

Pristine single-walled carbon nanohorns (SWNHs) were provided by Oak Ridge National Laboratories (ORNL). TEM was used to verify structure and inclusion of various particles within the CNH. CNHs were functionalized using carboxyl groups to make them water-soluble.

One approach took SWNHs and mixed them with KOH with mass ratio 1:40. This mixture was placed in a stainless steel capsule and shaken vigorously for 3 h, 30 min, 10 min, respectively. The final product was sonicated in pure water and dialyzed with tubing dialysis membrane (MWCO: 50000) until the pH is 7.

An alternative approach took purified SWNHs (5 mg) and placed them in 5 ml of dry *o*-dichlorobenzene and sonicated for 30 min to obtain a CNHs suspension solution. The latter solution was heated at 85°C for 3 days. Each day 50 mg of peroxide was added to the solution. After the reaction was completed, the suspension was cooled and poured into an Erlenmeyer flask containing a tetrahydrofuran and sonicated for 15 min. This solution was then filtered using a 0.45 μm pore size PTFE membrane. Functionalized SWNHs collected on the membrane, placed in 10 ml of ethanol, sonicated for 20 min, and filtered again. During the filtration, a large amount of ethanol was repeatedly used to completely wash off the unreacted peroxides and reaction byproducts. Finally functionalized SWNHs were vacuum-dried at 70°C overnight. Functionalized SWNHs (1 mg) were poured into 2 ml of PBS solution containing 1% Pluronic F-127 (PL-127) and sonicated for 30 min to obtain a 0.5 mg/ml homogenous solution. A final solution concentration of 0.1 mg/ml CNH was used for all experiments. Heating of cells with CNHs was done in PBS with 1% PL-127. Unheated controls were allowed to seed on slides for 24 hr and then incubated with functionalized CNHs (0.1 mg/ml) for 24 hours. To clarify, empty nanohorns were used in these experiments.

4.1.2. Nanohorn structure and imaging

Imaging was performed by our collaborators at Oak Ridge National Laboratories (ORNL) using a Hitachi HF-3300 TEM operated at 300 kV.

4.1.3. Temperature and heat generation

See **Chapter 2** for procedure details. Lethal heating time was 5 min at 3W laser power.

4.1.4. Cell viability

See **Chapter 2** for procedure details. Cell viability was carried out 24 hr post-seeding for unheated CNH controls and 16 hr post-seeding for heated samples.

4.2. Experimental results

4.2.1. Nanohorn structure and imaging

Carbon nanohorns were verified as dahlia-like structures having an overall diameter of between 80-100 nm. Dr. Harry Dorn's group had inserted $Gd_3N@C_{80}$ trimetallic nitride template endohedral metallofullerenes (TNT EMFs) into CNHs. Figure 4.1 shows various TEM images of dahlia-like CNHs with the inclusion of $Gd_3N@C_{80}$.

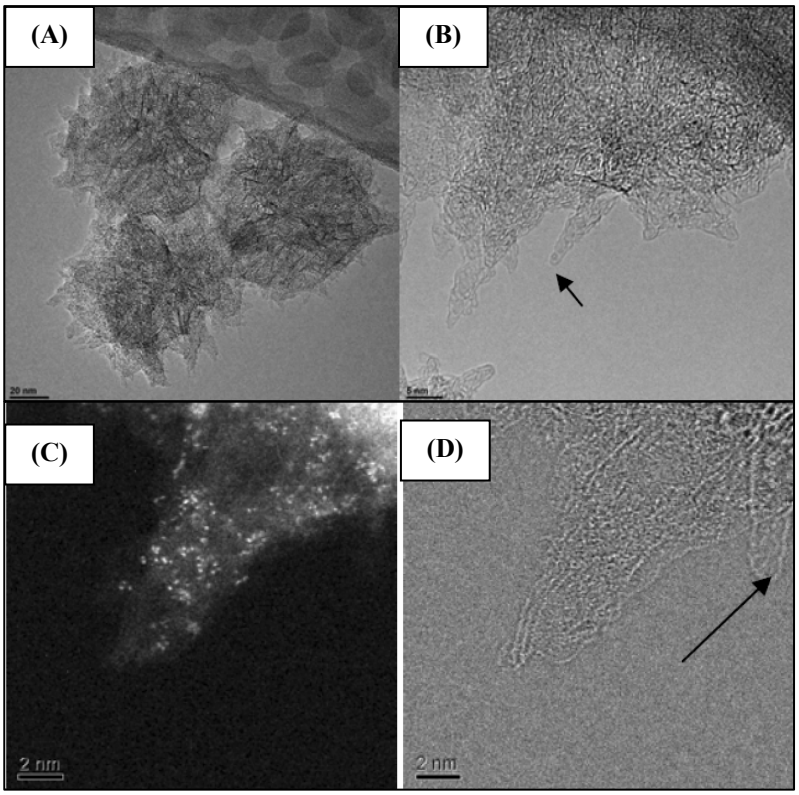

Figure 4.1. TEM images of Gd3N@C80@SWNH taken by collaborators at ORNL. (A) Low magnification TEM image showing the flower-like structure of the functionalized carbon SWNHs filled with Gd3N@C80 metallofullerenes, 20 nm scale bar; (B) High magnification micrograph from the SWNH edge showing the carbon nanohorn structure, as well as individual fullerene particles trapped inside cones, 5 nm scale bar; (C) STEM-HAADF image from the edge of a functionalized SWNH containing Gd3N@C80. Bright dots are the individual metal particles, 2 nm scale bar; (D) A bright field image from the same area showing SWNH caps of single graphene sheets (see arrow), 2 nm scale bar.

4.2.2. Temperature and heat generation

CNH were laser-irradiated at a power of 3W for 5 min (lethal setting). Temperature profiles were similar to MWNTs at this laser setting except maximum temperatures were slightly lower. Maximum temperatures for non-CNH and CNH samples were 31.43°C and 60.53°C,

respectively, with a standard deviation range between 0.72-1.16°C. Temperature profiles are shown for non-CNH and 0.1mg/ml CNH samples in Figure 4.2.

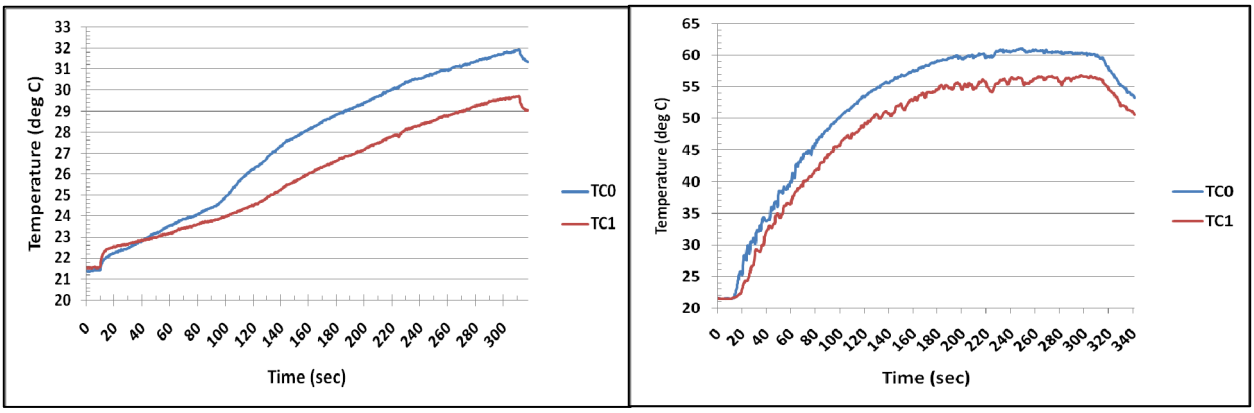

(A) **(B)**

Figure 4.2. Temperature plots of lethal heating (3W, 5 min) of PBS with 1% PL-127 (A) without and (B) with 0.1 mg/ml CNHs. (TC0 is 4 mm from laser center and TC1 is 7 mm from laser center).

Temperatures rose within the non-CNH and 0.1 mg/ml CNH samples by 7.5°C and 36.3°C, respectively. Standard deviations (σ) ranged from 2.6-3.2°C. Figure 4.3 shows this significant different in temperature elevation.

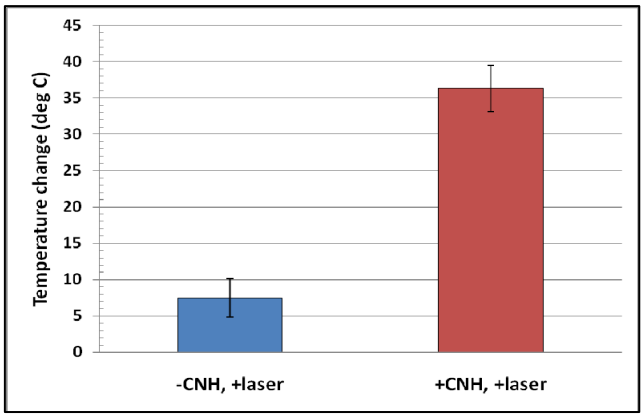

Figure 4.3. Temperature elevation without and with CNHs at lethal laser level (3W, 5min). Concentration of CNH was 0.1 mg/ml in PBS. N=3, σ = 2.6-3.2°C.

4.2.3. Cell viability

Cell viability remained high and comparable within the control groups. Upon laser application, samples not containing CNHs possessed a similar cell viability compared to controls. The only significant difference was seen in the lethal heating of samples with CNH inclusion. Figure 4.4 shows trypan blue staining of PC3 control and lethal heated cells.

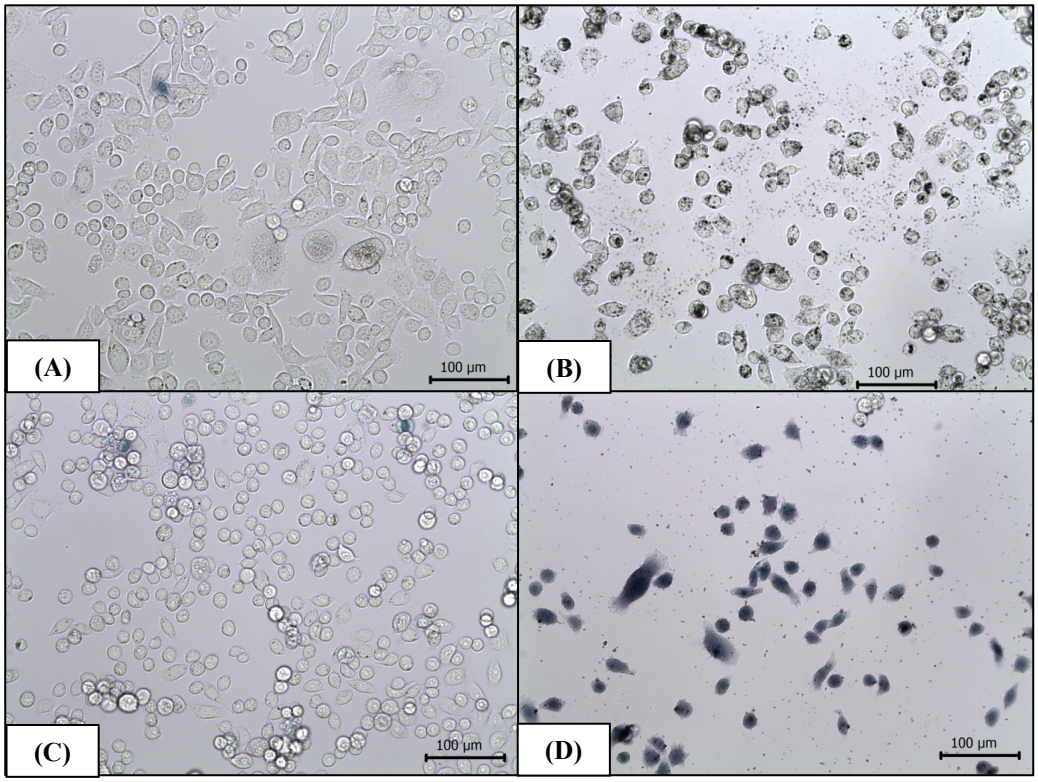

Figure 4.4. Trypan Blue staining of PC3 cells: (A) unheated without CNH, (B) unheated with CNH, (C) lethal heating without CNH, and (D) lethal heating with CNHs. Scale bar is 100 µm.

Mean cell viability for unheated non-CNH samples was 99.28%, for unheated CNH samples 99.35%, for lethally heated non-CNH samples was 98.39%, and for lethally heated CNH samples 4.85% (see Figure 4.5). The standard deviations ranged from 0.49 - 3.64%.

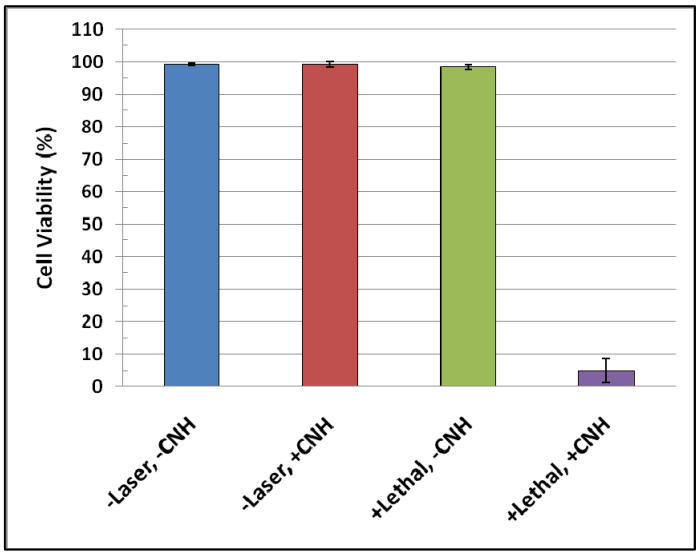

Figure 4.5. Cell viability of PC3 cells. Note the significant reduction in viable cells with lethal and CNHs. n=3, σ range: 0.49 - 3.64%.

4.3. Discussion and conclusions

Miyako et al. showed that CNHs have slight absorbance within the NIR wavelength range. This absorbance is less than MWNT, but is substantial enough to produce heat if illuminated by light of the correct wavelength range. This group has shown temperature elevations in 0.3 mg/ml and 0.025 mg/ml CNH solutions upon 1064 nm laser irradiation of 1-5W [48, 49]. With a concentration of 0.1 mg/ml CNH and laser power of 3W, similar temperature rises occurred in CNH samples in my studies. There was a large difference in maximum temperature (31.4°C for non-CNH and 60.5°C for CNH samples) and temperature elevation (7.5°C for non-CNH and 36.3°C for CNH samples).

Cell viability remained high in all groups except the lethal laser group with CNHs (cell viability = 4.85%). CNHs are more biocompatible because they are entirely metal free, unlike NTs. High cell viability in unheated groups shows that CNH were not inherently toxic to the cells. This data was further supported by research from other groups at the tissue and organism level that showed little toxicity of CNHs to tissue [104, 163].

The dramatic difference in cell viability in the heated CNH samples demonstrated the potential of CNH as a thermal enhancer to effectively kill cancer cells. Miyako et al. have shown elimination of phages and microbes by coupling NIR laser light with CNH inclusion [48, 49]. Because of large cavities within the CNH, other particles can be inserted into their

structure. Groups have already begun inserting drugs, imaging agents, and other nanoparticles [105, 106, 113, 115, 116, 159-162]. Some groups have utilized the large surface area of CNHs to attach antibodies specific to a virus or microbe of interest [48, 49]. This feature could be used to target cancer cells or other cells of interest by attachment of specific antibodies. Being able to use this particle as both an imaging and therapy agent is useful to image tumor areas, thermally eradicate the tissue, and better monitor the target tissue. The lethal combination of CNHs and NIR laser light shows these particles as a viable option for enhancing the thermal deposition and specificity of hyperthermia treatments for elimination of cancer.

Integration of CNHs into laser hyperthermia treatment could lead to enhanced thermal deposition and specificity to increase cancer cell injury and minimize healthy tissue injury. These factors would blend well with treatments combating poorly defined tumors regions or tumors within vital tissue. Enhancing thermal therapies and optimizing those therapies could decrease recovery times and reduce the risk of tumor recurrence.

Chapter 5: Future Prospects

5.1. Multi-walled nanotubes

5.1.1. Cell culture

Future work will include HSP staining of unresolved groups within the PC3 and RENCA cell samples to increase sample size to at least 3 samples per group. Additional cell viability data will be acquired to increase sample size within each lethal lased group. Cell internalization of the MWNT must undergo further scrutiny, since this theory is very dependent on nanotube and cell type. Staining of other subcellular components will enable researchers to mark the locations of nanotubes to further solidify MWNT transport into cells. This step may also lead to further understanding of the mechanisms behind the movement of MWNT into cells.

Varying laser power would be another direction to pursue. The gathered data would give a better picture of which laser parameters are more critical to affect cells with and without nanotubes from the various measures of temperature, cell viability, and HSP expression.

5.1.2. Phantoms and *in vivo* mouse tumor study

HSP staining will need to be conducted on unheated and heated phantoms with and without MWNTs. HSP expression will be evaluated in lased mouse tumors containing MWNTs to determine if phantoms provide a comparable model to tissue heating monitored by MRTI. To better understand heating phenomena, thermal camera technology will be used to visualize radial surface heating paired with thermocouples for depth measurements in each phantom. These technologies will allow better simultaneous temperature measurements within the phantoms. Further phantom studies would involve different "layers" (non-NT and MWNT) being assembled, irradiated, and evaluated for temperature elevation, cell viability, and HSP expression. This work would increase confidence of using MWNTs in embedded tumor therapy.

Future work is required to image and compare HSP intensities at different locations within heated tumors. Optimization of the antibodies is needed to ensure HSP expression. Once this protocol is optimized, HSP distribution can be compared with MRTI temperature mapping data to better understand the correlation between temperature and HSP expression distribution. Also, future work will include studying cell structure damage from H&E stained tumor tissue

structure at various depths and radii away from the laser beam and correlating that tissue damage evidence with HSP and temperature data.

5.2. Nanohorns

Using various laser powers and heating times would provide a better picture of the thermal properties of CNHs. CNH internalization studies should be conducted to see if these nanoparticles pass through cell membranes with more efficiency than cylindrical nanotubes. Also, defining the intracellular locations that CNH congregate would help shed light on the mechanisms of intercellular transport.

References:

1. **Prostate Cancer** [http://www.cancer.gov/cancertopics/wyntk/prostate/page2]
2. [http://www.prostatecancerfoundation.org]
3. Carroll PR, Carducci MA, Zietman AL, Rothaermel JM: **Report to the Nation on Prostate Cancer.** (Berman S, Britt GS eds.). pp. 1-130. Santa Monica: Prostate Cancer Foundation; 2005:1-130.
4. Scherr D, Swindle PW, Scardino PT: **National Comprehensive Cancer Network guidelines for the management of prostate cancer.** *Urology* 2003, **61:**14-24.
5. Swindle PW, Kattan MW, Scardino PT: **Markers and meaning of primary treatment failure.** *Urol Clin North Am* 2003, **30:**377-401.
6. Amin Z, Bown SG, Lees WR: **Local treatment of colorectal liver metastases: a comparison of interstitial laser photocoagulation (ILP) and percutaneous alcohol injection (PAI).** *Clin Radiol* 1993, **48:**166-171.
7. Nolsoe CP, Torp-Pedersen S, Burcharth F, Horn T, Pedersen S, Christensen NE, Olldag ES, Andersen PH, Karstrup S, Lorentzen T, et al.: **Interstitial hyperthermia of colorectal liver metastases with a US-guided Nd-YAG laser with a diffuser tip: a pilot clinical study.** *Radiology* 1993, **187:**333-337.
8. Vogl TJ, Mack MG, Muller PK, Straub R, Engelmann K, Eichler K: **Interventional MR: interstitial therapy.** *Eur Radiol* 1999, **9:**1479-1487.
9. Vogl TJ, Mack MG, Straub R, Engelmann K, Zangos S, Eichler K: **[Interventional MR-guided laser induced thermotherapy in oncologic indications. Status and prospects].** *Radiologe* 1999, **39:**764-771.
10. Seki T, Wakabayashi M, Nakagawa T, Imamura M, Tamai T, Nishimura A, Yamashiki N, Okamura A, Inoue K: **Percutaneous microwave coagulation therapy for patients with small hepatocellular carcinoma: comparison with percutaneous ethanol injection therapy.** *Cancer* 1999, **85:**1694-1702.
11. Gazelle GS, Goldberg SN, Solbiati L, Livraghi T: **Tumor ablation with radio-frequency energy.** *Radiology* 2000, **217:**633-646.
12. Hilger I, Andra W, Bahring R, Daum A, Hergt R, Kaiser WA: **Evaluation of temperature increase with different amounts of magnetite in liver tissue samples.** *Invest Radiol* 1997, **32:**705-712.
13. Hilger I, Hiergeist R, Hergt R, Winnefeld K, Schubert H, Kaiser WA: **Thermal ablation of tumors using magnetic nanoparticles: an in vivo feasibility study.** *Invest Radiol* 2002, **37:**580-586.
14. Jolesz FA, Hynynen K: **Magnetic resonance image-guided focused ultrasound surgery.** *Cancer J* 2002, **8 Suppl 1:**S100-112.
15. Kattan MW, Wheeler TM, Scardino PT: **Postoperative Nomogram for Disease Recurrence After Radical Prostatectomy for Prostate Cancer.** *Journal of Clinical Oncology* 1999, **17:**1499-1507.
16. **National Cancer Institute FactSheet: Staging: Questions and Answers** [http://www.prostate-cancer-institute.org/about-prostate-cancer/prostate-cancer-tests.html]
17. Hanks GE, Asbell S, Krall JM: **Outcome for lymph node dissection negative T-1b,T-2 (A-2,B) prostate cancer treated with external beam radiation therapy in RTOG 77-06.** *Int J Radiat Oncol Biol Phys* 1991, **21:**1099-1103.

18. Paulson DF, Moul JW, Walther PJ: **Radical prostatectomy for clinical stage T1-2N0M0 prostatic adenocarcinoma: long-term results.** *J Urol* 1990, **144:**1180-1184.
19. Walsh PC, Retik AB, Vaughan ED (Eds.): **Campbell's Urology**, 7th edition. Philadelphia, PA: WB Saunders Company; 1998.
20. Madersbacher S, Grobl M, Kramer G, Dirnhofer S, Steiner GE, Marberger M: **Regulation of heat shock protein 27 expression of prostatic cells in response to heat treatment.** *Prostate* 1998, **37:**174-181.
21. Gibbons NB, Watson RW, Coffey RN, Brady HP, Fitzpatrick JM: **Heat-shock proteins inhibit induction of prostate cancer cell apoptosis.** *Prostate* 2000, **45:**58-65.
22. Hirsch LR, Stafford RJ, Bankson JA, Sershen SR, Rivera B, Price RE, Hazle JD, Halas NJ, West JL: **Nanoshell-mediated near-infrared thermal therapy of tumors under magnetic resonance guidance.** *Proc Natl Acad Sci U S A* 2003, **100:**13549-13554.
23. Kiang JG, Tsokos GC: **Heat shock protein 70 kDa: molecular biology, biochemistry, and physiology.** *Pharmacol Ther* 1998, **80:**183-201.
24. Rylander MN: **Design of Hyperthermia Protocols for Inducing Cardiac Protection and Tumor Destruction by Controlling Heat Shock Protein Expression.** University of Texas at Austin, Biomedical Engineering; 2005.
25. Dresselhaus MS, Dresselhaus G, Avouris P (Eds.): **Carbon nanotubes : synthesis, structure, properties, and applications**. New York: Springer; 2001.
26. Schlesinger MJ, Santoro MG, Garaci E (Eds.): **Stress proteins : induction and function**. Berlin: Springer-Verlag; 1990.
27. Beere HM: **Death versus survival: functional interaction between the apoptotic and stress-inducible heat shock protein pathways.** *J Clin Invest* 2005, **115:**2633-2639.
28. Roigas J, Wallen ES, Loening SA, Moseley PL: **Effects of combined treatment of chemotherapeutics and hyperthermia on survival and the regulation of heat shock proteins in Dunning R3327 prostate carcinoma cells.** *Prostate* 1998, **34:**195-202.
29. Ciocca DR, Clark GM, Tandon AK, Fuqua SA, Welch WJ, McGuire WL: **Heat shock protein hsp70 in patients with axillary lymph node-negative breast cancer: prognostic implications.** *J Natl Cancer Inst* 1993, **85:**570-574.
30. Tomei LD, Cope FO (Eds.): **Apoptosis : the molecular basis of cell death**. Plainview, N.Y.: Cold Spring Harbor Laboratory Press; 1991.
31. Calderwood SK, Khaleque MA, Sawyer DB, Ciocca DR: **Heat shock proteins in cancer: chaperones of tumorigenesis.** *Trends Biochem Sci* 2006, **31:**164-172.
32. Soti C, Nagy E, Giricz Z, Vigh L, Csermely P, Ferdinandy P: **Heat shock proteins as emerging therapeutic targets.** *Br J Pharmacol* 2005, **146:**769-780.
33. Levine AJ, Momand J, Finlay CA: **The p53 tumour suppressor gene.** *Nature* 1991, **351:**453-456.
34. Rylander MN, Feng Y, Zhang Y, Bass J, Jason Stafford R, Volgin A, Hazle JD, Diller KR: **Optimizing heat shock protein expression induced by prostate cancer laser therapy through predictive computational models.** *J Biomed Opt* 2006, **11:**041113-041116.
35. Rylander MN, Feng Y, Bass J, Diller KR: **Heat shock protein expression and injury optimization for laser therapy design.** *Lasers Surg Med* 2007, **39:**731-746.
36. Rylander MN, Feng Y, Bass J, Diller KR: **Thermally induced injury and heat-shock protein expression in cells and tissues.** *Ann N Y Acad Sci* 2005, **1066:**222-242.

37. Song G, Ouyang G, Bao S: **The activation of Akt/PKB signaling pathway and cell survival.** *J Cell Mol Med* 2005, **9:**59-71.
38. Cornford PA, Dodson AR, Parsons KF, Desmond AD, Woolfenden A, Fordham M, Neoptolemos JP, Ke Y, Foster CS: **Heat shock protein expression independently predicts clinical outcome in prostate cancer.** *Cancer Res* 2000, **60:**7099-7105.
39. Vargas-Roig LM, Fanelli MA, Lopez LA, Gago FE, Tello O, Aznar JC, Ciocca DR: **Heat shock proteins and cell proliferation in human breast cancer biopsy samples.** *Cancer Detect Prev* 1997, **21:**441-451.
40. Georgopoulos C, Welch WJ: **Role of the major heat shock proteins as molecular chaperones.** *Annu Rev Cell Biol* 1993, **9:**601-634.
41. Craig EA, Weissman JS, Horwich AL: **Heat shock proteins and molecular chaperones: mediators of protein conformation and turnover in the cell.** *Cell* 1994, **78:**365-372.
42. Richards EH, Hickey E, Weber L, Masters JR: **Effect of overexpression of the small heat shock protein HSP27 on the heat and drug sensitivities of human testis tumor cells.** *Cancer Res* 1996, **56:**2446-2451.
43. Schlesinger MJ: **Heat shock proteins.** *J Biol Chem* 1990, **265:**12111-12114.
44. Kim HP, Morse D, Choi AM: **Heat-shock proteins: new keys to the development of cytoprotective therapies.** *Expert Opin Ther Targets* 2006, **10:**759-769.
45. Saleh A, Srinivasula SM, Balkir L, Robbins PD, Alnemri ES: **Negative regulation of the Apaf-1 apoptosome by Hsp70.** *Nat Cell Biol* 2000, **2:**476-483.
46. Kam NW, O'Connell M, Wisdom JA, Dai H: **Carbon nanotubes as multifunctional biological transporters and near-infrared agents for selective cancer cell destruction.** *Proc Natl Acad Sci U S A* 2005, **102:**11600-11605.
47. Bassil A, Puech P, Tubery L, Bacsa W, Flahaut E: **Controlled laser heating of carbon nanotubes.** *Applied Physics Letters* 2006, **88:**173113-.
48. Miyako E, Nagata H, Hirano K, Makita Y, Nakayama K-i, Hirotsu T: **Near-infrared laser-triggered carbon nanohorns for selective elimination of microbes.** *Nanotechnology* 2007, **18:**475103.
49. Miyako E, Nagata H, Hirano K, Sakamoto K, Makita Y, Nakayama K-i, Hirotsu T: **Photoinduced antiviral carbon nanohorns.** *Nanotechnology* 2008, **19:**075106.
50. Seo WS, Lee JH, Sun X, Suzuki Y, Mann D, Liu Z, Terashima M, Yang PC, McConnell MV, Nishimura DG, Dai H: **FeCo/graphitic-shell nanocrystals as advanced magnetic-resonance-imaging and near-infrared agents.** *Nat Mater* 2006, **5:**971-976.
51. Liu Z, Cai W, He L, Nakayama N, Chen K, Sun X, Chen X, Dai H: **In vivo biodistribution and highly efficient tumor targeting of carbon nanotubes in mice.** *Nature Nanotechnology* 2006, **2:**47-52.
52. Poole CP, Owens FJ: *Introduction to nanotechnology.* Hoboken, N.J.: John Wiley; 2003.
53. Webster S, Maultzsch J, Thomsen C, Liu J, Czerw R, Terrones M, Adar F, John C, Whitley A, Carroll DL: **Raman Characterization of Nitrogen Doped Multiwalled Carbon Nanotubes.** In*; San Francisco, Ca., United States*. Materials Research Society; 2003: 129-134.
54. Xu J, Xiao M, Czerw R, Carroll DL: **Optical limiting and enhanced optical nonlinearity in boron-doped carbon nanotubes.** *Chemical Physics Letters* 2004, **389:**247-250.

55. Torti SV, Byrne F, Whelan O, Levi N, Ucer B, Schmid M, Torti FM, Akman S, Liu J, Ajayan PM, et al: **Thermal ablation therapeutics based on CN(x) multi-walled nanotubes.** *Int J Nanomedicine* 2007, **2:**707-714.
56. Liu Z, Winters M, Holodniy M, Dai H: **siRNA delivery into human T cells and primary cells with carbon-nanotube transporters.** *Angew Chem Int Ed Engl* 2007, **46:**2023-2027.
57. Buzea C, Pacheco II, Robbie K: **Nanomaterials and nanoparticles: Sources and toxicity.** *Biointerphases* 2007, **2:**M17-55.
58. Kroto HW, Heath JR, Obrien SC, Curl RF, Smalley RE: **C-60-Buckminsterfullerene.** *Nature* 1985, **318:**162-163.
59. Polyachenko NH: **Carbon Nanomaterials for Oncology Treatment Options.** Wake Forest University Graduate School of Arts and Sciences, School of Biomedical Engineering and Sciences; 2007.
60. Liu J, Czerw R, Carroll DL: **Large-scale synthesis of highly aligned nitrogen doped carbon nanotubes by injection chemical vapor deposition methods. .** *Journal of Materials Research* 2005, **20:**538-543.
61. Dresselhaus MS, Dresselhaus G, Eclund PC (Eds.): **Science of Fullerenes and Carbon Nanotubes**: Academic Press Inc.; 1996.
62. de Vries IJM, Lesterhuis WJ, Barentsz JO, Verdijk P, van Krieken JH, Boerman OC, Oyen WJG, Bonenkamp JJ, Boezeman JB, Adema GJ, et al: **Magnetic resonance tracking of dendritic cells in melanoma patients for monitoring of cellular therapy.** *Nature Biotechnology* 2005, **23:**1407-1413.
63. Kostarelos K, Lacerda L, Pastorin G, Wu W, Wieckowski S, Luangsivillay J, Godefroy S, Pantarotto D, Briand J-P, Muller S, et al: **Cellular uptake of functionalized carbon nanotubes is independent of functional group and cell type.** *Nature Nanotechnology* 2007, **2:**108-113.
64. Blank VD, Nuzdin AA, Bagramov RK, Prokhorov VM: **A comparison of some thermodynamic parameters between superhard fullerite, some metals and some covalent elements.** *Carbon* 2001, **39:**905-908.
65. Kempa K, Rybczynski J, Huang ZP, Gregorczyk K, Vidan A, Kimball B, Carlson J, Benham G, Wang Y, Herczynski A, Ren ZF: **Carbon nanotubes as optical antennae.** *Advanced Materials* 2007, **19:**421-421.
66. Burke PJ, Li SD, Yu Z: **Quantitative theory of nanowire and nanotube antenna performance.** *IEEE Transactions on Nanotechnology* 2006, **5:**314-334.
67. Wang Y, Kempa K, Kimball B, Carlson JB, Benham G, Li WZ, Kempa T, Rybczynski J, Herczynski A, Ren ZF: **Receiving and transmitting light-like radio waves: Antenna effect in arrays of aligned carbon nanotubes.** *Applied Physics Letters* 2004, **85:**2607-2609.
68. Hanson GW: **Fundamental transmitting properties of carbon nanotube antennas.** *IEEE Transactions on Antennas and Propagation* 2005, **53:**3426-3435.
69. Schonenberger C, Forro L: **Multiwall carbon nanotubes.** *Physics World* 2000, **13:**37-41.
70. Hepplestone SP, Ciavarella AM, Janke C, Srivastava GP: **Size and temperature dependence of the specific heat capacity of carbon nanotubes.** *Surface Science* 2006, **600:**3633-3636.

71. Unfried K, Albrecht C, Klotz L-O, von Mikecz A, Grether-Beck S, SCHINS RPF: **Cellular responses to nanoparticles: Target structures and mechanisms.** *Nanotoxicology* 2007, **1:**52-71.
72. Smith DA, van de Waterbeemd H: **Pharmacokinetics and metabolism in early drug discovery.** *Curr Opin Chem Biol* 1999, **3:**373-378.
73. Heller D, Baik S, Eurell T, Strano M: **Single-walled carbon nanotube spectroscopy in live cells: Towards long-term labels and optical sensors. .** *Adv Mater* 2005, **17:**2793-2799.
74. Cherukuri P, Bachilo SM, Litovsky SH, Weisman RB: **Near-infrared fluorescence microscopy of single-walled carbon nanotubes in phagocytic cells.** *J Am Chem Soc* 2004, **126:**15638-15639.
75. Kam NW, Liu Z, Dai H: **Carbon nanotubes as intracellular transporters for proteins and DNA: an investigation of the uptake mechanism and pathway.** *Angew Chem Int Ed Engl* 2006, **45:**577-581.
76. Garcia-Garcia E, Andrieuxa K, Gilb S, Couvreura P: **Colloidal carriers and blood–brain barrier (BBB) translocation: A way to deliver drugs to the brain? .** *International Journal of Pharmaceutics* 2005, **298:**274-292.
77. Juvin P, Fournier T, Boland S, Soler P, Marano F, Desmonts JM, Aubier M: **Diesel particles are taken up by alveolar type II tumor cells and alter cytokines secretion.** *Arch Environ Health* 2002, **57:**53-60.
78. Kato T, Yashiro T, Murata Y, Herbert DC, Oshikawa K, Bando M, Ohno S, Sugiyama Y: **Evidence that exogenous substances can be phagocytized by alveolar epithelial cells and transported into blood capillaries.** *Cell Tissue Res* 2003, **311:**47-51.
79. Kukowska-Latallo JF, Candido KA, Cao Z, Nigavekar SS, Majoros IJ, Thomas TP, Balogh LP, Khan MK, Baker JR, Jr.: **Nanoparticle targeting of anticancer drug improves therapeutic response in animal model of human epithelial cancer.** *Cancer Res* 2005, **65:**5317-5324.
80. Singal M, Finkelstein JN: **Amorphous silica particles promote inflammatory gene expression through the redox sensitive transcription factor, AP-1, in alveolar epithelial cells.** *Exp Lung Res* 2005, **31:**581-597.
81. Kreyling WG, Semmler M, Erbe F, Mayer P, Takenaka S, Schulz H, Oberdorster G, Ziesenis A: **Translocation of ultrafine insoluble iridium particles from lung epithelium to extrapulmonary organs is size dependent but very low.** *J Toxicol Environ Health A* 2002, **65:**1513-1530.
82. Stone V, Shaw J, Brown DM, MacNee W, Faux SP, Donaldson K: **The role of oxidative stress in the prolonged inhibitory effect of ultrafine carbon black on epithelial cell function** *Toxicology in Vitro* 1998, **12:**649-659.
83. Gurr JR, Wang AS, Chen CH, Jan KY: **Ultrafine titanium dioxide particles in the absence of photoactivation can induce oxidative damage to human bronchial epithelial cells.** *Toxicology* 2005, **213:**66-73.
84. Hopwood D, Spiers EM, Ross PE, Anderson JT, McCullough JB, Murray FE: **Endocytosis of fluorescent microspheres by human oesophageal epithelial cells: comparison between normal and inflamed tissue.** *Gut* 1995, **37:**598-602.
85. Rothen-Rutishauser BM, Schurch S, Haenni B, Kapp N, Gehr P: **Interaction of fine particles and nanoparticles with red blood cells visualized with advanced microscopic techniques.** *Environ Sci Technol* 2006, **40:**4353-4359.

86. Peters A, Veronesi B, Calderón-Garcidueñas L, Gehr P, Chen LC, Geiser M, Reed W, Rothen-Rutishauser B, Schürch S, Schulz H: **Translocation and potential neurological effects of fine and ultrafine particles a critical update.** *Particle and Fibre Toxicology* 2006, **3:13**.
87. Nemmar A, Hoylaerts MF, Hoet PH, Dinsdale D, Smith T, Xu H, Vermylen J, Nemery B: **Ultrafine particles affect experimental thrombosis in an in vivo hamster model.** *Am J Respir Crit Care Med* 2002, **166:**998-1004.
88. Oberdorster G, Sharp Z, Atudorei V, Elder A, Gelein R, Lunts A, Kreyling W, Cox C: **Extrapulmonary translocation of ultrafine carbon particles following whole-body inhalation exposure of rats.** *J Toxicol Environ Health A* 2002, **65:**1531-1543.
89. Xia T, Kovochich M, Brant J, Hotze M, Sempf J, Oberley T, Sioutas C, Yeh JI, Wiesner MR, Nel AE: **Comparison of the Abilities of Ambient and Manufactured Nanoparticles To Induce Cellular Toxicity According to an Oxidative Stress Paradigm.** *Nano Lett* 2006, **6:**1794-1807.
90. Pantarotto D, Singh R, McCarthy D, Erhardt M, Briand JP, Prato M, Kostarelos K, Bianco A: **Functionalized carbon nanotubes for plasmid DNA gene delivery.** *Angew Chem Int Ed Engl* 2004, **43:**5242-5246.
91. Cai D, Mataraza JM, Qin ZH, Huang Z, Huang J, Chiles TC, Carnahan D, Kempa K, Ren Z: **Highly efficient molecular delivery into mammalian cells using carbon nanotube spearing.** *Nat Methods* 2005, **2:**449-454.
92. Kam NWS, Dai HJ: **Carbon nanotubes as intracellular protein transporters: generality and biological functionality.** *J Am Chem Soc* 2005, **127:**6021-6026.
93. Kam NWS, Jessop TC, Wender PA, Dai H: **Nanotube molecular transporters: internalization of carbon nanotube- protein conjugates into mammalian cells.** *J Am Chem Soc* 2004, **126** 6850- 6851.
94. Geiser M, Rothen-Rutishauser B, Kapp N, Schürch S, Kreyling W, Schulz H, Semmler M, Hof VI, Heyder J, Gehr P: **Ultrafine Particles Cross Cellular Membranes by Nonphagocytic Mechanisms in Lungs and in Cultured Cells.** *Environ Health Perspect* 2005 **113:**1555-1560.
95. Stefani D, Wardman D, Lambert T: **The implosion of the Calgary General Hospital: ambient air quality issues.** *J Air Waste Manag Assoc* 2005, **55:**52-59.
96. Penn A, Murphy G, Barker S, Henk W, Penn L: **Combustion-derived ultrafine particles transport organic toxicants to target respiratory cells. .** *Environmental Health Perspectives* 2005, **113:**956-963.
97. Li N, Sioutas C, Cho A, Schmitz D, Misra C, Sempf J, Wang M, Oberley T, Froines J, Nel A: **Ultrafine particulate pollutants induce oxidative stress and mitochondrial damage.** *Environ Health Perspect* 2003, **111:**455-460.
98. Porter A, Gass M, Muller K, Skepper JN, Midgley P, Welland M: **Visualizing the Uptake of C60 to the Cytoplasm and Nucleus of Human Monocyte-Derived Macrophage Cells Using Energy-Filtered Transmission Electron Microscopy and Electron Tomography.** *Acta Biomater* 2006, **2:**409–419.
99. Isobe H, Tanaka T, Maeda R, Noiri E, Solin N, Yudasaka M, Iijima S, Nakamura E: **Preparation, Purification, Characterization, and Cytotoxicity Assessment of Water-Soluble, Transition-Metal-Free Carbon Nanotube Aggregates.** *Angewandte Chemie International Edition* 2006, **45:**6676-6680.

100. Iijima S, Yudasaka M, Yamada R, Bandow S, Suenaga K, Kokai F, Takahashi K: **Nano-aggregates of single-walled graphitic carbon nano-horns.** *Chemical Physics Letters* 1999, **309:**165-170.
101. Iijima S, Ichihashi T: **Single-shell carbon nanotubes of 1 nm diameter.** *Nature* 1993, **363:**603-605.
102. Fan X, Tan J, Zhang G, Zhang F: **Isolation of carbon nanohorn assemblies and their potential for intracellular delivery.** *Nanotechnology* 2007, **18:**195103.
103. Kasuya D, Yudasaka M, Takahashi K, Kokai F, Iijima S: **Selective Production of Single-Wall Carbon Nanohorn Aggregates and Their Formation Mechanism.** *J Phys Chem B* 2002, **106:**4947-4951.
104. Miyawaki J, Yudasaka M, Azami T, Kubo Y, Iijima S: **Toxicity of Single-Walled Carbon Nanohorns.** *ACS Nano* 2007, **2:**213-226.
105. Miyawaki J, Yudasaka M, Imai H, Yorimitsu H, Isobe H, Nakamura E, Iijima S: **In vivo magnetic resonance imaging of single-walled carbon nanohorns by labeling with magnetite nanoparticles.** *Advanced Materials* 2006, **18:**1010-1014.
106. Yuge R, Ichihashi T, Shimakawa Y, Kubo Y, Yudasaka M, Iijima S: **Preferential Deposition of Pt Nanoparticles Inside Single-Walled Carbon Nanohorns.** *Advanced Materials* 2004, **16:**1420–1423.
107. Yoshitake T, Shimakawa Y, Kuroshima S, Kimura H, Ichihashi T, Kubo Y, Kasuya D, Takahashi K, Kokai F, Yudasaka M, Iijima S: **Preparation of fine platinum catalyst supported on single-wall carbon nanohorns for fuel cell application.** *Physica B: Condensed Matter* 2002, **323:**124-126.
108. Murata K, Hashimoto A, Yudasaka M, Kasuya D, Kaneko K, Iijima S: **The Use of Charge Transfer to Enhance the Methane-Storage Capacity of Single-Walled Nanostructured Carbon. .** *Adv Mater* 2004, **16:**1520–1522.
109. Bekyarova E, Murata K, Yudasaka M, Kasuya D, Iijima S, Tanaka H, Kahoh H, Kaneko K: **Single-Wall Nanostructured Carbon for Methane Storage.** *J Phys Chem B* 2003, **107:**4681-4684.
110. Murata K, Kaneko K, Kanoh H, Kasuya D, Takahashi K, Kokai F, Yudasaka M, Iijima S: **Adsorption Mechanism of Supercritical Hydrogen in Internal and Interstitial Nanospaces of Single-Wall Carbon Nanohorn Assembly.** *J Phys Chem B* 2002, **106:**11132-11138.
111. Murata K, Miyawaki J, Yudasaka M, Iijima S, Kaneko K: **High-density of methane confined in internal nanospace of single-wall carbon nanohorns.** *Carbon* 2005, **43:**2826-2830.
112. Yang CM, Kim YJ, Endo M, Kanoh H, Yudasaka M, Iijima S, Kaneko K: **Nanowindow-Regulated Specific Capacitance of Supercapacitor Electrodes of Single-Wall Carbon Nanohorns.** *J Am Chem Soc* 2007, **129:**20-21.
113. Matsumura S, Ajima K, Yudasaka M, Iijima S, Shiba K: **Dispersion of Cisplatin-Loaded Carbon Nanohorns with a Conjugate Comprised of an Artificial Peptide Aptamer and Polyethylene Glycol.** *Mol Pharmaceutics* 2007, **4:**723-729.
114. Murakami T, Fan J, Yudasaka M, Iijima S, Shiba K: **Solubilization of Single-Wall Carbon Nanohorns Using a PEG-Doxorubicin Conjugate.** *Mol Pharmaceutics* 2006, **3:**407-414.
115. Ajima K, Yudasaka M, Murakami T, Maigne A, Shiba K, Iijima S: **Carbon Nanohorns as Anticancer Drug Carriers.** *Mol Pharmaceutics* 2005, **2:**475-480.

116. Murakami T, Ajima K, Miyawaki J, Yudasaka M, Iijima S, Shiba K: **Drug-Loaded Carbon Nanohorns: Adsorption and Release of Dexamethasone in Vitro.** *Mol Pharmaceutics* 2004, **1:**399-405.
117. Murata K, Kaneko K, Kokai F, Takahashi K, Yudasaka M, Iijima S: **Pore structure of single-wall carbon nanohorn aggregates.** *Chem Phys Lett* 2000, **331:**14-20.
118. Chithrani BD, Ghazani AA, Chan WC: **Determining the size and shape dependence of gold nanoparticle uptake into mammalian cells.** *Nano Letters* 2006, **6:**662-668.
119. Fisher JW, Rylander MN: **Effective cancer laser therapy design through the integration of nanotechnology and computational treatment planning models.** In *Proceedings of SPIE; San Jose, CA*. Edited by Vo-Dinh T, Lakowicz JR. 2008: 68690D-68691-68611.
120. Liu J, Webster S, Carroll DL: **Temperature and flow rate of NH3 effects on nitrogen content and doping environments of carbon nanotubes grown by injection CVD method.** *J Phys Chem B* 2005, **109:**15769-15774.
121. Monteiro-Riviere NA, Inman AO, Wang YY, Nemanich RJ: **Surfactant effects on carbon nanotube interactions with human keratinocytes.** *Nanomedicine: Nanotechnology, Biology, and Medicine* 2005, **1:**293– 299.
122. Kirchner C, Liedl T, Kudera S, Pellegrino T, Munoz Javier A, Gaub HE, Stolzle S, Fertig N, Parak WJ: **Cytotoxicity of colloidal CdSe and CdSe/ZnS nanoparticles.** *Nano Lett* 2005, **5:**331-338.
123. Moore VC, Strano MS, Haroz EK, Hauge RH, Smalley RE: **Individually suspended single-walled carbon nanotubes in various surfactants.** *Nano Letters* 2003, **3:**1379-1382.
124. Rylander MN, Diller KR, Wang S, Aggarwal SJ: **Correlation of HSP70 expression and cell viability following thermal stimulation of bovine aortic endothelial cells.** *J Biomech Eng* 2005, **127:**751-757.
125. John T, Dennis S, Shinohara H: **Production, isolation, and characterization of group-2 metal-containing endohedral metallofullerenes.** *Applied Physics A* 1998, **66:**243-247.
126. Chen RJ, Bangsaruntip S, Drouvalakis KA, Kam NW, Shim M, Li Y, Kim W, Utz PJ, Dai H: **Noncovalent functionalization of carbon nanotubes for highly specific electronic biosensors.** *Proc Natl Acad Sci U S A* 2003, **100:**4984-4989.
127. Shim M, Kam N, Chen R, Li Y, Dai H: **Functionalization of carbon nanotubes for biocompatibility and biomolecular recognition.** *Nano Lett* 2002, **2:**285-288.
128. Liu Z, Davis C, Cai W, He L, Chen X, Dai H: **Circulation and long-term fate of functionalized, biocompatible single-walled carbon nanotubes in mice probed by Raman spectroscopy.** *Proc Natl Acad Sci U S A* 2008, **105:**1410-1415.
129. Matthew JE, Nazario YL, Roberts SC, Bhatia SR: **Effect of mammalian cell culture medium on the gelation properties of Pluronic F-127.** *Biomaterials* 2002, **23:**4615-4619.
130. Csermely P, Schnaider T, Soti C, Prohaszka Z, Nardai G: **The 90-kDa molecular chaperone family: structure, function, and clinical applications. A comprehensive review.** *Pharmacol Ther* 1998, **79:**129-168.
131. Garnier C, Protasevich I, Gilli R, Tsvetkov P, Lobachov V, Peyrot V, Briand C, Makarov A: **The two-state process of the heat shock protein 90 thermal denaturation: effect of calcium and magnesium.** *Biochem Biophys Res Commun* 1998, **249:**197-201.

132. Yonehara M, Minami Y, Kawata Y, Nagai J, Yahara I: **Heat-induced chaperone activity of HSP90.** *J Biol Chem* 1996, **271:**2641-2645.
133. Ding XZ, Smallridge RC, Galloway RJ, Kiang JG: **Increases in HSF1 translocation and synthesis in human epidermoid A-431 cells: role of protein kinase C and [Ca2+]i.** *J Investig Med* 1996, **44:**144-153.
134. Lacerda L, Raffa S, Prato M, Bianco A, Kostarelos K: **Cell-penetrating CNTs for delivery of therapeutics.** *Nanotoday* 2007, **2:**38-43.
135. Kam NWS, Liu Z, Dai H: **Functionalization of Carbon Nanotubes via Cleavable Disulfide Bonds for Efficient Intracellular Delivery of siRNA and Potent Gene Silencing.** *J Am Chem Soc* 2005, **127:**12492-12493.
136. Lopez CF, Nielsen SO, Moore PB, Klein ML: **Understanding nature's design for a nanosyringe.** *Proc Natl Acad Sci U S A* 2004, **101:**4431-4434.
137. Bianco A, Kostarelos K, Partidos CD, Prato M: **Biomedical applications of functionalised carbon nanotubes.** *Chem Commun (Camb)* 2005**:**571-577.
138. Kabanov AV, Chekhonin VP, Alakhov V, Batrakova EV, Lebedev AS, Melik-Nubarov NS, Arzhakov SA, Levashov AV, Morozov GV, Severin ES, et al.: **The neuroleptic activity of haloperidol increases after its solubilization in surfactant micelles. Micelles as microcontainers for drug targeting.** *FEBS Lett* 1989, **258:**343-345.
139. Kabanov AV, Batrakova EV, Alakhov VY: **Pluronic block copolymers for overcoming drug resistance in cancer.** *Adv Drug Deliv Rev* 2002, **54:**759-779.
140. Kabanov AV, Batrakova EV, Alakhov VY: **Pluronic block copolymers as novel polymer therapeutics for drug and gene delivery.** *J Control Release* 2002, **82:**189-212.
141. Krylova OO, Pohl P: **Ionophoric activity of pluronic block copolymers.** *Biochemistry* 2004, **43:**3696-3703.
142. Regev R, Katzir H, Yeheskely-Hayon D, Eytan GD: **Modulation of P-glycoprotein-mediated multidrug resistance by acceleration of passive drug permeation across the plasma membrane.** *FEBS J* 2007, **274:**6204-6214.
143. Jamshaid M, Farr SJ, Kearney P, Kellaway IW: **Poloxamer Sorption on Liposomes - Comparison with Polystyrene Latex and Influence on Solute Efflux.** *Int J Pharm* 1988, **48:**125-131.
144. Erukova VY, Krylova OO, Antonenko YN, Melik-Nubarov NS: **Effect of ethylene oxide and propylene oxide block copolymers on the permeability of bilayer lipid membranes to small solutes including doxorubicin.** *Biochim Biophys Acta* 2000, **1468:**73-86.
145. Batrakova EV, Li S, Miller DW, Kabanov AV: **Pluronic P85 increases permeability of a broad spectrum of drugs in polarized BBMEC and Caco-2 cell monolayers.** *Pharm Res* 1999, **16:**1366-1372.
146. Bendas ER, Tadros MI: **Enhanced transdermal delivery of salbutamol sulfate via ethosomes.** *AAPS PharmSciTech* 2007, **8:**E107.
147. Wong M: **Alginates in tissue engineering.** *Methods Mol Biol* 2004, **238:**77-86.
148. Thomas S: **Alginate dressings in surgery and wound management-Part 1.** *J Wound Care* 2000, **9**.
149. Lim F, Sun AM: **Microencapsulated islets as bioartificial endocrine pancreas.** *Science* 1980, **210:**908-910.

150. Soon-Shiong P, Heintz RE, Merideth N, Yao QX, Yao Z, Zheng T: **Insulin independence in a type 1 diabetic patient after encapsulated islet transplantation. .** *Lancet* 1994, **343:**950-951.
151. Joki T, Machluf M, Atala A, Zhu J, Seyfried NT, Dunn IF, Abe T, Carroll RS, Black PM: **Continuous release of endostatin from microencapsulated engineered cells for tumor therapy.** *Nat Biotechnol* 2001, **19:**35-39.
152. Cirone P, Bourgeois JM, Austin RC, Chang PL: **A novel approach to tumor suppression with microencapsulated recombinant cells.** *Hum Gene Ther* 2002, **13:**1157-1166.
153. Chang PL: **Microcapsules as bio-organs for somatic gene therapy.** *Ann N Y Acad Sci* 1997, **831:**461-473.
154. Chang SC, Rowley JA, Tobias G, Genes NG, Roy AK, Mooney DJ, Vacanti CA, Bonassar LJ: **Injection molding of chondrocyte/alginate constructs in the shape of facial implants.** *J Biomed Mater Res* 2001, **55:**503-511.
155. Fragonas E, Valente M, Pozzi-Mucelli M, Toffanin R, Rizzo R, Silvestri F, Vittur F: **Articular cartilage repair in rabbits by using suspensions of allogenic chondrocytes in alginate.** *Biomaterials* 2000, **21:**795-801.
156. Shang Q, Wang Z, Liu W, Shi Y, Cui L, Cao Y: **Tissue-engineered bone repair of sheep cranial defects with autologous bone marrow stromal cells.** *J Craniofac Surg* 2001, **12:**586-593; discussion 594-585.
157. Lee CS, Gleghorn JP, Won Choi N, Cabodi M, Stroock AD, Bonassar LJ: **Integration of layered chondrocyte-seeded alginate hydrogel scaffolds.** *Biomaterials* 2007, **28:**2987-2993.
158. Ishihara Y, Calderon A, Watanabe H, Okamoto K, Suzuki Y, Kuroda K, Suzuki Y: **A precise and fast temperature mapping using water proton chemical shift.** *Magn Reson Med* 1995, **34:**814-823.
159. Ajima K, Maigne A, Yudasaka M, Iijima S: **Optimum Hole-Opening Condition for Cisplatin Incorporation in Single-Wall Carbon Nanohorns and Its Release.** *J Phys Chem B* 2006, **110:**19097-19099.
160. Ajima K, Yudasaka M, Maigne A, Miyawaki J, Iijima S: **Effect of Functional Groups at Hole Edges on Cisplatin Release from Inside Single-Wall Carbon Nanohorns.** *J Phys Chem B* 2006, **110:**5773-5778.
161. Hashimoto A, Yorimitsu H, Ajima K, Suenaga K, Isobe H, Miyawaki J, Yudasaka M, Iijima S, Nakamura E: **Selective deposition of a gadolinium(III) cluster in a hole opening of single-wall carbon nanohorn.** *Proceedings of the National Academy of Sciences* 2004, **101:**8527-8530.
162. Yuge R, Yudasaka M, Miyawaki J, Kubo Y, Ichihashi T, Imai H, Nakamura E, Isobe H, Yorimitsu H, Iijima S: **Controlling the Incorporation and Release of C60 in Nanometer-Scale Hollow Spaces inside Single-Wall Carbon Nanohorns.** *J Phys Chem B* 2005, **109:**17861-17867.
163. Lynch RM, Voy BH, Glass DF, Mahurin SM, zhao B, Hu H, Saxton AM, Donnell RL, Cheng M-d: **Assessing the pulmonary toxicity of single-walled carbon nanohorns.** *Nanotoxicology* 2007, **1:**157 - 166.